Elektrische stromen in apolaire vloeistoffen met surfactanten

Electric Currents in Nonpolar Liquids with Surfactants

Filip Beunis

Promotor: prof. dr. ir. K. Neyts
Proefschrift ingediend tot het behalen van de graad van
Doctor in de Ingenieurswetenschappen:Toegepaste Natuurkunde

Vakgroep Elektronica en Informatiesystemen
Voorzitter: prof. dr. ir. J. Van Campenhout
Faculteit Ingenieurswetenschappen
Academiejaar 2007 - 2008

UNIVERSITEIT
GENT

ISBN 978-90-8578-208-7
NUR 959, 924
Wettelijk depot: D/2008/10.500/27

Filip Beunis

Preface

This book is not the result of five years of hard work. At no moment did I have the feeling that I was doing something else than playing and doing what I wanted to do. The fact that all this fun now leads to a PhD degree is of course important, mainly since it will allow me to keep on doing what I like. But the degree is not the real prize. '*I've already got the prize. The prize is the pleasure of finding things out (R. Feynman)*'

A lot of people have contributed to this pleasure, and to the results that are a consequence of it. I could not have done it, nor would I have wanted to do it, without them.

In the first place, I would like to thank my parents. Mama and Papa, while most people that I mention in this preface helped me finishing this PhD,

you helped me to get to the start of it. your unconditional love and support, and the example you set for me, made me the person that I am today.

I would also like to thank my promotor. Kristiaan, you have a way of guiding your PhD students that is more about asking questions than about providing answers, more about understanding than about knowing, more about giving ideas than about assigning tasks. I could not have wished for a better mentor.

If coming to work meant having fun, it is mainly because my colleagues are my friends. People of the physical electronics group, I really enjoy working with you. I saw a whole floor of PhD students finishing, and a whole floor starting. The group of professors (that are all a little bit eccentric in their own way) provided continuity in an atmosphere that I found very stimulating. You all helped me taking things seriously when I had to, and relativizing them when I could. You are with too many to mention you all, but it would especially be unforgivable if I forgot the people that I shared an office with. Gert, Andriy, Youri, Filip, Hans, Yvan, Karel, Matthias and Bart, thanks!

Two of my colleagues deserve a special mention. Filip S and Matthias, I saw you evolving from naïve thesis students into good scientists. It makes me proud to imagine that I played a part in that evolution. I wonder if you know how much you teached me, partly by forcing me to order my thoughts to be able to explain things to you, partly by explaining me your own thoughts.

I would also like to thank Alwin Verschueren from Philips Research. Alwin, the meetings we had always meant an explosion of new ideas, which finally resulted in the book you are holding. I hope my results will be useful for you and for Philips.

While my colleagues inspired me at work, my other friends and my family gave me the necessary perspective. A lot of ideas didn't come when I was in the office, but when I was at home, in a bar or outside, with you. Thanks for that!

Finally, Andrea, my partner in everything. You were both the motivation and the distraction. Thank you for your patience and for your impatience, they were both necessary! It's a pleasure finding things out with you, because of you, for you, and about you!

Filip Beunis

Table of contents

Samenvatting

Elektrische stromen in apolaire vloeistoffen met surfactanten

Een vloeistof kan polair of apolair zijn, afhankelijk van de verdeling van lading in haar moleculen. Surfactantmoleculen hebben zowel een polair als een apolair deel, waardoor ze adsorberen op oppervlakken en grotere aggregaten vormen. In een apolaire vloeistof vormen ze inverse micellen, die ladingen kunnen stabiliseren die anders niet zouden kunnen bestaan. Gedurende mijn doctoraatsonderzoek heb ik de eigenschappen van geladen inverse micellen onderzocht.

De belangrijkste motivatie om ladingen in mengsels van apolaire vloeistof en surfactant te onderzoeken is de relevantie voor elektroforetische beeldschermen. In de zoektocht naar elektronisch papier, dat de goede visuele eigenschappen van gedrukt papier combineert met de mogelijkheid om de afgebeelde informatie te wijzigen, zijn

elektroforetische beeldschermen een veelbelovende technologie. De resultaten van mijn onderzoek dragen bij tot een beter begrip van mengsels van surfactant en apolaire vloeistof, en vormen de basis voor een model dat het gedrag van elektroforetische beeldschermen beschrijft.

Ik heb mengsels onderzocht van de apolaire vloeistof n-dodecaan en het surfactant OLOA 1200, die gebruikt worden in elektroforetische beeldschermen. Een dunne laag van het mengsel wordt gesandwiched tussen planaire elektrodes. Langdurig kortsluiten van de elektrodes zorgt voor een homogene distributie van inverse micellen in het device. Na kortsluiting wordt een spanningsstap aangelegd over de elektrodes en wordt de resulterende elektrische stroom gemeten. Om bruikbare informatie uit deze metingen te kunnen halen, heb ik een gevoelige meetopstelling ontwikkeld. De combinatie van de eendimensionale geometrie en de eenvoudige beginvoorwaarde laat een gemakkelijke interpretatie van de resultaten toe. Uit de metingen kunnen waarden voor de mobiliteit en de gemiddelde concentratie van inverse micellen bepaald worden.

Uit de mobiliteitsmetingen kon ik verschillende eigenschappen van inverse micellen afleiden. Ik heb waarden gevonden voor de effectieve straal en het aantal surfactantmoleculen in een inverse micelle. De concentratie aan inverse micellen blijkt afhankelijk te zijn van de surfactantconcentratie en van de dikte van het device. Ik verklaar dit door concentratie-afhankelijke micellizatie en oppervlakte-adsorptie van surfactantmoleculen. In geometrieën met microscopische dimensies zijn

deze processen beide belangrijk. Ik stel een model voor dat toelaat de concentratie aan geladen en neutrale inverse micellen te voorspellen voor een gegeven dikte en surfactantconcentratie. Dit model komt overeen met de metingen. Ik leid ook waarden af voor de surfactantconcentratie onder dewelke geen inverse micellen worden gevormd (de kritische micelle concentratie), en voor de oppervlakteconcentratie van geadsorbeerde surfactantmoleculen op de elektrodes.

De gemeten elektrische stroom op korte tijdsschaal is een gevolg van de beweging van geladen inverse micellen die aanwezig zijn in het device op het ogenblik dat de stap in de spanning wordt aangelegd. De beweging van deze ladingen kan worden beschreven met de Poisson-Nernst-Planck vergelijkingen, die drift in het elektrisch veld, diffusie, en de invloed van de ladingen op het veld beschrijven. Ondanks het belang van deze vergelijkingen is er geen algemene oplossing gekend. Ik onderzoek vier speciale gevallen, waarin vereenvoudigende veronderstellingen kunnen gemaakt worden. Voor deze gevallen leid ik analytische uitdrukkingen af die nuttig zijn om de dynamica van ladingstransport in apolaire vloeistoffen met surfactant te begrijpen. De theoretische resultaten komen overeen met numerieke simulaties en stroommetingen. Dit bevestigt dat drift en diffusie de twee dominante transportmechanismes zijn voor inverse micellen in een apolaire vloeistof.

Nadat er een evenwicht tussen drift en diffusie bereikt is voor een zekere spanning, bewegen de ladingen niet meer en zou de elektrische stroom nul moeten zijn. De metingen tonen echter dat er een kleine stroom blijft vloeien gedurende lange tijd. Dit is een gevolg van de beweging van

nieuw gegenereerde geladen inverse micellen. Ik meet deze 'quasi' steady state stroom in devices met verschillende eigenschappen en voor verschillende spanningen. Een analyse van hoe de stroom afhangt van verschillende parameters laat me toe een model voor te stellen voor de generatie en recombinatie van geladen inverse micellen. Deze reacties komen voor in de bulk tussen twee inverse micellen en aan oppervlakken tussen een micelle en de geadsorbeerde surfactantlaag. Het reactiemechanisme is verschillend voor de twee gevallen, maar beide zijn nodig om de metingen te verklaren.

Samen met drift en diffusie, kunnen de mechanismes voor generatie en recombinatie in de bulk en aan de oppervlakken gecombineerd worden in een model dat zowel de transient als de (quasi) steady state in alle metingen goed beschrijft.

Summary

Electric currents in nonpolar liquids with surfactants

A liquid can be polar or nonpolar, depending on the distribution of charge in its constituent molecules. Surfactant molecules have both a polar and a nonpolar part, as a result of which they adsorb at interfaces and self-aggregate into larger structures. In nonpolar liquids they form inverse micelles, which can stabilize charges that could not exist otherwise. During my PhD research, I investigated the properties of charged inverse micelles.

The main motivation for investigating charges in mixtures of nonpolar liquids and surfactants is the relevance in electrophoretic displays. In the search for paper-like displays, which combine the good viewing characteristics of printed paper with the ability to change the displayed information, electrophoretic displays are a promising technology. The

results of my research contribute to a better understanding of mixtures of surfactant and nonpolar liquid, and provide the basis for a model to describe the behavior of electrophoretic displays.

I investigated mixtures of the nonpolar liquid n-dodecane and the surfactant OLOA 1200, which are used in electrophoretic displays. A thin layer of the mixtures is sandwiched between two planar electrodes. Short-circuiting the electrodes for a long time ensures a homogeneous distribution of inverse micelles throughout the device. After short-circuiting, a voltage step is applied over the electrodes and the resulting electric current is measured. To derive useful information from these measurements, I developed a sensitive measurement setup. The combination of the one-dimensional geometry and the simple initial condition allows a straightforward interpretation of the results. Values for the mobility and the average concentration of charged inverse micelles can be obtained from these measurements.

From the current measurements, I was able to derive several properties of the inverse micelles. I found values for the effective radius and for the number of surfactant molecules in an inverse micelle. Measurements of the inverse micelle concentration indicate a dependence on the surfactant concentration and on the thickness of the device. I explain this by concentration dependent micellization and surface adsorption of surfactant molecules. In geometries with microscopic dimensions, these processes are both important. I propose a model which allows to predict the concentrations of neutral and charged inverse micelles for a given thickness and surfactant concentration. I also derive values for the

surfactant concentration below which no micelles are formed (the critical micelle concentration) and for the surface concentration of adsorbed surfactant molecules on the electrodes.

The electric current measured on a short timescale is a result of the movement of charged inverse micelles present in the device at the moment when the voltage step is applied. The movement of these charges can be described with the Poisson-Nernst-Planck equations, which describe drift in the electric field, diffusion, and the influence of charges on the electric field. Despite the importance of these equations, no general solution is known. I investigate four special cases, in which simplifying assumptions can be made. For these cases, I derive analytical expressions which are useful to understand the dynamics of charge transport in nonpolar liquids with surfactant. The theoretical results agree with numerical simulations and current measurements. This confirms that drift and diffusion are the two dominant transport mechanisms for inverse micelles in a nonpolar liquid.

After an equilibrium between drift and diffusion is reached for a certain applied voltage, the charges do not move anymore and the electric current should be zero. The measurements however show that a small current keeps flowing for a very long time. This is a result of the movement of newly generated charged inverse micelles. I measured this 'quasi' steady state current in devices with different properties and for different voltages. An analysis of how the current depends on various parameters allows me to propose a model for the generation and recombination of charged inverse micelles. These reactions happen in the

bulk between two micelles and also at the surfaces between a micelle and the adsorbed surfactant layer. The mechanism of the reaction is different for the two cases, but both are necessary to explain the measurements.

Together with drift and diffusion, the mechanisms of generation and recombination in the bulk and at the surfaces can be combined in a model which describes both the transient and the (quasi) steady state of all the measurements I performed.

List of symbols

Symbol	Unit	Description
$\hat{A}$	$A \cdot s^{-1}$	Fitting parameter
$\hat{B}$	A	Fitting parameter
c	no unit	Weight fraction of surfactant in nonpolar liquid
c_{cmc}	no unit	Critical micelle concentration
$C(t)$	no unit	Integration function
$\hat{C}$	A	Fitting parameter
C_{empty}	F	Capacitance of an empty device
C_i	no unit	Eigenvalues, used in the solution of the Nernst-Planck equation
d	m	Thickness of a device
d_{IL}	m	Thickness of an insulating layer

Symbol	Unit	Description
D	$m^2 \cdot s^{-1}$	Diffusion constant of particles in a viscous medium or inverse micelles in dodecane
$\hat{D}$	s^{-1}	Fitting parameter
$E(x,t)$	$V \cdot m^{-1}$	Electric field, measured in the positive x-direction
$\tilde{E}(\tilde{x},\tilde{t})$	no unit	Normalized electric field
$E_{bulk}(t)$	$V \cdot m^{-1}$	Electric field in the bulk
$E_{DL}(x,t)$	$V \cdot m^{-1}$	Electric field in the double layer
$E_{el}(t)$	$V \cdot m^{-1}$	Electric field at the electrode
$E_{el,qss}$	$V \cdot m^{-1}$	Electric field at the electrode in quasi steady state
$E_{int}(t)$	$V \cdot m^{-1}$	Electric field at the interface of the double layer and the space charge region
$E_{ss}(x)$	$V \cdot m^{-1}$	Electric field in steady state
$E_{SC}(x,t)$	$V \cdot m^{-1}$	Electric field in the (positive) space charge region
f	No unit	Correction factor to take insulating layers into account
$I(t)$	A	Electric current, flowing from the external circuit towards the electrode at $x = -d/2$
$\tilde{I}(\tilde{t})$	no unit	Normalized electric current
I_0	A	Initial electric current on application of a voltage step, after the capacitive charge has been supplied to the electrodes but before any charge in the device has moved
I_{qss}	A	Quasi steady state current
$I_{sim}(t)$	A	Simulated electric current
$I_{th}(t)$	A	Theoretical electric current

Symbol	Unit	Description
$J(x,t)$	A·m^{-2}	Electric current density, measured in the positive x-direction
$\tilde{J}(\tilde{x},\tilde{t})$	no unit	Normalized electric current density
$J_{el,qss}$	A·m^{-2}	Electric current density at an electrode in quasi steady state
$J_{qss}(x)$	A·m^{-2}	Electric current density in quasi steady state
k	J·K^{-1}	Constant of Boltzmann
K	no unit	Equilibrium constant of disproportionation / comproportionation of inverse micelles
l	m	Distance between two particles
$m(x,t)$	m^{-3}	Total concentration of both positively and negatively charged particles or inverse micelles
$\tilde{m}(\tilde{x},\tilde{t})$	no unit	Normalized total concentration
m_{mic}	kg	Mass of an inverse micelle
m_{mol}	kg	Mass of a surfactant molecule
$\overline{n}(t)$	m^{-3}	Average concentration of one polarity of charged particles or inverse micelles
$n_0(x,t)$	m^{-3}	Concentration of neutral inverse micelles
$\overline{n}_0(t)$	m^{-3}	Average concentration of neutral inverse micelles
$n_{0,el,qss}$	m^{-3}	Concentration of neutral inverse micelles near the electrode in quasi steady state
$n_+(x,t)$	m^{-3}	Concentration of positively charged particles or inverse micelles
$\tilde{n}_+(\tilde{x},\tilde{t})$	no unit	Normalized concentration of positive charges
$n_{+,el,qss}$	m^{-3}	Concentration of positively charged inverse micelles near the electrode in quasi steady state

Symbol	Unit	Description
$n_{+,ss}(x)$	m^{-3}	Steady state concentration of positively charged particles or inverse micelles
$n_{-}(x,t)$	m^{-3}	Concentration of negatively charged particles or inverse micelles
$\tilde{n}_{-}(\tilde{x},\tilde{t})$	no unit	Normalized concentration of negative charges
$n_{-,el,qss}$	m^{-3}	Concentration of negatively charged inverse micelles near the electrode in quasi steady state
$n_{-,ss}(x)$	m^{-3}	Steady state concentration of negatively charged particles or inverse micelles
$n_{DL}(x,t)$	m^{-3}	Concentration of (positive) charges in the (positive) double layer
$n_{int}(t)$	m^{-3}	Concentration of (positive) charges at the interface of the (positive) double layer and space charge region
$n_{SC}(x,t)$	m^{-3}	Concentration of (positive) charges in the (positive) space charge region
$\overline{n}_{tot}$	m^{-3}	Average concentration of all inverse micelles
N	no unit	Aggregation number, number of surfactant molecules in one inverse micelle
q	C	Absolute value of the electric charge of one charged particle or inverse micelle
q_e	C	Elementary charge
Q_{cap}	$C \cdot m^{-2}$	Capacitive surface charge density on an electrode
$Q_{el}(t)$	$C \cdot m^{-2}$	Surface charge density on an electrode
$Q_{ind}(t)$	$C \cdot m^{-2}$	Induced surface charge density on an electrode

Symbol	Unit	Description
$Q_s(t)$	C·m^{-2}	Surface charge density of charged particles or inverse micelles near an electrode
Q_{tot}	C·m^{-2}	Total charge (per unit of electrode area) carried by particles or inverse micelles of one polarity
R	m	Effective radius of an inverse micelle
S	m^2	Surface area on which surfactant molecules are adsorbed
S_{el}	m^2	Surface area of an electrode
S_{tot}	m^2	Surface area enclosed by glue pattern
t	s	Temporal coordinate
$\tilde{t}$	no unit	Normalized time
$t_{x\%}$	s	Time when the simulated electric current reaches x % of its initial value
t_{ss}	s	Time when steady state is reached after a voltage step at $t = 0$
T	K	Absolute temperature
U_k	J	Kinetic energy
U_p	J	Potential energy
V_A	V	Applied voltage, measured at the electrode at $x = -d/2$ with the other electrode grounded
V_T	V	Thermal voltage
x	m	Spatial coordinate
$\tilde{x}$	no unit	Normalized position
$X_{\pm,i}(x)$	no unit	Eigenfunctions, used in the solution of the Nernst-Planck equation

Symbol	Unit	Description
Z	no unit	Absolute value of the valency of a charged particle or inverse micelle
Z_i	no unit	Valency of charged particle i
α	$m^3 \cdot s^{-1}$	Bulk recombination constant
β	$m^3 \cdot s^{-1}$	Bulk generation constant
γ	no unit	Dimensionless factor, used in the space charge limited regime
γ'	no unit	Corrected dimensionless factor, used in the space charge limited regime
Δ	no unit	Normalized root mean square error between theory and simulation
ε	no unit	Relative dielectric constant of a medium or dodecane
ε_0	$F \cdot m^{-1}$	Dielectric permittivity of vacuum
ε_{IL}	no unit	Relative dielectric constant of an insulating layer
ζ	$m^{-1} \cdot V^{-1} \cdot s^{-1}$	Surface generation constant
η	Pa·s	Viscosity of dodecane
λ	no unit	Dimensionless parameter, a measure for the charge content of a device
λ_B	m	Bjerrum length
λ_{DL}	m	Width of a double layer, or Debye length
$\lambda_{SC}(t)$	m	Thickness of a space charge region
μ	$m^2 \cdot V^{-1} \cdot s^{-1}$	Mobility
ν	m^{-2}	Surface concentration of adsorbed surfactant molecules
$\rho(x,t)$	$C \cdot m^{-3}$	Charge density

Symbol	Unit	Description
$\tilde{\rho}(\tilde{x},\tilde{t})$	no unit	Normalized charge density
ρ_m	kg·m^{-3}	Mass density of dodecane
$\rho_{ss}(x)$	C·m^{-3}	Steady state of the charge density
$\rho_{tr}(x,t)$	C·m^{-3}	Transient part of the charge density
σ	Ω·m	Resistivity of dodecane
τ_{dep}	s	Depletion time
τ_{DL}	s	Double layer charging time
τ_{scr}	s	Screening time
τ_{sep}	s	Separation time
τ_{tr}	s	Transit time
φ	no unit	Dimensionless parameter, a measure for the applied voltage
$\Psi_0(x,t)$	m^{-2}·s^{-1}	Flux of neutral inverse micelles, measured in the positive x-direction
$\Psi_{0,ads}$	m^{-2}·s^{-1}	Flux of neutral inverse micelles adsorbing at a surface from the liquid
$\Psi_+(x,t)$	m^{-2}·s^{-1}	Flux of positively charged particles or inverse micelles
$\tilde{\Psi}_+(\tilde{x},\tilde{t})$	no unit	Normalized flux of positive charges
$\Psi_{+,ads}$	m^{-2}·s^{-1}	Flux of positively charged inverse micelles adsorbing at a surface from the liquid
$\Psi_{+,inj}$	m^{-2}·s^{-1}	Flux of positively charged inverse micelles injected from the surface into the liquid
$\Psi_-(x,t)$	m^{-2}·s^{-1}	Flux of negatively charged particles or inverse micelles
$\tilde{\Psi}_-(\tilde{x},\tilde{t})$	no unit	Normalized flux of negative charges

Symbol	Unit	Description
$\Psi_{-,ads}$	$m^{-2} \cdot s^{-1}$	Flux of negatively charged inverse micelles adsorbing at a surface from the liquid
$\Psi_{-,inj}$	$m^{-2} \cdot s^{-1}$	Flux of negatively charged inverse micelles injected from the surface into the liquid

Filip Beunis

Chapter 1
Introduction

A liquid can be polar or nonpolar, depending on the distribution of charge in its constituent molecules. Surfactant molecules have both a polar and a nonpolar part, as a result of which they adsorb at interfaces and self-aggregate into larger structures. In a nonpolar liquid they form inverse micelles, which can stabilize charges that could not exist otherwise. During my PhD research, I investigated the properties of charged inverse micelles. This chapter provides the necessary background and describes electrophoretic display technology, the application which was the main motivation for my work. The results of my research, outlined in this chapter, contribute to a better understanding of mixtures of surfactant and nonpolar liquid, and provide the basis for a model to describe the behavior of electrophoretic displays.

1.1. Introduction

Liquids can be broadly divided into two categories: polar liquids and nonpolar liquids. The distinction between the two is based on the distribution of electric charge within the constituent molecules (figure 1). In polar liquids the molecules have a permanent dipole moment: their positive and negative charges are not distributed in the same way. This occurs when some atoms in the molecule attract electrons more than other atoms. In nonpolar liquids, the molecules do not have a permanent dipole moment: positive and negative charges are distributed in the same way throughout the molecule. The distinction between polar and nonpolar liquids is not absolute, but rather an indication of the relative position of a liquid on a continuous scale of polarities, measured by the relative dielectric constant ε (no unit) of the liquid. Water is considered to be polar because its relative dielectric constant is 80, a relatively high value. The relative dielectric constant of dodecane is 2, a relatively low value, so it is considered nonpolar. Other liquids, such as acetone with a relative dielectric constant of 20, are more difficult to categorize.

When a liquid is used as a solvent, its polarity is an important property. As a general rule, polar solutes can only be dissolved in polar solvents and nonpolar solutes can only be dissolved in nonpolar solvents. This is a result of the thermodynamics involved in the interactions between solvent and solute molecules. In terms of enthalpy and entropy, it is more favorable for a molecule to be surrounded by molecules with a similar polarity than by molecules with another polarity. This difference arises from the attractions between the molecules. Between nonpolar

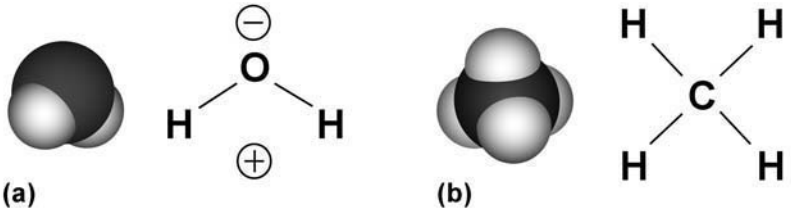

Figure 1:
Example of (a) a polar molecule (water), and (b) a nonpolar molecule (methane). (a) Water is polar because the oxygen atom attracts electrons more than the hydrogen atoms. Since the molecule is asymmetrical, this results in a dipole. (b) Methane is nonpolar because in the carbon-hydrogen bonds the electrons are not attracted more to one atom than to another. In addition, the molecule is symmetrical.

molecules there is in general no significant attraction. In polar liquids however, dipole attraction causes the enthalpy of the system to decrease when the polar molecules are closer to each other. In some polar liquids, in particular in water, hydrogen bonds are formed, which contribute even more to the decrease of enthalpy. This is the reason why water and oil do not mix, but rather separate into two distinct phases. In addition to the decrease of enthalpy, the preference for a higher entropy will favor 'unordered' systems over 'ordered' ones. Which of these different factors is dominant depends on the specific liquids that are used and on the proportions in which they are (attempted to be) mixed.

Some molecules consist of both polar (or hydrophilic) parts and nonpolar (or hydrophobic) parts. Such molecules are called amphiphilic, and their

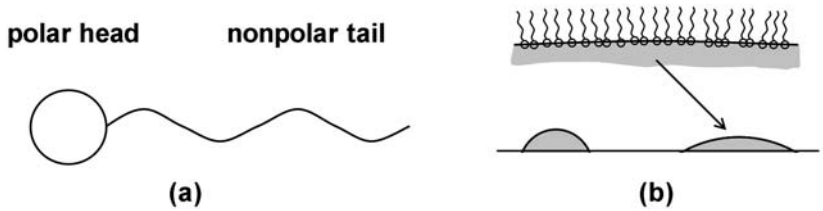

Figure 2:
(a) Schematic representation of an amphiphilic molecule, with a polar head and a nonpolar tail. Such molecules are also called surfactants, because of their ability to lower the surface tension of a liquid in contact with for instance air (b). This results in a water droplet in contact with air on a surface to have a smaller contact angle if surfactant is added than in the case of pure water.

polar and nonpolar parts are called the heads and the tails, respectively (figure 2(a)). Because of their dual nature, these molecules tend to adsorb at interfaces between substances with different polarity, with their heads directed towards the polar substance and their tails directed towards the nonpolar substance. This can happen at the interface of two liquids, the interface of a gas and a liquid and the interface of a solid and a liquid. Because this adsorption lowers the surface tension of the interface (figure 2(b)), amphiphilic molecules are also called surfactants.

Surfactant molecules do not only adsorb at interfaces, but also self-aggregate [1][2][3]. Because it is energetically favorable for the polar head groups to be in a polar environment, they tend to concentrate together. The structures which are formed this way have a polar core, consisting of

the head groups, and a nonpolar shell, consisting of the apolar tails pointing outwards. These aggregates are called inverse micelles, in analogy with the micelles formed in polar liquids [4] (figure 3), where the nonpolar tails of surfactant molecules concentrate together. The mechanisms of micelle formation and inverse micelle formation are however not completely the same. An increase of entropy is the driving factor in the formation of micelles. In the case of inverse micelles, the driving factor is a decrease of enthalpy, as a result of attraction between the polar heads. The inverse micelles can however not grow indefinitely because of sterical hindrance, resulting in an optimal size of inverse micelles.

The polar interior of inverse micelles is an environment with unique properties. This environment allows chemical reactions which do not occur in normal circumstances, so surfactant can serve as a catalyst in nonpolar liquids [5]. They are widely used in the investigation of enzymatic reactions [6][7], the fabrication of nanoparticles [8], the stabilization of soot in engine oil [9] or in drug delivery [10]. All these applications are based on the fact that a small polar volume is physically separated from the nonpolar environment by a layer of surfactant molecules. This situation also allows for the existence of free charges in nonpolar liquid [11][12]. The use of surfactant as a charging agent has several practical applications, and is the main motivation for this work.

The behavior of charges in polar liquids has been studied intensively and is largely understood. In nonpolar liquids, due to stronger electrostatic interactions, the presence of free charges is less likely and can in most

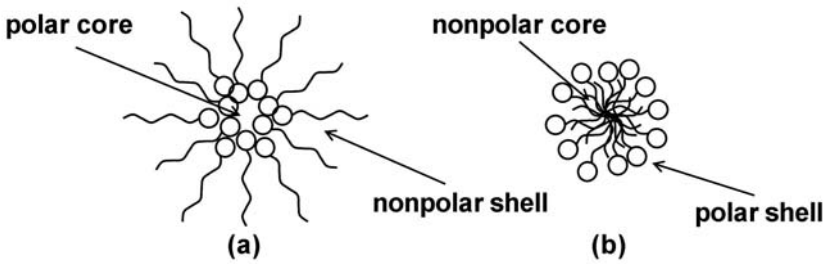

Figure 3:

Schematic representation of (a) an inverse micelle and (b) a micelle. In a nonpolar liquid, surfactant molecules concentrate their heads together and form inverse micelles (a) with a polar core and a nonpolar shell. In a polar liquid, the molecules concentrate their tails together, resulting in a micelle (b) with a nonpolar core and a polar shell.

cases be neglected. In many practical situations however, their presence is important, and can result in undesired effects [13][14] or useful applications. Charges in nonpolar liquids have received much less research attention than in polar liquids, and are therefore not as well understood. During my PhD research, I performed electric current measurements to obtain information about charges in mixtures of a nonpolar liquid and a surfactant.

The remainder of this chapter provides the necessary background and motivation for my work, as well as a quick overview of the following chapters. In section 2, I explain how surfactant can stabilize free electric charges which could otherwise not exist in nonpolar liquid. This property is used in practical applications, one of which is electrophoretic ink, which I describe in section 3. The need to understand better the behavior of

charged inverse micelles in electrophoretic ink is the main motivation for my research. Section 4 provides a quick overview of this research and summarizes the results I obtained.

This chapter demonstrates that charges in mixtures of a nonpolar liquid and a surfactant are important in practical applications. The results of my PhD research, reported in this work, provide a better understanding of the origin, the properties and the behavior of these charges.

1.2. Charge in nonpolar liquid

Most nonpolar liquids have very good insulating properties, but their conductivity increases by several orders of magnitude if a surfactant is added. This is a result of the fact that the surfactant molecules can provide the separation which is necessary for opposite charges to overcome the electrostatic attraction.

1.2.1. Bjerrum length

The ratio between charged and neutral particles in a liquid is the result of an equilibrium between different reactions. On a microscopic scale, these reactions occur because of collisions between the particles, which are in constant thermal motion. During each collision between two particles a number of forces come into play. When two oppositely charged particles collide, one of these forces is the electrostatic force, which attracts the two particles towards each other (figure 4). The potential energy U_p (unit: J) with reference zero at large distance is inversely proportional with the distance l (unit: m) between the particles:

$$U_p = \frac{Z_1 Z_2 q_e^2}{4\pi\varepsilon\varepsilon_0 l}. \qquad (1)$$

In this equation, Z_1 and Z_2 (no unit) are the numbers of elementary charges of the particles; q_e is the elementary charge (q_e = 1.602×10^{-19} C); ε is the relative dielectric constant of the medium and ε_0 is the dielectric permittivity of vacuum (ε_0 = 8.854×10^{-12} F·m^{-1}).

If the electrostatic force would be the only force acting on the particles, all

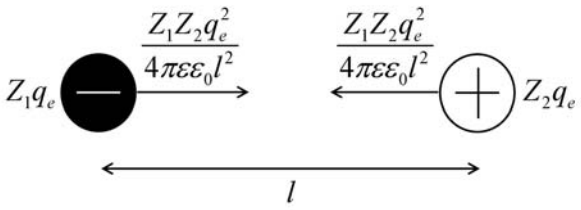

Figure 4:
Two charged particles with opposite polarity are attracted towards each other by the electrostatic force. The magnitude of this force is proportional with the charge on each of the particles and with the square of the distance between them. The polarity of the medium is also important: the electrostatic force is inversely proportional with the relative dielectric constant of the medium. This results in a stronger attraction in nonpolar liquids than in polar liquids.

charges would eventually pair up with an opposite charge and in equilibrium no charges could exist. The reason why this is not the case is that the kinetic energy associated with the thermal motion of the particles can overcome the electrostatic attraction. U_k (unit: J) is a measure for the average kinetic energy:

$$U_k = kT\,, \tag{2}$$

with k the constant of Boltzmann (k = 1.38×10^{-23} J·K^{-1}) and T (unit: K) the absolute temperature.

The two energies in equations (1) and (2) are equal in magnitude for a certain distance between two opposite charges, which is called the Bjerrum length λ_B (unit: m):

$$\lambda_B = \left| \frac{Z_1 Z_2 q_e^2}{4\pi\varepsilon\varepsilon_0 kT} \right|. \quad (3)$$

The Bjerrum length is thus a measure for the distance at which oppositely charged particles have to remain separated to prevent irreversible electrostatic binding. This separation can be achieved just by the size of the charges themselves, or by encapsulating them in a larger structure. In more elaborate models [15][16], there is no sharply defined critical distance, but the conclusion is always that the equilibrium between charged and neutral particles shifts in favor of charged particles for larger particle sizes (including the encapsulation).

In water (ε = 80) and for univalent charges, the Bjerrum length in equation (3) can be calculated as 0.7 nm. As an example, the center-to-center distance in a NaCl crystal (normal kitchen salt) is 0.28 nm. Although this distance is smaller than the Bjerrum length, the shell of water molecules which forms around ions through dipole interactions is sufficient to allow the existence of Na^+ and Cl^- ions (figure 5).

In nonpolar liquids the situation is different, as a result of the low relative dielectric constant. In dodecane (ε = 2) for instance, the Bjerrum length for univalent charges is 28 nm. For charges in pure dodecane, there is nothing that prevents them from approaching each other closer than the Bjerrum length. Therefore, very few charges can exist in equilibrium and pure dodecane is a good insulator.

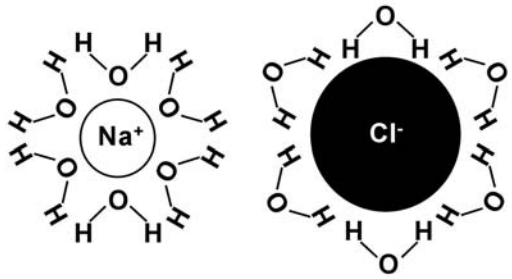

Figure 5:
For salt (NaCl) to dissolve in water, the Na^+ and Cl^- ions have to remain separated over a distance estimated by the Bjerrum length, which is 0.7 nm in water. The formation of a shell of water molecules around the ions, as a result of the attraction between the charge and the dipole, provides a barrier that keeps the ions separated over this distance. For that reason, salt dissolves very well in water.

1.2.2. Surfactant as charging agent

In a nonpolar liquid, charges can only exist if they are encapsulated in large structures, which prevent them from approaching each other closer than the Bjerrum length. This can be achieved by adding a surfactant to the liquid. The adsorption of surfactant molecules on charged species provides a separating layer which can keep charges apart.

In the polar core of an inverse micelle, neutral groups can dissociate into oppositely charged ions. These groups can originate from impurities (for instance water) in the nonpolar liquid, or can be on the heads of the surfactant molecules. When the negative and the positive charge resulting from a dissociation both remain confined in the polar core, the

inverse micelle remains neutral. The inverse micelles can interact with each other and exchange their contents [17][18] during a collision. This can result in a separation of two oppositely charged inverse micelles (figure 6(a)). This charging mechanism of inverse micelles will be discussed in more detail in chapters 3 and 5. Univalent charges can be stabilized in inverse micelles, but for higher valences the necessary separation distance increases. In chapter 4 I will show that in the mixture I investigate, only univalent charges are present.

Surfactant can also stabilize charges on the surface of colloidal particles in a nonpolar liquid. Surface groups on these particles can dissociate, and a layer of surfactant molecules adsorbed on the surface of the particle provides the necessary separation with the counterion (figure 6(b)). Around the counterion itself, an inverse micelle forms.

1.2.3. Applications

The use of surfactant as charging agent has many applications. In most of these applications, an electric charge on colloidal particles suspended in a nonpolar liquid allows manipulating the particles.

Liquid immersion development [19] is an alternative for the dry toner used in printers or copiers. In this process, a patterned electrostatic image is created by the exposure of a charged photoconductor to an inhomogeneous light source. A suspension of charged pigment particles in a nonpolar liquid is then brought in contact with the surface, and the charged pigment neutralizes the electrostatic image, thereby creating a

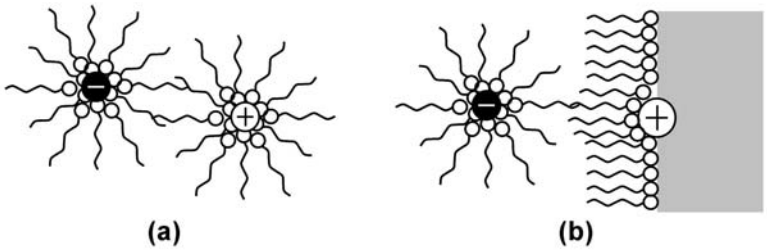

Figure 6:
The Bjerrum length in a nonpolar liquid is bigger than in a polar liquid. Ions can only remain separated over a large enough distance when a surfactant is added. Ions encapsulated by surfactant molecules result in charged inverse micelles (a). On a surface, charges can exist because they are separated from counterions by an adsorbed surfactant layer (b). The counterion is stabilized in an inverse micelle.

real image. Electrostatic lithography [20] is based on the same principle. In ink jet printing [21], a stream of ink with a carefully controlled conductivity is broken into small droplets by an electric field. The droplets can then be guided to the paper with a very high accuracy.

With electrophoretic deposition [22], very homogeneous layers of different materials can be coated onto a conducting surface. Electrodeposition is usually done from polar solutions, but nonpolar liquids are used for instance to produce ceramic coatings. The conductive surface is immersed in a liquid containing charged particles of the coating material. Using the surface as an electrode and another counterelectrode to apply a voltage over the liquid, the particles are attracted towards the

surface and attach to it. Baking attaches the coating permanently to the surface.

Colloidal crystals are used to model atomic systems [23]. The interactions between colloidal particles in a nonpolar liquid are controlled by varying the amount of charges in the liquid and by an electric field. The effect of the electric field on the properties of the suspension (the electrorheological effect) is also used in electrically triggered pumps, brakes and robotic joints [24][25]. In these applications, the electric field causes the viscosity of the liquid to increase significantly.

Electrophoretic displays are based on the movement of charged pigment particles in a nonpolar liquid under the influence of an electric field. The purpose of my research is to increase the understanding of this technology, so that a model describing its behavior can be developed. Therefore, I describe this application in more detail in the following section.

1.3. Electrophoretic displays

The main motivation for investigating charges in mixtures of nonpolar liquid and surfactant is the relevance in electrophoretic displays. In the search for paper-like displays, which combine the good viewing characteristics of printed paper with the ability to change the displayed information, electrophoretic displays are a promising technology.

1.3.1. Electronic paper

Despite the progress of electronic displays in the last decades, printed paper is still a popular medium to show information. This has different reasons, but an important one is the fact that printed paper has superior viewing characteristics when compared to electronic displays. In addition, paper is lightweight, flexible, cheap and doesn't need an energy source to maintain an image. Of course, in contrast to electronic displays, the information is static.

Electronic paper [26][27][28][29] is the common denominator for technologies that aim to combine the advantages of printed paper with the ability to change the information content. Being a concept, it is not clearly defined what properties a technology should have to be qualified as electronic paper [30], but it should possess at least some of the following characteristics. The viewing characteristics should be similar to those of printed paper, being high contrast, high resolution and wide viewing angle. It should be reflective rather than transmittive and energy should only be needed to change the information, not to maintain it. A lot

of attention also goes to the possibility to make flexible displays [31][32]. Finally, for a commercial breakthrough the ability to display color and the switching speed are important parameters.

For the implementation of electronic paper many technologies are being investigated. Historically the first one was 'Gyricon', based on the rotation of particles with different colors on both sides [33][34]. Technologies with liquid crystals [35][36][37][38] have the advantage to be based on a mature display technology. Electrochromic displays use a change in color as a result of an electrochemical reaction to form an image [39][40][41][42]. A recent technology, electrowetting, allows video-rate switching [43][44]. The most promising technology however, which starts to be commercially available, is the electrophoretic display.

1.3.2. Electrophoretic displays

Electrophoretic displays [45][46] are based on the movement of charged pigment particles under the influence of an electric field. The most straightforward implementation is illustrated in figure 7. Positively charged white particles (i.e. titanium oxide [47][48][49]) and negatively charged black particles (i.e. carbon black [50]) are suspended in a clear nonpolar liquid and placed between two electrodes, of which at least one has to be transparent. When a voltage is applied over the electrodes, the pigment particles move and gather near the electrodes. Depending on the polarity of the voltage, the positively charged black particles or the negatively charged white particles are present near the transparent electrode. When this pixel is viewed from the side of the transparent

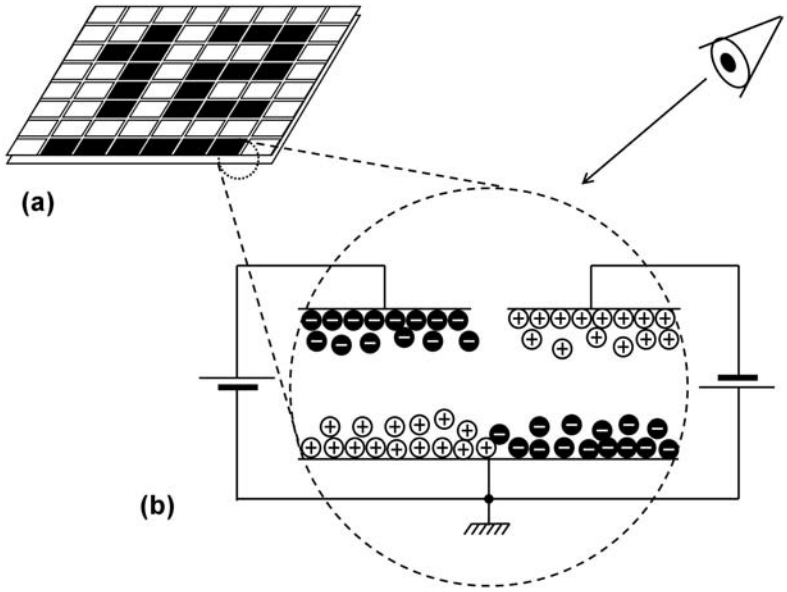

Figure 7:

An image in the most straightforward implementation of an electrophoretic display is formed by a pattern of pixels which can be black or white (a). The color of a pixel is controlled by the polarity of the voltage over two electrodes (b). Between the electrodes is electrophoretic ink, a transparent liquid containing positively charged white pigment particles and negatively charged black pigment particles. When a voltage is applied, the particles will move towards the electrode with the opposite polarity. An observer looking at the structure through a transparent electrode sees (for each pixel) the color of the pigment particles concentrated near that electrode.

electrode, one either sees it black or white. A display is constructed by combining many of these pixels.

In practice, the suspension is enclosed in smaller structures such as microcapsules or microcups [51][52][53][54], which prevent the lateral motion of pigment particles. This lateral motion is the result of a flow in the liquid, and causes the pixels to color inhomogeneously. The use of microcapsules allows thin films of 'electrophoretic ink' to be easily applied on almost any surface.

In recent years, applications using electrophoretic display technology started to become commercially available (figure 8). However, for a real commercial breakthrough, improvement is still necessary. The shortest switching time for electrophoretic displays today is of the order of a few tenths of a second, which is much too slow for video-rate applications. But most important is probably the difficulty to make a color display with electrophoretic technology. The basic reason for this is that differently colored pigments are distinguished by their electric polarity, which can only have two values, positive or negative. To make a color display based on subtractive colors, three colors on a white background have to be controlled independently, which is beyond using only the polarity of the applied voltage. To tackle these problems, a better understanding of the physical and chemical mechanisms underlying the working of electrophoretic displays is necessary.

Figure 8:
Examples of applications using electrophoretic display technology. (a) A test project from a newspaper with e-book readers based on electrophoretic ink proved a success. (b) Shelf labels and (c) indicators on memory sticks only need to change their information occasionally. No power is needed to maintain the image. The same principle results in longer battery time in mobile telephones (d).

1.3.3. Stabilization of charged pigment

The liquid in which the pigment particles are suspended should have good insulating properties, which is why a nonpolar liquid is used. A polar liquid would act approximately as a conductor, in which no electric field can exist. However, the pigment particles need to have a stable electric charge, which is unlikely in a nonpolar liquid. In addition, small pigment particles tend to coagulate, forming bigger agglomerates than intended (figure 9(a)). Both these problems are solved by adding surfactant to the nonpolar liquid.

The surfactant molecules adsorb at the surface of the pigment particles.

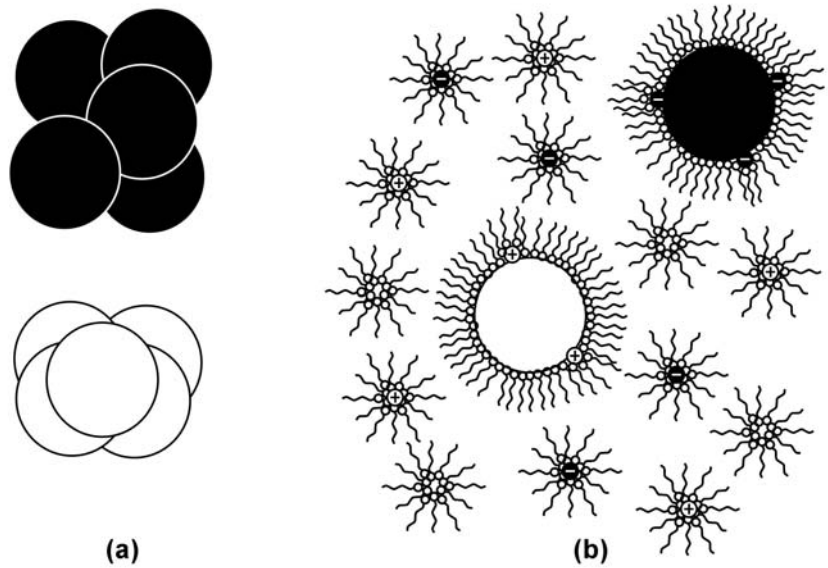

Figure 9:

(a) When no surfactant is added, pigment particles in a nonpolar liquid are not charged and form bigger aggregates. (b) When a surfactant is added, the pigment particles are encapsulated by surfactant molecules, and are sterically stabilized. In addition, depending on the nature of the surface, the pigment can become positively or negatively charged. The suspension can then be used for electrophoretic displays. However, the surfactant molecules also self-aggregate, forming inverse micelles. These micelles can also stabilize charges, resulting in the liquid behaving as an electrolyte. This can have negative effects on the performance when the suspension is used in an electrophoretic display.

Because of this layer of surfactant, the pigment particles can not come close enough together to coagulate (figure 9(b)). This mechanism is called steric stabilisation [55][56][57]. The surfactant layer also allows charges to exist on the surface of the particles [58][59], by separating them physically from their counterions (figure 9(b)). The charge can be the result of the dissociation of acid or basic sites on the surface of the particle. Depending on the nature of these sites, the particle will become positively or negatively charged. There is a lot of discussion about the mechanisms responsible for the charging of colloidal particles in a nonpolar liquid [60][61][62][63][64], and a lot more research is needed.

Charges are stabilized not only at the surface of colloidal pigment particles, but also in inverse micelles (figure 9(b)). Because of this, the liquid behaves as an electrolyte, even although it is nonpolar. The number of charged inverse micelles is usually bigger than the number of charges on the particles. Therefore, they will have a significant influence on the behavior of the electrophoretic display. In chapter 4 I explain how the movement of charged inverse micelles can screen the electric field, which slows down the movement of the pigment particles and thus increases the switching time of the electrophoretic display. Understanding the behavior of (charged) inverse micelles in nonpolar liquid is essential to be able to model and simulate the behavior of electrophoretic displays.

1.4. Overview of this work

During my PhD research, I performed current measurements to investigate charged inverse micelles in mixtures of nonpolar liquid and surfactant. The following paragraphs give a quick overview of the different aspects of this research and summarize the results I obtained.

1.4.1. Electric current measurements

I investigated mixtures of the nonpolar liquid n-dodecane and the surfactant OLOA 1200, which are used in electrophoretic displays. A thin layer of the mixtures is sandwiched between two planar electrodes. Since the electrodes are much larger than the thickness of the device, the geometry can be considered one-dimensional. Short-circuiting the electrodes for a long time ensures a homogeneous distribution of inverse micelles throughout the device. After short-circuiting, a voltage step is applied over the electrodes and the resulting electric current is measured. To derive useful information from these measurements, I developed a sensitive measurement setup. The combination of the one-dimensional geometry and the simple initial condition allows a straightforward interpretation of the results. Values for the mobility and the average concentration of charged inverse micelles can be obtained from these measurements.

1.4.2. Micellization and surface adsorption

From measurements of the mobility, I was able to derive several

properties of the inverse micelles. I found values for the effective radius and for the number of surfactant molecules in an inverse micelle. Measurements of the inverse micelle concentration indicate a dependence on the surfactant concentration and on the thickness of the device. I explain this by concentration dependent micellization and surface adsorption of surfactant molecules. In geometries with microscopic dimensions, these processes are both important. I propose a model which allows to predict the concentrations of neutral and charged inverse micelles for a given thickness and surfactant concentration and agrees well with the experiments. I also derive values for the surfactant concentration below which no micelles are formed (the critical micelle concentration) and for the surface concentration of adsorbed surfactant molecules on the electrodes.

1.4.3. Drift and diffusion of inverse micelles

The electric current measured on a short timescale is a result of the movement of charged inverse micelles present in the device at the moment when the voltage step is applied. The movement of these charges can be described with the Poisson-Nernst-Planck equations, which describe drift in the electric field, diffusion, and the influence of charges on the electric field. Despite the importance of these equations, no general solution is known. I investigate four special cases, in which simplifying assumptions can be made. For these cases, I derive analytical expressions which are useful to understand the dynamics of charge transport in nonpolar liquids with surfactant. The theoretical results agree with numerical simulations and current measurements. This confirms that

drift and diffusion are the two dominant transport mechanisms for inverse micelles in a nonpolar liquid.

1.4.4. Inverse micelle reactions

After an equilibrium between drift and diffusion is reached for a certain applied voltage, the charges do not move anymore and the electric current should be zero. The measurements however show that a small current keeps flowing for a very long time. This is a result of the movement of newly generated charged inverse micelles. I measured this 'quasi' steady state current in devices with different properties and for different voltages. An analysis of how the current depends on various parameters allows me to propose a model for the generation and recombination of charged inverse micelles. These reactions happen in the bulk between two micelles and also at the surfaces between a micelle and the adsorbed surfactant layer. The mechanism of the reaction is different for the two cases, but both are necessary to explain the measurements. Together with drift and diffusion, these mechanisms can be combined in a model which describes both the transient and the (quasi) steady state of all the measurements I performed.

1.5. Conclusions

Surfactants molecules in nonpolar liquids adsorb at interfaces and self-aggregate into inverse micelles. The layers of surfactant which are formed in this way provide a barrier which keeps opposite charges separated, stabilizing them on the surface of colloidal particles or in the interior of inverse micelles. Surfactants are used as charging agents in many applications, one of which is electrophoretic display technology. In electrophoretic displays, the movement of charged pigment particles in a nonpolar liquid under the influence of an electric field causes the pixels to change color. Charged inverse micelles can influence the behavior of these displays.

During my PhD research, I investigated inverse micelles in a nonpolar liquid by performing current measurements. This allowed me to obtain information about the structure of inverse micelles, the properties of the micellar solution, the transport mechanisms involved in the movement of inverse micelles and the reactions responsible for their generation.

These results contribute to the understanding of surfactants and charges in nonpolar liquids. This understanding is necessary to construct a model describing the behavior of electrophoretic displays. Such a model would be helpful in the design of new implementations of electrophoretic displays which overcome the shortcomings that still exist today.

Chapter 2
Electric current measurements

In this work, I investigate surfactant in nonpolar liquid by measuring electric currents. I use devices with planar electrodes containing a mixture of dodecane and OLOA 1200, over which a voltage step is applied after short-circuiting the device for a long time. The resulting electric current decreases quickly over several orders of magnitude, and continues for a long time. To monitor this behavior accurately, an elaborate measurement setup is required. I combined different pieces of equipment to obtain useful measurements. Because of the one-dimensional structure and the simple initial condition, a general interpretation of the current curve and the estimation of some basic properties is possible.

2.1. Introduction

Due to the low dielectric constant resulting in strong electrostatic interactions, free charges are unlikely to exist in nonpolar liquids [12]. Surfactants can be used as charging agents to stabilize free charges in a nonpolar liquid by encapsulating them in inverse micelles [11]. Understanding the origin, the properties and the behavior of these charges is important in practical applications such as electrophoretic ink [46]. Measurements of electric currents in devices with a nonpolar liquid and a surfactant can reveal information about charges in the mixture [65].

Because the concentration of charges in nonpolar liquids is low, the resulting currents are small, ranging from picoamperes to microamperes per cm^2 [66]. Moreover, the current contains different information at different timescales, ranging from milliseconds to hours [18]. Therefore, currents need to be measured fast and accurately over a wide range and during a long time. For my research, I developed a setup which fulfills these requirements. In this chapter, I describe how I measure and interpret electric currents in devices containing nonpolar liquid and surfactant.

The structure of the devices and the liquid and surfactant that I used are described in section 2 of this chapter. In section 3 I show how I combined different pieces of equipment to develop the setup with which I measured the electrical currents in these devices. These measurements provide indirect information about the charges in the mixture. The general methods that I used to interpret these currents are explained in

section 4.

The measurement setup and basic interpretation that I describe in this chapter are essential for the rest of this work. They are used to obtain information about mixtures of nonpolar liquid and surfactant. Analyzing this information provides insight in the physical mechanisms underlying the structure, the transport and the interactions of charged inverse micelles in these mixtures.

2.2. Devices with nonpolar liquid and surfactant

Different nonpolar liquids and different surfactants are used in the research community. AOT is the most widely studied surfactant [67][68][69], because it is soluble in water (polar) and alkanes (nonpolar) and forms micelles (or inverse micelles) in both [70][71]. During my PhD research I studied OLOA 1200 in dodecane, because it has been used a lot in electrophoretic displays [72][73][74]. I investigated this mixture by placing it in a device with planar electrodes at a distance much smaller than the square root of the area, which results in a one-dimensional configuration.

2.2.1. Dodecane and OLOA 1200

In this work I use dodecane as nonpolar liquid. Dodecane is an alkane with twelve carbon atoms: $C_{12}H_{26}$. It exists in 355 different isomeric forms. I used n-dodecane (Aldrich, purity: 99.9%) [75], the isomer in which all carbon atoms are ordered in one single chain (figure 10). The most important physical properties of dodecane that will be used in this work are its relative dielectric constant ε:

$$\varepsilon = 2\,, \tag{4}$$

its resistivity σ (unit: Ω·m):

$$\sigma = 10^{13}\ \Omega \cdot \mathrm{m}\,, \tag{5}$$

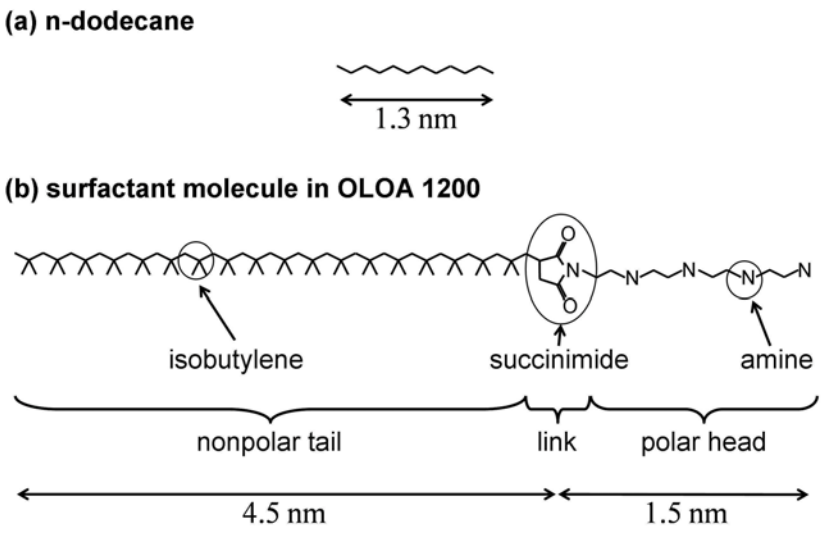

Figure 10:

The chemical structure of (a) an n-dodecane molecule and (b) a surfactant molecule in OLOA 1200. (a) The nonpolar liquid that I use in this work is n-dodecane, an alkane whose molecules are built up of 12 carbon atoms in a single chain. (b) As surfactant I use OLOA 1200, a mixture of mineral oil and molecules as shown in the figure. The nonpolar tail is a chain of isobutylene groups, a branched hydrocarbon which dissolves well in dodecane. The polar character of the head is a result of the amine groups, which contain a lone electron pair. The nonpolar tail and the polar head are linked by a succinimide group. The indicative lengths in the figure are calculated based on typical bond lengths and bond angles.

its mass density ρ_m (unit: kg·m^{-3}):

$$\rho_m = 750\ \mathrm{kg \cdot m^{-3}}, \tag{6}$$

and its (absolute) viscosity η (unit: Pa·s):

$$\eta = 1.4 \times 10^{-3}\ \mathrm{Pa \cdot s}. \tag{7}$$

The combination of these properties make dodecane appropriate for use in electrophoretic displays [76][77].

As surfactant I used OLOA 1200 (Chevron), which was originally intended as a lubricating oil additive [78][79]. Its easy adsorption on surfaces and its good charge stabilizing properties make it popular in nonpolar colloidal solutions in general [55][80][81] and electrophoretic ink in particular [72][73][74]. It is also increasingly used for research purposes [12][82]. However, Chevron does not disclose the exact chemical formulation of OLOA 1200. The company describes it as a mixture of 50 wt% mineral oil and 50 wt% polyisobutylene succinimide with a molecular mass of around 1700. In the literature one can find that chain(s) containing amine groups are attached on the succinimide [12][82], although it is not clear if there is only one chain or two chains. Different authors use different lengths for the polyisobutylene tail [83][84], the most common value being 18 isobutylene groups [82][85]. Figure 10 shows a representative formula for the molecule, but probably OLOA 1200 contains a mixture of molecules with different numbers of chains and different chain lengths. For a qualitative description however, these differences are not important. The polyisobutylene chain is the nonpolar tail of the surfactant molecule, dissolving well in hydrocarbons. The amine groups are basic sites,

responsible for the polar character of the head and the ability to adsorb on surfaces [86]. The succinimide acts as the link between the nonpolar tail and the polar head group(s). Although it does not correspond to the molecular formula in figure 10, I will use the molecular mass provided by the manufacturer (which is more consistent with two polar chains), which results in a mass of one molecule m_{mol} (unit: kg):

$$m_{mol} = 2.8\times10^{-24}\ \mathrm{kg}\ . \tag{8}$$

Using typical bond lengths and bond angles, the length of one surfactant molecule (assuming 18 isobutylene groups) is estimated to be about 6 nm, of which the nonpolar tail is 4.5 nm and the polar head is 1.5 nm.

For my PhD research I made several mixtures of dodecane and OLOA 1200 in different proportions, ranging from 0.001 wt% to 10 wt% OLOA. Considering that only half of the OLOA consists of surfactant molecules, the weight fraction c (no unit) of surfactant is then:

$$c = \frac{1}{2}\left(\frac{\mathrm{wt\%\ OLOA}}{100\ \mathrm{wt\%}}\right). \tag{9}$$

I assume that the viscosity, the mass density and the relative dielectric constant of the mixtures are the same as those of pure dodecane. The resistivity however will change considerably, because of the stabilization of free charges in inverse micelles formed by the surfactant molecules [12].

2.2.2. Device structure

I measured mixtures of dodecane and OLOA 1200 in devices with planar electrodes (figure 11). These devices consist of two glass plates with a surface area of one square inch and a thickness of 1.1 mm. The glass is coated on one side with a 20 nm thick indium tin oxide (ITO) layer. ITO [87][88] is used as a transparent conductor, and has a sheet resistance of about 100 Ω per square. I used ITO for the electrodes because it is common in display technology [89][90]. The coated glass plates are purchased from Delta Technologies. By photolithography, a square pattern is defined in the ITO, resulting in an electrode area S_{el} (unit: m^2) of 1 cm^2 (Figure 11(a)). In some devices, I spincoated a thin polyimide layer (around 50 nm) on the electrodes. In other devices, the electrodes remain uncoated.

The glass plates are attached to each other (with the electrodes facing the inside) using a UV-curing glue in which spacer beads have been mixed. The glue is applied as a pattern around the electrodes and encloses a surface area S_{tot} (unit: m^2), which varies from device to device between 2 cm^2 and 4 cm^2. The spacer beads keep the glass plates at a distance d (unit: m) of each other. Before filling the devices, I always measured their capacitance C_{empty} (unit: F). This allowed me to accurately estimate the device thickness using

$$d = \frac{\varepsilon_0 S_{el}}{C_{empty}}, \tag{10}$$

which is important because the manufacturers of spacer beads specify the size with relatively large tolerance.

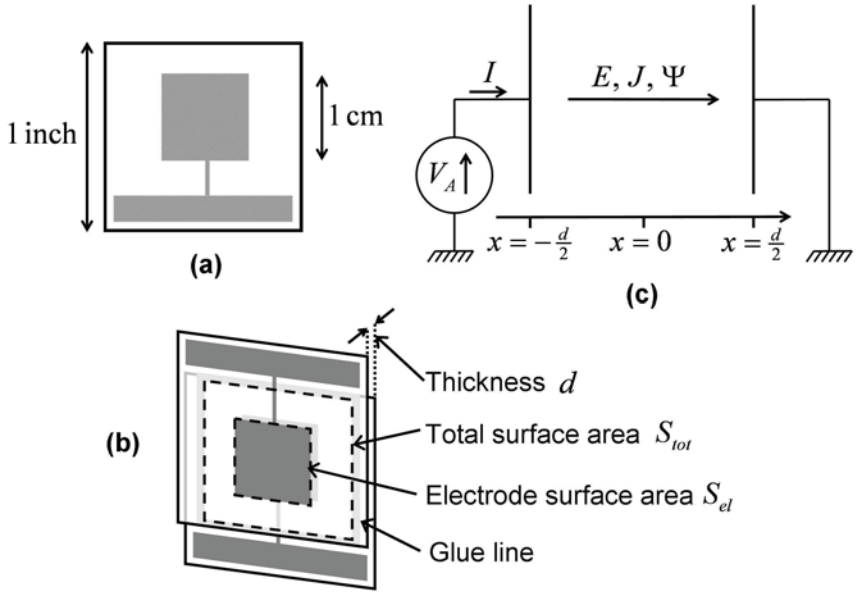

Figure 11:

The devices that I used for the current measurements consist of two glass plates of one square inch with a 1 cm² ITO electrode connected with a contact area (a). The two glass plates are assembled so that the electrodes overlap and the contact areas are not covered (b). They are glued together using a UV-curing glue in which spacer beads have been mixed. The size of the electrodes is much bigger than the distance between them, so the structure can be considered to be one-dimensional (c). The conventions that I use in this work for the directions in which the applied voltage V_A, the external current I, the electric field E, the current density J and the particle fluxes Ψ are measured are indicated in the figure.

Through an opening left in the glue pattern, the device is filled with a mixture of dodecane and OLOA 1200, using capillary force. Two more openings allow the air to escape from the device. After filling, the openings are sealed with two-component glue.

The surface area of the electrodes is much bigger than the distance between them, so the device can be considered as a one-dimensional structure, in which all quantities depend only on one spatial coordinate x (unit: m). In this work, I always take the reference position $x = 0$ in the middle of the device (Figure 11(c)), so the left electrode is at position $x = -d/2$ and the right electrode at position $x = d/2$. Voltages are measured at the electrode at $x = -d/2$, with the other electrode grounded. Electric fields, current densities and particle fluxes are all measured in the positive x-direction. The external current is defined as the electrical current flowing from the external circuit towards the electrode at $x = -d/2$.

2.3. Current measurement setup

Currents in devices with a nonpolar liquid and a surfactant need to be measured fast and accurately over a wide range and during a long time. This requires an elaborate measurement setup, which combines different pieces of equipment with a computer to coordinate and synchronize them. In this section I describe the setup that I developed and used to do the current measurements during my PhD research.

More specifically, I measured currents as a response to a step in the voltage applied over the device electrodes. This situation results in some general characteristics of the current which can be used in the design of the setup. The electric current on application of a voltage step will typically be larger and change faster at short times than on longer time scales [66]. This means that a tradeoff between speed and accuracy can be made. Some equipment, such as an oscilloscope, can measure fast but with limited accuracy. Other equipment, such as an electrometer, can measure accurately, but at a slow rate [91]. Therefore, measuring the current simultaneously with different pieces of equipment offers the possibility to choose the best result at every timescale.

2.3.1. Measurement setup

Figure 12 shows a schematic representation of the setup I developed. The current to be measured is supplied to an amplifying stage which converts the current into a voltage between -200 V and 200 V proportional to the current. This stage is part of a Keithley 6517A electrometer [91]. The initial

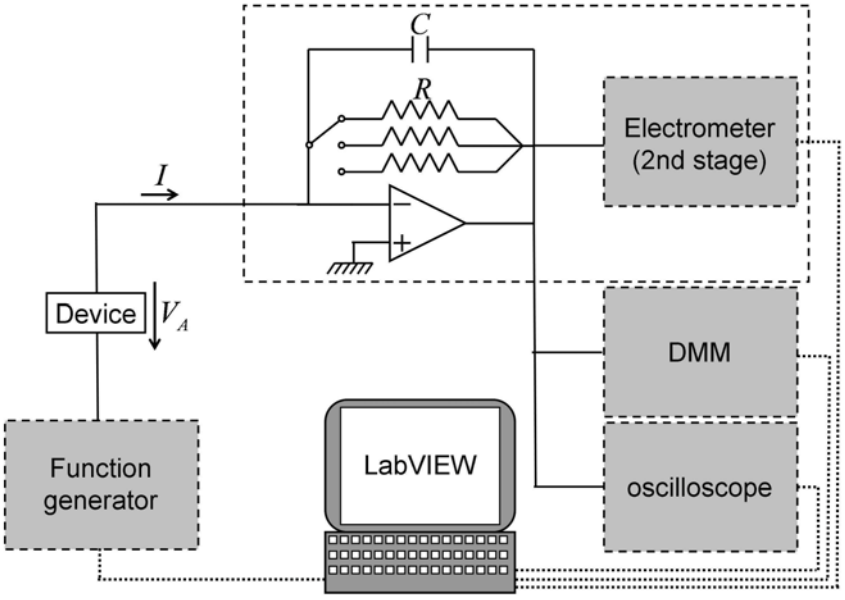

Figure 12:

Schematic overview of the electrical current measurement setup used for this work. A voltage step, generated by a function generator, is applied over the electrodes of the device and the resulting electrical current is converted to a voltage in the first amplifying stage of an electrometer. This voltage is then simultaneously measured by several oscilloscope channels, a digital multimeter and the second stage of the electrometer, which all have different ranges and resolutions, both in time as for the voltage. The different measurements are combined by a computer into one curve. The computer also controls and synchronizes all the equipment. Control lines and trigger lines are not shown on this figure.

amplification factor has to be set manually before the measurement to one of the values 1 V/mA, 1 V/μA or 1 V/nA. The resulting voltage is then measured by different instruments. For the shortest timescale (0 to 100 ms) the voltage is measured with a time resolution of 50 μs by four oscilloscope channels which are configured for different ranges. The first channel, for which I use a ×10 probe, can measure between -200 V and 200 V, with a resolution of roughly 0.5 V. The range of the second channel is ± 20 V, with a resolution of 50 mV. The third and fourth channels have ranges of ± 2 V and ± 0.2 V, with resolutions of 5 mV and 0.5 mV. For an intermediate timescale (10 ms to 1.5 s) the voltage is measured with a time resolution of 1 ms using a Keithley 2000 digital multimeter, which can measure up to 200 V with a resolution of 0.1 mV. On a long timescale (more than 1 s), the voltage is measured with a time-resolution of 0.1 s using the second stage in the electrometer, which can measure up to 200 V with a resolution of 5 μV. Additionally, after 10 s I change the time resolution to 1 s, which provides enough time between two measurement points so that the range of the first stage of the electrometer can be changed automatically. This way, the full accuracy of the electrometer (down to 0.1 pA and up to 20 mA) becomes available. Figure 13 shows a schematic overview of the current ranges that can be measured accurately at different times.

A computer with a LabView program is used to control and synchronize the measurement instruments and the waveform generator used to apply a voltage over the cell. The results from the different equipment are combined by the program to obtain one curve for the current over all timescales.

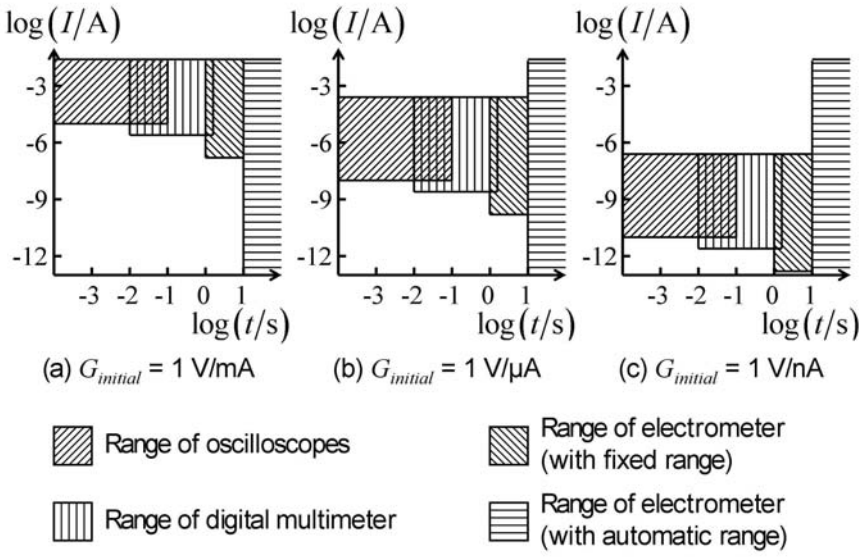

Figure 13:

The electrical current which flows to devices containing mixtures of nonpolar liquid and surfactant has to be measured fast and accurately, over a wide range and during a long time. Different pieces of equipment are suited for measurements in different regions of the time-current plane. This figure indicates, for each piece of equipment, the range for which it is useful. The measurement setup is configured differently for initial currents in the range of milliamperes (a), microamperes (b) or nanoamperes (c). The overlapping regions are used to compensate differences in the current offset. They allow the reconstruction of one current curve from the different measurements.

2.3.2. Bandwidth limitation

To limit the noise generated in different parts of the setup, the bandwidth is reduced by placing a capacitor in series with the resistor of the first amplifying stage [91]. This filters out contributions on a timescale smaller than the RC time constant. However, it also limits the smallest time at which an accurate measurement is possible. This effect is more important for higher amplifications, because in that case a higher resistance is required. In most of my measurements, the results become reliable around 1 ms after the application of the step in the voltage. This is sufficiently small for the purposes of this work.

2.3.3. Experimental validation of the accuracy

As described in the previous paragraph, the accuracy at short timescales is limited by the bandwidth of the measurement setup. The value for the accuracy depends on several parameters, such as the initial amplification factor, the applied voltage and the capacity of the device. At long timescales, the accuracy is limited because of random noise and a possible offset current. At these timescales, there is enough time between measurements for the measurement setup to adapt its range automatically. I tested the setup on a discrete capacitor (10 pF and low leakage), on an empty device,and in open circuit. In all these cases, and for voltages up to 5 V, the measured currents remain well below 0.1 pA, which I consider to be the limit for reliable measurements. I also measured a device filled with dodecane, but without surfactant. Also in this case, the current remains below the measurement sensitivity.

2.4. Interpretation of current measurements

A typical current measurement with the setup described in the previous section is shown in figure 14. This current is a result of the movement of charges inside the device. From the current at different timescales, it is possible to obtain information about different mechanisms responsible for the behavior of the charges. In all the measurements reported in this work, the electrodes of the devices have been short-circuited for several minutes before a voltage step was applied. In the absence of an electric field, diffusion of charges results in a homogeneous distribution of charges throughout the device. This is a simple initial condition, which allows a relatively easy interpretation of the current.

2.4.1. Ramo's theorem

The physics that relate the current supplied to the electrodes with the movement of charges in the device are expressed by Ramo's theorem [92][93][94][95]. This theorem states that the charge on the electrodes is the sum of a capacitive contribution (due to the voltage difference between the electrodes) and a contribution from the charge density with opposite sign and weighed by the potential at the corresponding location. For the one-dimensional situation relevant in this work, Ramo's theorem (for the charge per unit surface on the left electrode Q_{el} (unit: C·m^{-2}) and assuming global electroneutrality) can be written as:

$$Q_{el} = \frac{\varepsilon\varepsilon_0}{d} V_A + \frac{1}{d} \int_{-d/2}^{d/2} \rho x dx , \qquad (11)$$

in which V_A (unit: V) is the applied voltage and ρ (unit: C·m^{-3}) is the

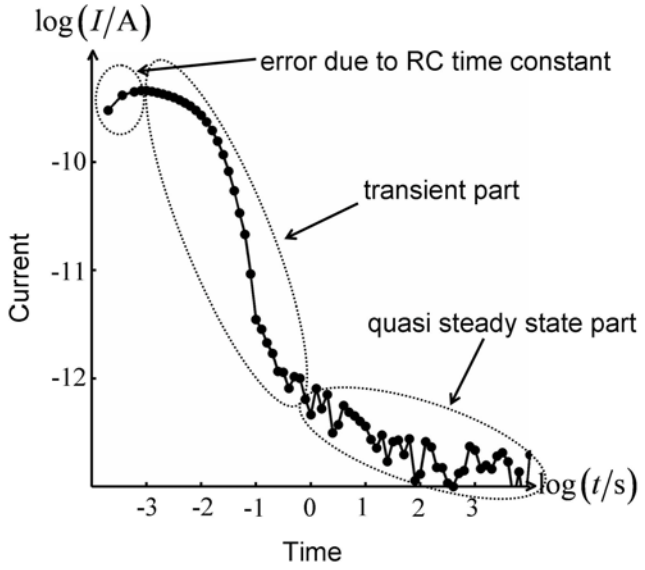

Figure 14:

A typical electrical current, measured on application of a voltage step over the electrodes of a device with nonpolar liquid and surfactant. Different parts of the curve are a result of different mechanisms involved in the behavior of charges. For times smaller than a millisecond, the measurement is inaccurate as a result of the RC-time constant of the measurement setup. The current on a small timescale is largely the result of the movement of charges which are initially present in the device. It decreases as the charges assume a new equilibrium position. On a larger timescale, the current is a result of the movement of charges generated during the measurement. It decreases much slower, and can go on for several hours.

charge density in the device.

Taking the derivative with respect to time t (unit: s) of equation (11), and multiplying with the electrode surface area yields an expression for the external current I (unit: A). For a voltage step from 0 to V_A at t=0, this expression is:

$$I = \frac{\varepsilon\varepsilon_0 S_{el}}{d} V_A \delta(t) + \frac{S_{el}}{d} \int_{-d/2}^{d/2} \frac{\partial \rho}{\partial t} x dx \,. \qquad (12)$$

The dirac impulse represents the charging of the capacitor, and will be neglected in the rest of this work.

2.4.2. Current on different timescales

The shape of the electrical current (figure 14) can be roughly divided in two parts. The first part occurs at a relatively short timescale, the second part occurs at a longer timescale. The difference between these two parts lies in the origin of the charges whose movement is responsible for the current. Initially, the charges which are present in the device at the moment that the voltage step is applied, move to reach a new equilibrium distribution between drift and diffusion. This results in a large current at short timescales, which decreases as the distribution approaches equilibrium. I will investigate this decrease in detail in chapter 4. If only charges that are present from the beginning could move, then this current should go to zero. However, in the measurements one sees a small current remaining for a very long time. I call this the 'quasi' steady state current. It is not really in steady state, since it still decreases very slowly. However, on the timescale of the movement of the charges this

current is approximately constant. The current on a longer timescale is a result of the movement of additional charges, generated during the time that the voltage is applied. This generation can be a result of different mechanisms, which I discuss in more detail in chapter 5.

2.4.3. Estimation of average concentration and mobility

Even without fully understanding the shape of the electrical current, it is possible to derive some important quantitative values from it [96][97][98]. The first of these values is the initial average concentration of positive or negative charges. I always assume global electroneutrality and an opposite valency $\pm Z$ (unit: 1) for positive and negative charges, which means that these concentrations have the same value $\overline{n}$ (unit: m^{-3}) for both polarities. This quantity can be derived from the integral of the measured electrical current over time (figure 15), when a large voltage step (more than 1 V) is applied. Initially, positive and negative charges are homogeneously distributed, so the charge density in the liquid is zero. Ramo's theorem (equation (11)) shows that the surface charge density on the electrodes just after applying the voltage is:

$$Q_{el}\left(t=0\right)=\frac{\varepsilon\varepsilon_0}{d}V_A. \tag{13}$$

In the following, the time t=0 refers to the moment at which the voltage has been applied, the capacitive current has been supplied to the cell, but the charges have not yet started their motion under influence of the field. At sufficiently large voltages, the electric field will cause the charges to move until they reach the oppositely charged electrode, where they stop moving. When all the charges have arrived at the electrodes, there is

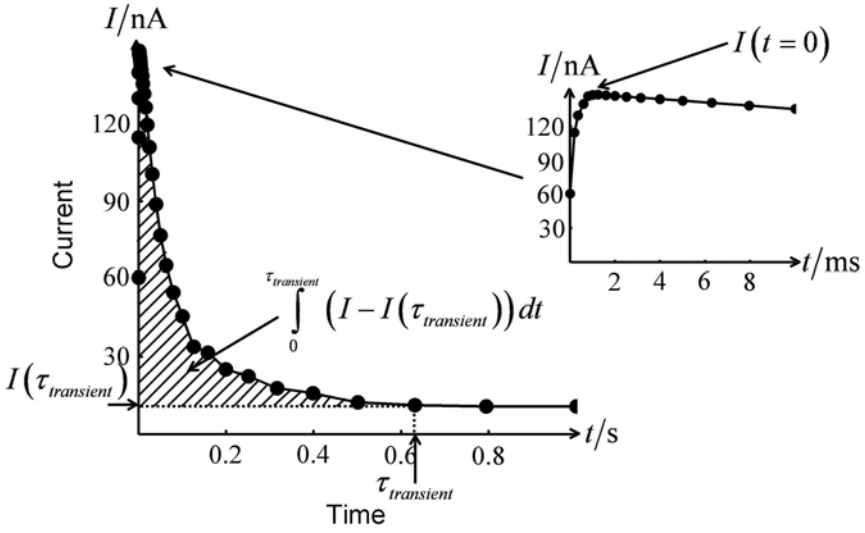

Figure 15:

For voltage steps from zero volts to a large voltage, some properties of the mixture of nonpolar liquid and surfactant can be easily derived from a current measurement, using equations (16) and (18). The estimation of the average concentration of charged inverse micelles is based on the integral of the electrical transient current. One has to take into account the quasi steady state current which is also present in the measurement. The mobility can be estimated based on the initial current. Because of the RC time constant of the measurement setup, the best estimation for the initial current is usually not the first measurement point, but rather the maximum value of the measured current.

an additional charge on the electrodes which is approximately equal to the total charge in the device:

$$Q_{el}\left(t \to \infty\right) - Q_{el}\left(t = 0\right) = Zq_e \overline{n} d \,. \tag{14}$$

The electrical current supplied to the electrodes is the derivative over time of the charge on the electrodes, multiplied by the electrode area, so equation (14) can be written as:

$$\overline{n} = \frac{1}{Zq_e S_{el} d} \int_0^\infty I dt \,. \tag{15}$$

In this equation, the quasi steady state current should not be taken into account. To correct for the fact that the current does not become zero after the transient period, and the fact that during the transient period there is already a contribution of generated charges, I modify equation (15) into the following, more realistic formula:

$$\overline{n} = \frac{1}{Zq_e S_{el} d} \int_0^{t_{ss}} \left(I - I\left(t_{ss}\right)\right) dt \,. \tag{16}$$

In this equation, t_{ss} (unit: s) is the time when the current has reached its quasi steady state value. In chapter 5, I describe a formal way to estimate this time, but in most cases a (subjective) visual estimation is sufficient for equation (16).

The second value that can easily be derived from the electrical current measurement is the mobility of the charges. Initially, all charges are homogeneously distributed. At the moment when the voltage is applied the electric field is therefore homogeneous throughout the device, and all charges move with the same speed. Because of these simple initial conditions, the initial current can easily be calculated (see chapter 4):

$$I\left(t=0\right)=\frac{2Zq_e\bar{n}\mu V_A S_{el}}{d}. \tag{17}$$

In this equation, the mobility μ (unit: $m^2 \cdot V^{-1} \cdot s^{-1}$) is the proportionality constant between the speed of a charge and magnitude of the electric field. Using the average concentration of charges obtained with equation (16), one can find the mobility:

$$\mu=\frac{I\left(t=0\right)d}{2Zq_e\bar{n}V_A S_{el}}. \tag{18}$$

Because of the RC time constant discussed in the previous section, the first measurement point will not represent the initial current accurately. Therefore, it is better to use the maximum value of the current to approximate the initial current.

2.5. Conclusions

Surfactants in nonpolar liquids can stabilize free charges, which would otherwise not exist. These charges can be investigated by measuring the electrical current supplied to a device containing a mixture of nonpolar liquid and surfactant.

During my PhD research, I investigated mixtures of n-dodecane and OLOA 1200. This mixture is suited for use in electrophoretic displays. I put these mixtures in a one-dimensional device with planar ITO electrodes.

Nonpolar liquids, even with surfactant, contain few charges and the electrical currents are small. I developed a setup which can measure electrical currents fast and accurately over a wide range and during a long time. This measurement setup is especially suited to measure currents when a voltage step is applied over the electrodes.

Before each measurement that I report in this work, the electrodes are shortcircuited for a long time. The charges are then homogeneously distributed at the moment of the voltage step. This simple initial condition allows an easy interpretation of some aspects of the electric current measurements.

Chapter 3
Micellization and surface adsorption

Surfactant molecules in a nonpolar liquid adsorb at interfaces and form inverse micelles. In structures with microscopic dimensions these processes can not be considered independent from each other, but have to be combined in one model. I performed electric current measurements on different devices and derived values for the mobility and average concentration of charged inverse micelles. These results allow calculating several properties of the structure of inverse micelles. To explain the dependencies of the concentration of inverse micelles on the surfactant concentration, the thickness of the device and the nature of the surfaces, I propose a model combining inverse micellization and surface adsorption of surfactant molecules.

3.1. Introduction

Because of their amphiphilic nature, surfactant molecules in a nonpolar liquid can adsorb at interfaces between the liquid and any other substance in contact with it [86][99]. These interfaces can be between the liquid and macroscopic surfaces [100][101][102], such as those confining the liquid, or between the liquid and microscopic surfaces, such as those of colloidal particles dissolved in the bulk of the liquid [103][104]. The surfactant molecules also self-aggregate into inverse micelles [2], which can stabilize an electric charge [17]. These are all competing processes [82], but in most applications, because of their macroscopic dimensions, the bulk processes can be considered independently from the adsorption at the confining surfaces.

Nonpolar liquids with surfactant are also used in an increasing number of applications with microscopic dimensions, such as electrophoretic displays [45][46] or in microfluidics [105]. When the ratio between the volume and the surface of the container is small, bulk properties such as the concentration of inverse micelles [18] or the charge on colloidal particles [64] may depend on the geometry and the properties of the confining surfaces. In this situation it is important to have a model which combines micellization and surface adsorption to describe the behavior of surfactant in a nonpolar liquid [99].

I performed accurate transient current measurements on layers with different thicknesses of mixtures with different concentrations of surfactant in a nonpolar liquid. These measurements allow for the

estimation of the mobility and the average concentration of charged inverse micelles. I explain these measurements using a simple model for micelle formation, charging, and surface adsorption.

In section 2 of this chapter, I report measurements on two different series of devices. In one series the electrodes are coated with a thin layer (around 50 nm) of polyimide. In the other series the electrodes are left uncoated. In section 3 I analyze the values for the mobility obtained from these measurements to derive several properties of the structure of the inverse micelles. An analysis of the charge concentration, in section 4, allows me to find the concentrations of both charged and neutral inverse micelles. These concentrations are dependent on the nature of the surfaces and on the thickness of the device, which I explain, in section 5, by surface adsorption.

The model that I propose for micellization and surface adsorption explains all the dependencies observed in the measurements, and allows me to estimate several properties of the micellar solution and of the adsorbed surface layer. The obtained values are necessary to describe the shape of electric transient current curves that is discussed in chapter 4.

3.2. Measurements

3.2.1. Method

The devices used for the measurements consist of two glass plates, coated with a transparent ITO-electrode with surface area S_{el} = 1 cm^2 (figure 11). I made two series of devices. In the first series, the plates are spincoated with a thin (around 50 nm) layer of polyimide at the side of the electrode. In the other series, the plates are left uncoated. Spacer beads keep the two plates separated at a distance d. The glass plates are glued together by a pattern which encloses a surface area S_{tot}, which varies between 2 cm^2 and 4 cm^2 for different devices. The space between the plates is filled with a mixture of high purity (99.9%) n-dodecane (Aldrich) and different weight percentages of OLOA 1200, which contains 50 wt% mineral oil and 50 wt% of the surfactant polyisobutylene succinimide (Chevron).

The devices are initially shortcircuited for a sufficient amount of time to obtain a homogeneous distribution of charges. Then, at time t = 0, a voltage step to V_A = 3 V is applied and the resulting transient current is measured. This voltage is high enough to separate the charges completely, which allows to estimate the average concentration of charged inverse micelles of each polarity $\overline{n}$ from the integral of the measured transient current $I(t)$. From the initial value of the transient current, the mobility μ of the charged inverse micelles can then be estimated (see chapter 2).

3.2.2. Results

Figure 16 shows the concentration $\overline{n}$ (obtained as described in the previous section) as a function of the surfactant weight fraction, for devices with different thicknesses and with a polyimide coating. The concentration of charges is approximately proportional to the surfactant weight fraction. Figure 17 shows the measured concentration $\overline{n}$ as a function of the surfactant weight fraction, for devices with different thicknesses and without polyimide coating. For higher weight fractions of surfactant the concentration of charges is approximately proportional to the surfactant weight fraction. For lower weight fractions of surfactant there is a dependence on the thickness of the device. The mobility is approximately the same for all measurements, with average 8.8×10^{-10} $m^2V^{-1}s^{-1}$. These experimental observations allow for the estimation of a number of properties of the inverse micelles formed by the surfactant molecules.

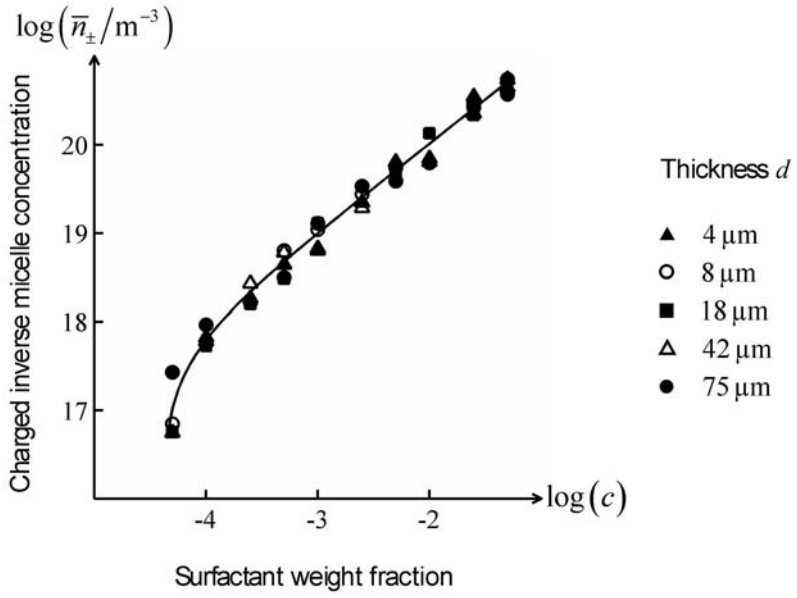

Figure 16:

The measured concentration of charged inverse micelles as a function of the surfactant weight fraction, for devices with different thicknesses and with a polyimide layer spincoated on the electrode side of the glass plates. Except for the lowest surfactant concentration, the inverse micelle concentration is proportional with the surfactant weight fraction. There is no dependence on the thickness of the device. The plotted curve is the best fit corresponding to the described model for inverse micellization. The fact that the charged inverse micelle concentration goes to zero for small surfactant weight fractions is explained by a critical micelle concentration, under which no inverse micelles are formed.

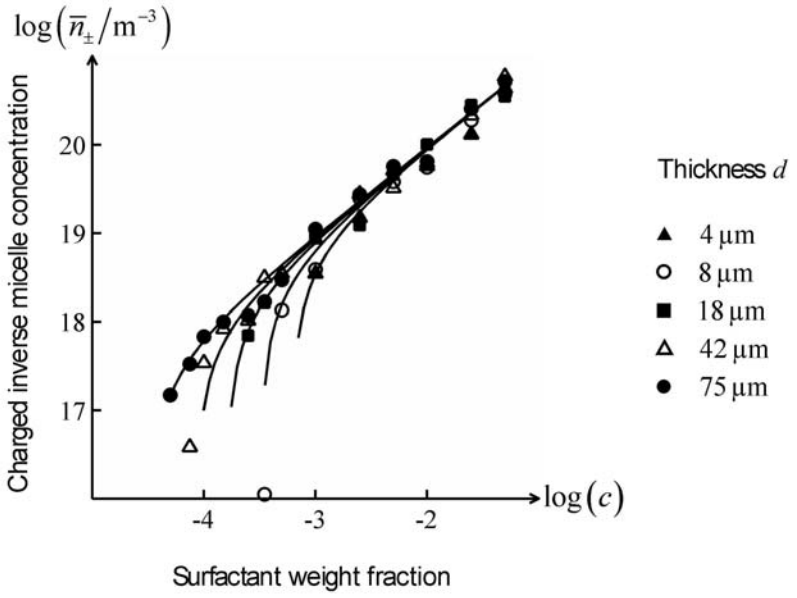

Figure 17:

The measured concentration of charged inverse micelles in function of the surfactant weight fraction, for devices with different thicknesses and with uncoated electrodes. At high surfactant concentrations, the inverse micelle concentration behaves the same way as in the case with a polyimide coating on the electrodes. At lower surfactant concentrations, there is a dependence on the thickness of the device. The plotted curve is the best fit with these measurements based on a model for inverse micellization and surface adsorption of surfactant molecules. The dependence on the thickness is explained by assuming that adsorbed surface layers of surfactant molecules are formed, leaving less molecules to form inverse micelles.

3.3. Structure of inverse micelles

3.3.1. Effective radius

I assume that the shape of all charged and neutral inverse micelles is approximately spherical, and can be described by the same effective radius R (unit: m). With this assumption, the mobility of the charged inverse micelles is related to their valency Z, their effective radius R and to the viscosity of the liquid η, according to Stokes's law:

$$\mu = \frac{Zq_e}{6\pi\eta R}. \tag{19}$$

In chapter 1 it was already indicated that the valency of charged inverse micelles can only be ± 1, and this will be proven in chapter 4. With this fact, and knowing the viscosity of dodecane (η = 1.4×10^{-3} kg·m^{-1}·s^{-1}), equation (19) can be used to estimate the average effective radius of the inverse micelles from the value for the average mobility (μ = 8.8×10^{-10} m^2·V^{-1}·s^{-1}), reported in section 3.2.:

$$R = \frac{Zq_e}{6\pi\eta\mu} = 7.6\,\text{nm}. \tag{20}$$

This value agrees with the length of a surfactant molecule (6 nm), calculated in chapter 1. Other works report a dependency of the inverse micelle size on the water content in the nonpolar liquid [106][107]. I did not investigate this dependency, but since I took no precautions to keep the dodecane in a water-free environment, I assume that the concentration of water molecules is always at the saturation value, and thus the same in all my measurements.

3.3.2. Aggregation number

From equation (20), the average volume of an inverse micelle is calculated as 1840 nm^3. If one assumes that an inverse micelle has approximately the same density as pure dodecane (ρ_m = 750 kg/m^3), its mass m_{mic} (unit: kg) can be estimated as

$$m_{mic} = \frac{4\pi}{3}\rho_m R^3 = 1.38\times10^{-21}\,\mathrm{kg}\,. \tag{21}$$

In chapter 1 I calculated the mass of one surfactant molecule m_{mol} to be 2.8×10^{-24} kg. From this value and equation (21), the aggregation number N (without unit), which is the average number of surfactant molecules per inverse micelle, can be calculated as

$$N = \frac{m_{mic}}{m_{mol}} = 490\,. \tag{22}$$

3.4. Properties of inverse micellar solution

3.4.1. Charging of inverse micelles

If all inverse micelles consist of approximately the same number of surfactant molecules, one expects the total inverse micelle concentration $\overline{n}_{tot}$ (unit: m^{-3}) including both charged and neutral inverse micelles, to increase proportionally with the weight fraction of surfactant molecules c according to:

$$\Delta\overline{n}_{tot} = \frac{\rho_m}{m_{mol}N}\Delta c \tag{23}$$

Figure 16 shows that, in the case of devices with a polyimide coating on the electrodes, the concentration of charged inverse micelles increases proportionally with the surfactant weight fraction and therefore, because of equation (23), proportionally with the total inverse micelle concentration. This indicates that the charged inverse micelles are the result of a disproportionation reaction rather than a dissociation reaction. With a dissociation / association reaction (figure 18(a)), one neutral inverse micelle would split into two oppositely charged micelles and vice versa, resulting in an equilibrium in which the charged inverse micelle concentration is proportional to the square root of the neutral inverse micelle concentration $\overline{n}_0$ (unit: m^{-3}):

$$M_0 \rightleftharpoons M_- + M_+ \quad \Rightarrow \quad \overline{n} \propto \sqrt{\overline{n}_0}\ . \tag{24}$$

With a disproportionation / comproportionation reaction however (figure 18(b)), two neutral inverse micelles exchange a charge so that two oppositely charged inverse micelles are formed, resulting in a

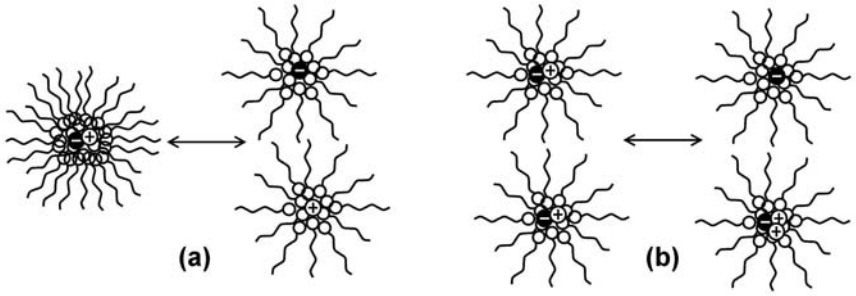

Figure 18:
Schematic representation of (a) a (hypothetical) dissociation / association reaction, in which a (bigger) neutral inverse micelle splits into two oppositely charged inverse micelles (and vice versa), and (b) a disproportionation / comproportionation reaction, in which two neutral inverse micelles exchange a charge, forming two oppositely charged inverse micelles (and vice versa).

proportionality between the neutral and charged inverse micelle concentrations:

$$2M_0 \rightleftharpoons M_- + M_+ \quad \Rightarrow \quad \overline{n} \propto \overline{n}_0 . \tag{25}$$

This justifies the assumption in section 3.3. that all inverse micelles (neutral and charged) contain the same number of surfactant molecules. If the equilibrium constant of the disproportionation / comproportionation reaction is K (without unit):

$$K = \frac{\overline{n}^2}{\overline{n}_0^2} , \tag{26}$$

the relation between the concentration of charged inverse micelles and the total inverse micelle concentration is

$$\overline{n}_{\pm} = \frac{\sqrt{K}}{1+2\sqrt{K}}\overline{n}_{tot}. \tag{27}$$

3.4.2. Concentration of inverse micelles

Figure 16 shows that under a certain surfactant weight fraction the charged inverse micelle concentration is zero. I explain this by assuming that a minimal weight fraction of surfactant molecules c_{cmc} (without unit) is necessary before inverse micelles can be formed. In polar liquids this 'critical micelle concentration' is a well known phenomenon, in nonpolar liquids it is more controversial [108][109]. Using this assumption and equation (23) results in a relation between the surfactant weight fraction and the total inverse micelle concentration:

$$\overline{n}_{tot} = \frac{\rho_m}{m_{mol}N}\left(c - c_{cmc}\right). \tag{28}$$

Combining equations (27) and (28), the charged inverse micelle concentration can be expressed in function of the surfactant weight fraction:

$$\overline{n} = \frac{\sqrt{K}}{1+2\sqrt{K}}\frac{\rho_m}{m_{mol}N}\left(c - c_{cmc}\right). \tag{29}$$

The unknown equilibrium constant K and the critical micelle concentration c_{cmc} can be used to fit equation (29) with the measurements in figure 16 on devices with a polyimide coating on the electrodes. The best fit is plotted on figure 16 and is found for the equilibrium constant

$$K = 3.9\times10^{-4}, \tag{30}$$

and the critical micelle concentration

$$c_{cmc} = 4.1\times10^{-5}. \tag{31}$$

The value for K corresponds to one positively charged and one negatively charged inverse micelle in every 53 inverse micelles. The critical micelle concentration in equation (31) corresponds to an OLOA 1200 weight percentage of 0.0082 wt%. The fact that K is much smaller than one indicates that there is an important reduction in electrostatic energy if two oppositely charged inverse micelles recombine. The important role of the electrostatic energy in such reactions make the generation of doubly charged inverse micelles unlikely.

3.5. Surface adsorption of surfactant molecules

3.5.1. Model for micellization and surface adsorption

Figure 17 indicates that, in the devices with uncoated electrodes, the concentration of charged inverse micelles (and according to equation (27) also the total concentration of inverse micelles) depends on the thickness of the device, which can not be explained by bulk micellization. For each thickness there is a different critical value of the weight fraction of surfactant molecules below which no charge could be measured. Figure 19 shows that this critical value increases inversely proportional with the thickness of the device.

In the devices with uncoated electrodes, I attribute the missing micelles in the bulk at low concentrations to two effects: a minimal weight fraction of surfactant molecules c_{cmc} in the bulk is needed before inverse micelles can be formed and the surfactant preferably covers the surfaces of the structure up to a surface concentration of surfactant molecules ν (unit: m^{-2}). The total mass of surfactant molecules is then distributed over three categories (figure 20): inverse micelles in the bulk, adsorbed at the two surfaces or individual surfactant molecules in the bulk:

$$\begin{aligned} c\rho_m S_{tot} d = {} & \bar{n}_{tot} N m_{mol} S_{tot} d \\ & + 2\nu m_{mol} S \\ & + c_{cmc}\rho_m S_{tot} d \end{aligned} \quad . \qquad (32)$$

In this equation, S (unit: m^2) is the surface area (on one plate) on which molecules become adsorbed. At this point I leave the possibilities open

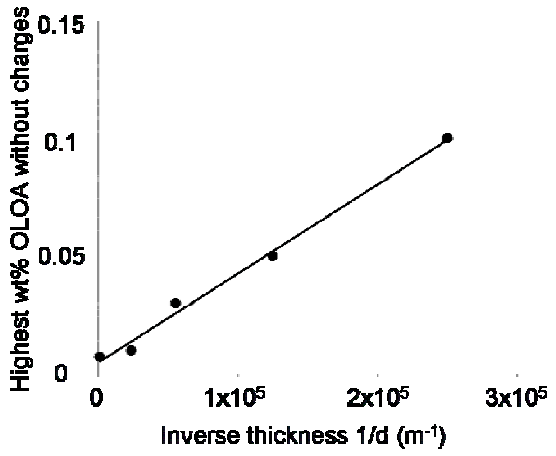

Figure 19:

In devices with uncoated electrodes, no charge could be measured for the lowest concentrations of surfactant. The critical value of the surfactant weight fraction below which no charge was measured is dependent on the thickness of the device. This figure shows the lowest weight fraction of surfactant for which charge could be measured, in function of the inverse of the thickness of the device. The critical value is (except for a constant term) inversely proportional with the thickness.

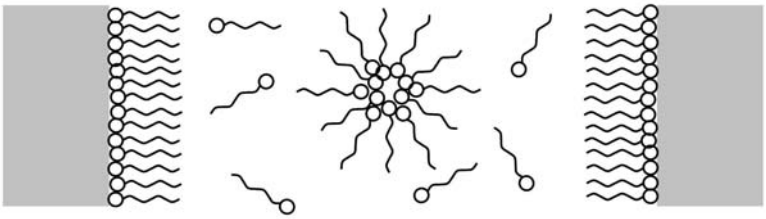

Figure 20:
In a mixture of a nonpolar liquid and surfactant, the surfactant molecules exist in three different forms. A small amount of molecules remains dissolved as monomers in the liquid. Other molecules are adsorbed at interfaces. The remaining molecules self-aggregate and form inverse micelles.

that the molecules are adsorbed only at the electrodes ($S = S_{el}$), only at the glass ($S = S_{tot} - S_{el}$), or at the complete surface ($S = S_{tot}$).

Combining equation (27) with equation (32), the concentration of charged micelles can be found as:

$$\bar{n} = \frac{\sqrt{K}}{1+2\sqrt{K}} \frac{1}{N} \left(\frac{\rho_m}{m_{mol}} (c - c_{cmc}) - 2\nu \frac{S}{S_{tot}} \frac{1}{d} \right). \qquad (33)$$

This expression is qualitatively consistent with the measurements in figures 16 and 19. The quantities S, K, c_{cmc} and ν can be used to find a quantitative fit of equation (33) to the measurements.

3.5.2. Experimental fit

In the measurements I don't see a dependence on S_{tot}, which indicates that the surfactant is adsorbed both at the electrodes and at the glass, so that $S = S_{tot}$, and S_{tot} disappears from equation (33). Fitting the slope of the curves in figure 17 yields

$$K = 3.2 \times 10^{-4}, \tag{34}$$

corresponding, through equation (27), with one positively and one negatively charged inverse micelle in every 58 inverse micelles. This result agrees with the result in the previous section for coated electrodes, which indicates that the charging process is independent of the surfaces. Fitting the slope of the curve in figure 19 yields

$$\nu = 0.46 \text{ nm}^{-2}, \tag{35}$$

or one adsorbed surfactant molecule per 2.2 nm^2. Finally, fitting the intercept value at high thicknesses in figure 19 yields

$$c_{cmc} = 3.5 \times 10^{-5}, \tag{36}$$

corresponding to 0.007 wt% of OLOA 1200. Like the value for K, this value for the critical micelle concentration agrees with the value found in the previous section for devices with a polyimide coating on the electrodes.

The fact that an adsorbed surface layer is formed on uncoated electrodes and not on electrodes coated with a polyimide layer can be understood by considering the polarity of the surfaces. Polyimide is a dielectric

material, with a relative dielectric constant of only 3. The difference with the relative dielectric constant of dodecane (ε=2), and therefore the driving force for surface adsorption is small. The electrode material is indium tin oxide (ITO), which is a relatively good conductor. The free charges in the electrodes will make it much more likely for the surfactant molecules to adsorb on this surface [110].

3.6. Conclusions

Surfactant molecules in a nonpolar liquid adsorb at surfaces and form inverse micelles, some of which become charged. In devices with small dimensions these processes can not be considered independently.

Analysis of transient current measurements allowed me to estimate the mobility and concentration of charged inverse micelles. From these values, I derived characteristics about the structure and concentration of the inverse micelles, the charging mechanism leading to charged inverse micelles and the surface density of surfactant molecules in an adsorbed surface layer.

Chapter 4
Drift and diffusion of inverse micelles

Surfactant molecules in nonpolar liquids self-aggregate into inverse micelles, some of which carry an electrical charge. The Nernst-Planck-Poisson equations model the effects of diffusion and drift in the electric field on the charges, and the change in the electric field induced by the charges. despite their importance, no general solution is known. In this chapter I investigate the dynamical behavior after application of a voltage on a plan-parallel device which has been short-circuited for a long time. I derive approximate analytical expressions for the charge distribution and electric field as a function of time and position, for four extreme cases. The theoretical formulas agree with simulations and measurements.

4.1. Introduction

Surfactant molecules in nonpolar liquids self-aggregate into inverse micelles, some of which carry an electrical charge. The movement of charges in a viscous medium under the influence of an electric field in a plan-parallel device is a very general problem. It lies at the basis of the understanding of electrolytes [111], semiconductors [112], plasmas [113] and many other applications. The Nernst-Planck-Poisson equations [114][115][116] model the effects of diffusion and drift in the electric field on the charges, and the change in the electric field induced by the charges. In most applications other equations have to be added to model mechanisms such as chemical reactions in the bulk [17][18] or at the electrodes [117], or to include sterical effects [118][119], but the basic problem is always the same. However, despite the importance of the Nernst-Planck-Poisson equations, no general solution is known.

The behavior of charges in a planar structure can be totally different, depending on the properties of the device and the driving conditions [120][121]. In the case of thick devices with a high charge content, driven at relatively small voltages, which is the relevant situation in many applications, the Nernst-Planck-Poisson equations can be linearized and solved [120][121]. However, for larger voltages, in thin devices or for lower charge concentrations, non-linear effects [120][121][122] make the solution much more difficult. These situations become increasingly important with the ongoing miniaturization and the growing use of non-polar media, such as in liquid crystal displays [123][124] and electrophoretic ink [45][46]. The nonlinear effects are sometimes treated

as higher order deviations from the linear case [121]. However, I take a different approach and investigate four extreme cases (one of them being the linear case). These regimes provide an understanding of the dominant effects in cases which are not well understood today, and provide a different perspective to investigate the Nernst-Planck-Poisson equations.

In this chapter I investigate the dynamical behavior after application of a voltage on a plan-parallel device which has been short-circuited for a long time. In section 2, I derive approximate analytical expressions for the charge distribution and electric field as a function of time and position, for each of the four regimes. I compare these analytical descriptions with numerical simulations. In section 3 of this chapter I describe under which circumstances each of the four regimes is applicable. In section 4, I compare the theoretical formulas with current measurements for mixtures of nonpolar liquid and surfactant which, depending on the conditions, can exhibit the behavior of each of the four regimes.

The analytical expressions for the current provide a way to determine several properties of the mixture, such as the concentration, mobility and valence of the charges. A similar approach has been followed in another work [125] to derive analytical expressions for the steady state distribution of charges in an electric field, which are confirmed by measurements.

4.2. Theoretical description

The plan-parallel device is approximated with a one-dimensional structure (figure 21), in which all quantities are only dependent on the spatial coordinate x and on the time t. This structure is bound by two electrodes separated by a distance d. The reference position $x=0$ is chosen in the middle of the structure, so the left electrode is at position $x=-d/2$ and the right electrode at position $x=d/2$. Between the two electrodes, the symmetric electrolyte is described by a dielectric medium containing positive and negative charges, which are identical except for their polarity. The dielectric permittivity of the medium is $\varepsilon\varepsilon_0$, with ε_0 the dielectric permittivity of vacuum and ε the relative dielectric constant of the medium. The charges carry a charge $\pm q=\pm Zq_e$ (unit: C) and their distribution in the medium is described by the concentrations $n_+(x,t)$ (unit: m^{-3}) and $n_-(x,t)$ (unit: m^{-3}) for positive and negative charges, respectively. Alternatively, the distribution can be described by the charge concentration $\rho(x,t)$ and the total concentration $m(x,t)$ (unit: m^{-3}), related to n_+ and n_- by

$$\rho = q(n_+ - n_-) \tag{37}$$

and

$$m = n_+ + n_-. \tag{38}$$

For $t<0$, the electrodes are at the same potential, and all charges are homogeneously distributed. At the reference time ($t=0$), a voltage V_A is applied over the electrodes, so that the left electrode is at potential V_A

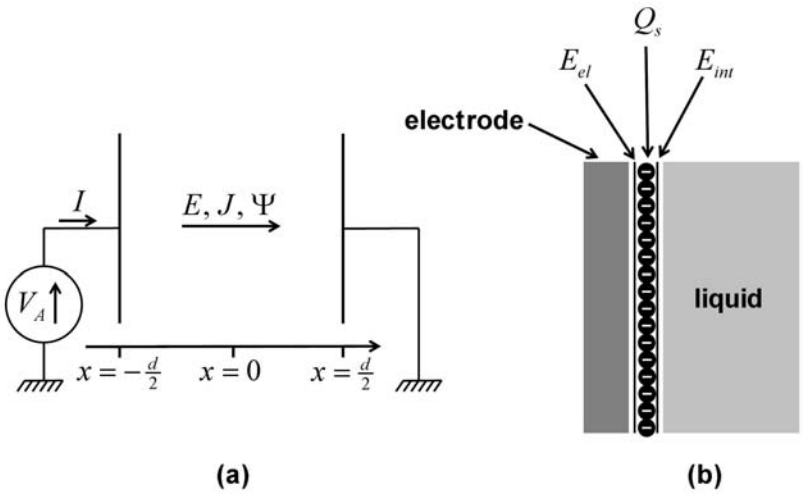

Figure 21:

(a) Schematical representation of the 1-dimensional structure considered in this chapter. The conventions used for the directions in which different quantities are measured are indicated on the figure. In some cases, a surface charge will exist at the electrodes (b). In these cases, E_{el} *is defined as the electric field between the surface charge and the electrode and* E_{int} *is defined as the electric field at the liquid side of the surface charge. The surface charge* Q_s *and the fields* E_{el} *and* E_{int} *are however all at the same position* $x = \pm d/2$.

and the right electrode is at potential 0. The electric field $E(x,t)$ (unit: V·m^{-1}), which is measured in the positive x-direction, is related to this voltage through:

$$\int_{-d/2}^{d/2} E dx = V_A , \tag{39}$$

and to the distribution of charges through Gauss's equation (which is equivalent to Poisson's equation):

$$\varepsilon\varepsilon_0 \frac{\partial E}{\partial x} = \rho . \tag{40}$$

The movement of the charges is the result of drift in the electric field and diffusion. It can be described by the Nernst-Planck equation:

$$\Psi_{\pm} = \pm\mu n_{\pm} E - D\frac{\partial n_{\pm}}{\partial x} . \tag{41}$$

$\Psi_{+}(x,t)$ (unit: m^{-2}s^{-1}) and $\Psi_{-}(x,t)$ (unit: m^{-2}s^{-1}) are the fluxes of positive and negative charges in the positive x-direction. The mobility μ and the diffusion constant D (unit: m^2·s^{-1}) are the same for positive and negative charges and are related by Einstein's formula:

$$\frac{D}{\mu} = V_T . \tag{42}$$

The thermal voltage V_T (unit: V) is defined as kT/q, in which k is Boltzmann's constant and T is the absolute temperature of the device. At this point let us assume that no charges can appear or disappear in the bulk, so the following continuity equation holds:

$$\frac{\partial n_{\pm}}{\partial t} = -\frac{\partial \Psi_{\pm}}{\partial x} . \tag{43}$$

Let us also assume that the electrodes are perfectly blocking, so at the

boundaries of the structure no charges can appear or disappear, and the fluxes there have to be zero, so $\Psi_{\pm}(-d/2,t)=0$ and $\Psi_{\pm}(d/2,t)=0$. As a result of these boundary conditions ,Eqs. (41) and (43), the average concentrations of positive and negative charges have to be constant in time. Because I assume global neutrality, both average concentrations have to be equal, and this value is defined as

$$\overline{n}=\tfrac{1}{d}\int_{-d/2}^{d/2} n_{\pm}dx\,. \tag{44}$$

Equivalently, the total charge in the device per unit electrode surface Q_{tot} (unit: C·m^{-2}) is constant in time:

$$Q_{tot}=q\int_{-d/2}^{d/2} n_{\pm}dx=q\overline{n}d\,. \tag{45}$$

The charge (per unit of electrode surface) $Q_{el}(t)$ on the left electrode (and $-Q_{el}$ on the right electrode) consists of electrons or holes, so it is of a different nature than the charges in the liquid. It is the sum of two contributions: a capacitive charge Q_{cap} (unit: C·m^{-2}) as a result of the applied voltage, and an induced charge $Q_{ind}(t)$ (unit: C·m^{-2}) as a result of the charges between the electrodes: $Q_{el}=Q_{cap}+Q_{ind}$. The capacitive charge can be expressed as $Q_{cap}=\varepsilon\varepsilon_0 V_A/d$ and the induced charge can be calculated using Ramo's theorem [92][93][94][95], which states that (in the situation considered here) the induced charge is proportional with the first geometrical momentum of the charge distribution: $Q_{ind}=\tfrac{1}{d}\int_{-d/2}^{d/2}\rho x dx$. The external current $I(t)$, flowing towards the left electrode and away from the right electrode, is then $I=S_{el}dQ_{el}/dt=S_{el}Q_{cap}\delta(t)+S_{el}\,dQ_{ind}/dt$. The Dirac impulse is a result of

the voltage step and the fact that the electrodes are perfect conductors, and will be omitted in the rest of this work. The external current can then be calculated from $\frac{\partial}{\partial x}\left(J+\varepsilon\varepsilon_0\frac{\partial}{\partial t}E\right)=0$ (see further), using Eqs. (39), (40) and the fact that E is symmetric around $x=0$, as:

$$I=\varepsilon\varepsilon_0\frac{dE_{el}}{dt}S_{el}, \tag{46}$$

in which $E_{el}(t)$ (unit: V·m^{-1}) is the electric field at the electrode. The current can also be calculated using Eq. (43), as:

$$I=\frac{S_{el}}{d}\int_{-d/2}^{d/2}Jdx, \tag{47}$$

in which $J(x,t)$ (unit: A·m^{-2}) is the current density inside the structure: $J=q(\Psi_+-\Psi_-)$.

At $t=0$ the concentrations $n_\pm$ are homogeneous, so the second term in Eq. (41), which represents diffusion, is zero. Since the concentrations are also equal, the charge concentration ρ is zero and, because of Eq. (40), the electric field E is homogeneous and, because of Eq. (39), equal to V_A/d. Using Eqs. (41) and (47) the following expression for the initial current I_0 (unit: A) is found:

$$I_0=\frac{2q\bar{n}\mu V_A S_{el}}{d}. \tag{48}$$

After $t=0$, The current will decrease because of a combination of three different reasons. The first reason is a result of the geometry of the structure: when charges reach the electrodes at $x=\pm d/2$, they can not move any further and stop contributing to the current. The second reason is diffusion, which, as can be seen in Eq. (41), tends to displace the charges towards the original homogeneous distribution, thereby preventing them

to separate completely. The third reason is (partial or almost complete) screening of the electric field: when charges become separated, the electric field in the bulk will decrease as a result of Eqs. (39) and (40), and this slows down the separation of charges by drift. Each of these reasons can be more or less important, depending on different parameters. In section 3 of this chapter the conditions which determine the relative importance of the different effects are discussed in more detail, but already now it can be understood intuitively that the effect of diffusion is smaller for higher voltages V_A (compared to he thermal voltage V_T) and the effect of screening is larger for a higher total charge Q_{tot} (compared to the capacitive charge Q_{cap}). The effect of the geometry is always present.

The Nernst-Planck-Poisson equations can be written in the following dimensionless form:

$$\tilde{\Psi}_{\pm} = \pm\tilde{n}_{\pm}\tilde{E} - \frac{1}{\varphi}\frac{\partial \tilde{n}_{\pm}}{\partial \tilde{x}}, \tag{49}$$

$$\frac{\partial \tilde{\Psi}_{\pm}}{\partial \tilde{x}} = -\frac{1}{\varphi}\frac{\partial \tilde{n}_{\pm}}{\partial \tilde{t}}, \tag{50}$$

$$\frac{\partial \tilde{E}}{\partial \tilde{x}} = \frac{\lambda}{2\varphi}\left(\tilde{n}_{+} - \tilde{n}_{-}\right), \tag{51}$$

$$\int_{-1/2}^{1/2} \tilde{E}\, d\tilde{x} = 1, \tag{52}$$

in which the dimensionless coordinates are defined as $\tilde{x} = x/d$ and $\tilde{t} = Dt/d^2$, and the dimensionless variables as $\tilde{n}_{\pm} = n_{\pm}/\overline{n}$, $\tilde{E} = Ed/V_A$ and $\tilde{\Psi}_{\pm} = 2q\Psi_{\pm}/I_0$. Eqs. (49)-(52) are only dependent on two dimensionless parameters:

$$\varphi = \frac{V_A}{V_T}, \tag{53}$$

$$\lambda = \frac{2q}{\varepsilon\varepsilon_0 V_T}\bar{n}d^2. \tag{54}$$

The parameter φ can easily be understood to be the normalized applied voltage. The interpretation of the parameter λ is less straightforward. Using the definition of the total charge in equation (45), equation (54) can be written as $\lambda = Q_{tot}/\frac{1}{2}C_{device}V_T$, with $C_{device} = \varepsilon\varepsilon_0/d$ the capacity (per unit of electrode surface) of the device. Therefore, λ can be interpreted as the normalized total charge in the device. It is possible to identify each possible situation with a point in the (φ, λ) parameter-plane. I will focus on values for φ between 0.1 and 1000 and values for λ between 0.1 and 10^6. The following derived dimensionless quantities will also be used: $\tilde{\rho} = \rho/q\bar{n}$, $\tilde{m} = m/\bar{n}$, $\tilde{J} = J/I_0$ and $\tilde{I} = I/I_0$.

In the following paragraphs, I will discuss four limiting cases. In the 'geometry limited' regime, the effects of diffusion and screening are neglected. In the 'space charge limited' regime, diffusion is still neglected, but the charge content is so high that the electric field in the bulk is almost completely screened by transient space charge regions, which are formed as positive and negative charges become separated. In the 'diffusion limited' regime, the voltage is so low that diffusion is dominant, but the total charge is also low enough so that the electric field remains homogeneous. Finally, in the 'double layer limited' regime, the interplay between diffusion and screening in the limit of a very low voltage and a very high charge content results in the formation of diffuse double layers which almost completely screen the electric field in the bulk.

4.2.1. Regimes without diffusion

In the limiting case when drift is the dominant transport mechanism, the diffusion term in Eq. (41) is neglected and:

$$\Psi_{\pm} = \pm \mu n_{\pm} E \,. \tag{55}$$

The combination of Eq. (55) and the blocking electrode boundary conditions has some important consequences. A first consequence is that a positive surface charge builds up near the negative electrode and a negative surface charge builds up near the positive electrode. These surface charges have no effect on the electric field in the device since they are infinitesimally close to the electrodes and induce an exactly opposite image charge. A second consequence of neglecting diffusion is that, adjacent to the electrodes, space charge regions with thickness $\lambda_{SC}(t)$ (unit: m) occur where charges of one polarity are completely absent, resulting in an unbalanced space charge of the other polarity.

The dynamics of these space charge regions can be divided into two phases. In the first phase, the positive and negative space charge regions grow because of the movement of charges with the opposite polarity in the bulk between the space charge regions. During this separation phase, the concentrations n_+ and n_- in the bulk are equal to their initial value $\overline{n}$, resulting in a homogeneous electric field $E_{bulk}(t)$ (unit: V·m^{-1}). The charge distribution and the electric field in the whole device during the separation phase can therefore be described by:

$$\begin{cases} n_{\pm} = 0 & for \quad -d/2 < \pm x < -\left(d/2 - \lambda_{SC}\right) \\ n_{\pm} = \overline{n} & for \quad -\left(d/2 - \lambda_{SC}\right) < \pm x < \left(d/2 - \lambda_{SC}\right) \\ n_{\pm} = n_{SC}\left(\pm x, t\right) & for \quad \left(d/2 - \lambda_{SC}\right) < \pm x < d/2 \end{cases}, \tag{56}$$

and

$$\begin{cases} E = E_{SC}\left(-x, t\right) & for \quad -d/2 < x < -\left(d/2 - \lambda_{SC}\right) \\ E = E_{bulk}\left(t\right) & for \quad -\left(d/2 - \lambda_{SC}\right) < x < \left(d/2 - \lambda_{SC}\right) \\ E = E_{SC}\left(x, t\right) & for \quad \left(d/2 - \lambda_{SC}\right) < x < d/2 \end{cases}, \tag{57}$$

in which $n_{SC}\left(x,t\right)$ (unit: m^{-3}) and $E_{SC}\left(x,t\right)$ (unit: $V \cdot m^{-1}$) are functions which are equal to the concentration of positive charges and to the electric field in the space charge layer closest to the negative electrode. Since only one polarity is present in this region, Eq. (40) results in:

$$n_{SC} = \frac{\varepsilon\varepsilon_0}{q}\frac{\partial E_{SC}}{\partial x}. \tag{58}$$

The speed at which the space charge regions grow is equal to the speed of the charges in the bulk:

$$\frac{d\lambda_{SC}}{dt} = \mu E_{bulk}. \tag{59}$$

The second phase starts when the space charge layers occupy the whole device ($2\lambda_{SC} = d$) and positive and negative charges are completely separated. After this separation time τ_{sep} (unit: s), the space charge regions shrink because of the movement of the charges inside the regions. In the bulk, n_+ and n_- are now both zero, so E_{bulk} is still homogeneous. Therefore, during this depletion phase, one can write:

$$\begin{cases} n_{\pm} = 0 & for \quad -d/2 < \pm x < -\left(d/2 - \lambda_{SC}\right) \\ n_{\pm} = 0 & for \quad -\left(d/2 - \lambda_{SC}\right) < \pm x < \left(d/2 - \lambda_{SC}\right) \\ n_{\pm} = n_{SC}\left(\pm x, t\right) & for \quad \left(d/2 - \lambda_{SC}\right) < \pm x < d/2 \end{cases}. \tag{60}$$

The electric field is still described by Eq. (57). Because of continuity of the electric field, during the depletion phase the borders of the space charge layers move according to:

$$\frac{d\lambda_{SC}}{dt} = -\mu E_{bulk}\,. \tag{61}$$

The depletion phase ends when the bulk is completely depleted of charges, at the depletion time τ_{dep} (unit: s), and the steady state situation is reached. Since all charges are at the electrodes and compensated by an image charge on the electrodes, the induced charge Q_{ind} in steady state is equal to the total charge Q_{tot} in the device. This is expressed as:

$$\int_0^{\infty} I dt = S_{el} Q_{tot}\,. \tag{62}$$

Depending on the total charge Q_{tot} in the device, the charge in the space charge regions will screen the electric field in the bulk partially or completely during the transient. In the following paragraphs, I discuss the two limiting cases of an undisturbed field (geometry limited regime) and of an almost completely screened field (space charge limited regime).

4.2.1.1. Geometry limited regime

In the limiting case in which the electric field is not screened at all, Eqs. (39) and (40) can be replaced by $E = V_A/d$. The time dependency of the thickness of the space charge regions follows then from Eqs. (59) and (61):

$$\begin{cases} \lambda_{SC} = \mu \dfrac{V_A}{d} t & \text{for } 0 \le t \le \tau_{sep} = \tau_{tr}/2 \quad \text{(separation phase)} \\ \lambda_{SC} = d - \mu \dfrac{V_A}{d} t & \text{for } \tau_{sep} \le t \le \tau_{dep} = \tau_{tr} \quad \text{(depletion phase)} \\ \lambda_{SC} = 0 & \text{for } \tau_{dep} \le t \quad \text{(steady state)} \end{cases}, \qquad (63)$$

in which the transit time τ_{tr} (unit: s) is the time that a charge needs to cross the whole thickness of the device when the field is not screened: $\tau_{tr} = d^2/\mu V_A$. Since the electric field is homogeneous, all charges move with the same speed, so the concentrations during the separation phase ($0 \le t \le \tau_{sep}$) are described by $n_{SC} = \overline{n}$. Using Eqs. (47) and (55), this results in the external current decreasing linearly over time during both the separation and the depletion phase:

$$I = I_0 \left(1 - \frac{t}{\tau_{tr}} \right), \qquad (64)$$

until steady state is reached at $t = \tau_{tr}$, after which the current remains zero.

I solved the system of (dimensionless) Eqs. (49)-(52) numerically using a forward Euler algorithm, for different situations. In figure 22, the analytical formulas are compared with these numerical results for the case with λ=0.1 and φ=1000. This situation is representative for the geometry limited regime, as will be demonstrated in section 3 of this chapter. Fig. 22 shows that the electric field is indeed homogeneous and constant over time. Because of this, the charges move at a homogeneous speed, and variations of the concentrations and current densities only occur at the borders between the bulk layer and the space charge layers. In the

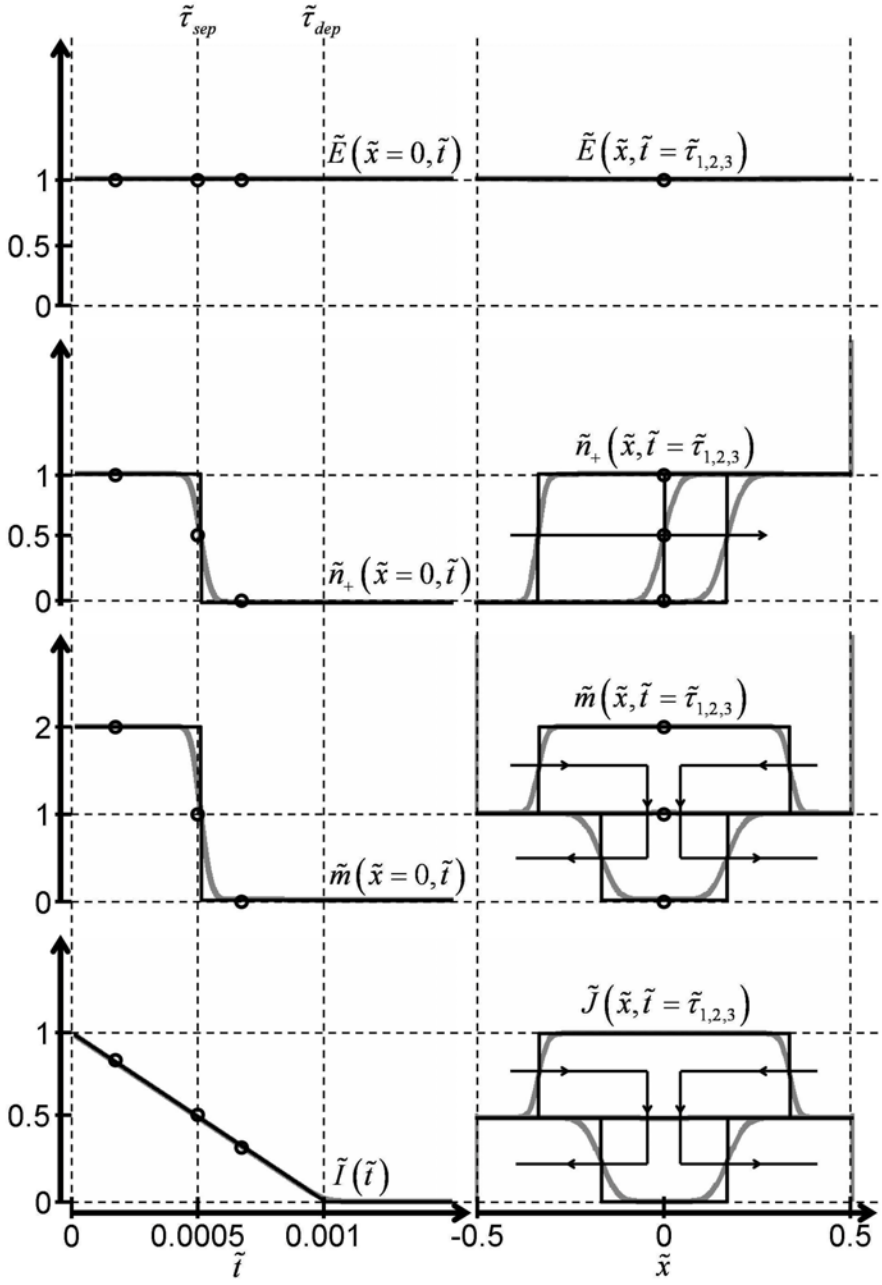
$\tilde{\tau}_{sep}$
$\tilde{\tau}_{dep}$
$\tilde{E}(\tilde{x}=0,\tilde{t})$
$\tilde{E}(\tilde{x},\tilde{t}=\tilde{\tau}_{1,2,3})$
$\tilde{n}_+(\tilde{x},\tilde{t}=\tilde{\tau}_{1,2,3})$
$\tilde{n}_+(\tilde{x}=0,\tilde{t})$
$\tilde{m}(\tilde{x},\tilde{t}=\tilde{\tau}_{1,2,3})$
$\tilde{m}(\tilde{x}=0,\tilde{t})$
$\tilde{J}(\tilde{x},\tilde{t}=\tilde{\tau}_{1,2,3})$
$\tilde{I}(\tilde{t})$
0
0.0005
0.001
$\tilde{t}$
-0.5
0
0.5
$\tilde{x}$

Figure 22:

Comparison between theory (black curves) and simulation (grey curves) for λ=0.1 and φ=1000 (representative for the geometry limited regime). Where the grey curves are not visible, they are coinciding with the black curves. On the left, the electric field, the concentration of positive charges and the total concentration in the middle of the device, as well as the external current, are shown in function of time. On the right, the electric field, the concentration of positive charges, the total concentration and the current density are shown as a function of position at times $\tilde{\tau}_1$ = 0.00033, $\tilde{\tau}_2$ = 0.0005 and $\tilde{\tau}_3$ = 0.00067. The dots on the left indicate these three times, the dots on the right indicate the position from the corresponding curves on the left. One can see that the assumption of a constant and homogeneous electric field is justified by the simulation. The theory for the geometry limited regime agrees with the numerical results, except for the fact that in the simulation, diffusion causes the sharp variations predicted in the analytical formulas, to be more gradual. This has however no significant effect on the dynamics of the regime.

analytical formulas, these positions and the separation and depletion times are sharply defined, because of neglecting diffusion. In the simulation, with diffusion, the variations occur over broader intervals. However, it can be seen that this has no significant influence on the dynamics of the charge transport.

The surface charge density near the electrodes $Q_s(t)$ (unit: C·m^{-2}) can easily be calculated by taking the difference between the total charge and the integral of Eqs. (56) or (60): $Q_s = q\bar{n}\mu V_A t/d$. Introducing diffusion yields a more accurate description of the distribution of charges near the electrodes. The surface charge is then spread out over a thin 'double layer'. Assuming that the charge during the transient, that has up to now been modeled as a surface charge, is distributed in the same way as in the steady state distribution [125], one finds:

$$n_{DL} = \frac{Q_s}{qd}\frac{V_A}{V_T} e^{-\frac{V_A}{V_T}\left(\frac{1}{2}-\frac{x}{d}\right)}, \tag{65}$$

in which $n_{DL}(x,t)$ (unit: m^{-3}) is the excess concentration close to the electrode on the right hand side. Fig. 23 shows that these expressions agree well with the simulation results.

4.2.1.2. Space charge limited regime

When the charge content is sufficiently large, the charge in the space charge regions has an important screening effect on the electric field in the bulk. Therefore, the electric field in the bulk is lower than the electric field in the space charge regions. During the separation phase, charges which move from the bulk region into a space charge region accelerate in

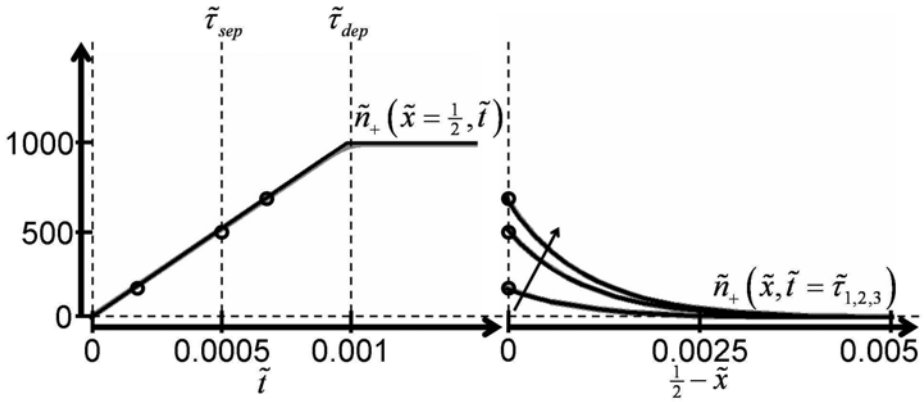

Figure 23:

Comparison between theory (black curves) and simulation (grey curves) for λ=0.1 and φ=1000 (representative for the geometry limited regime). Where the grey curves are not visible, they are coinciding with the black curves. On the left, the concentration of positive charges at the electrode is shown as a function of time. On the right, the concentration of positive charges in the double layer is shown as a function of place at times $\tilde{\tau}_1$ = 0.00033, $\tilde{\tau}_2$ = 0.0005 and $\tilde{\tau}_3$ = 0.00067. The dots on the left indicate these three times, the dots on the right the position from the corresponding curve on the left.

the inhomogeneous field, leading to an inhomogeneous concentration in the space charge regions. In [122], it was shown that in this situation, when drift is dominant and the field in the bulk region is almost completely screened, the electric current density J is approximately homogeneous over the whole device. In the section discussing the double layer limited regime it will be shown that this is also true when diffusion is present, making the homogeneity of the current density a typical characteristic if screening is a limiting mechanism. This can be understood by combining Eqs. (40) and (43) to obtain $\frac{\partial}{\partial x}\left(J+\varepsilon\varepsilon_0\frac{\partial}{\partial t}E\right)=0$. When the electric field is almost completely screened its value is almost constant in time. The high charge content however still results in a high current density. Therefore, in this case the second term in this equation can be neglected compared to the first term and the current density should be homogeneous.

Using Eqs. (40) and (55), the equality of the current densities in the bulk and in the space charge regions leads to:

$$\frac{\mu}{2}\frac{\partial}{\partial x}\left(E_{SC}^2\right)=\frac{2\mu q\bar{n}}{\varepsilon\varepsilon_0}E_{bulk}\,. \tag{66}$$

Using the continuity of the electric field at the boundary between the space charge regions and the bulk, the solution of this differential equation is:

$$E_{SC}=\sqrt{E_{bulk}^2+\frac{4q\bar{n}}{\varepsilon\varepsilon_0}\left(x+\lambda_{SC}-\frac{d}{2}\right)E_{bulk}}\,. \tag{67}$$

The field in the space charge region near the right interface is defined as $E_{int}(t)=E_{SC}(d/2,t)$ (unit: V·m^{-1}), so

$$\frac{E_{int}^2 - E_{bulk}^2}{E_{bulk}} = \frac{4q\overline{n}}{\varepsilon\varepsilon_0}\lambda_{SC}\,. \tag{68}$$

Note that E_{int} is not the same as the field at the electrode, used in Eq. (46), because there is a positive surface charge between the space charge region and the negative electrode.

Assuming that the voltage drop over the bulk region can be neglected compared to the voltage drop over the space charge regions, and using Eqs. (67) and (68), integration of Eq. (39) results in:

$$V_A = \frac{\varepsilon\varepsilon_0}{3q\overline{n}}\frac{E_{int}^3 - E_{bulk}^3}{E_{bulk}}\,. \tag{69}$$

Using Eqs. (68) and (69), in which $E_{int} \gg E_{bulk}$ is assumed, and Eq. (59), the following differential equation for λ_{SC}: $\frac{d}{dt}\left(\lambda_{SC}^4\right) = \frac{9}{16}\mu\varepsilon\varepsilon_0 V_A^2 q^{-1}\overline{n}^{-1}$ is found. With $\lambda_{SC}(0) = 0$ as initial condition, the solution of this differential equation is:

$$\lambda_{SC} = \frac{d}{2}\left(\frac{t}{\tau_{sep}}\right)^{\frac{1}{4}}, \tag{70}$$

in which the separation time is given by:

$$\tau_{sep} = \frac{1}{8\gamma}\tau_{tr}\,, \tag{71}$$

with the dimensionless factor γ defined as:

$$\gamma = \frac{9}{8}\frac{Q_{cap}}{Q_{tot}}\,. \tag{72}$$

Using the fact that the electric current density is homogeneous over the whole device, the external current during the separation phase can be calculated as:

$$I = \gamma I_0 \left(\frac{t}{\tau_{sep}} \right)^{-\frac{3}{4}}. \tag{73}$$

At τ_{sep}, the space charge regions occupy the whole device, and can not be supplied with charges from the bulk region anymore. During the depletion phase, the remaining charge in the space charge regions moves to the electrodes, λ_{SC} decreases to zero, the current drops to zero and the electric field becomes homogeneous. This happens fast compared to the decrease of the current during the separation phase, because the electric field in the space charge regions during the depletion phase is large compared to the electric field in the bulk during the separation phase. Therefore, it is justified to neglect the duration $\tau_{dep} - \tau_{sep}$ of the depletion phase compared to the duration of the separation phase τ_{sep}, and to assume $\tau_{dep} \approx \tau_{sep}$. With this assumption, integrating the current as in Eq. (73) shows that Eq. (62) holds: $\int_0^{\infty} Idt = \int_0^{\tau_{dep}} Idt = \int_0^{\tau_{sep}} Idt = S_{el} Q_{tot}$.

At $t = 0$, the expression for the current in Eq. (73) becomes infinite. The reason for this is that the assumption that the field is screened does not hold at very short times (at $t = 0$, the field is homogeneous and the current should be I_0). Therefore, the screening time τ_{scr} (unit: s) is defined as the time at which the current in Eq. (73) becomes equal to I_0, after which it can be assumed that the screening assumption is justified. τ_{scr} can be calculated as:

$$\tau_{scr} = \frac{\gamma^{\frac{1}{3}}}{8} \tau_{tr}. \tag{74}$$

Before this screening time one can assume that the current remains approximately equal to I_0. However, with this assumption the integral of

the current is not equal to $S_{el}Q_{tot}$ anymore. Therefore, the current during the separation phase is renormalized by introducing γ' (without unit), defined by the condition $\tau_{scr}I_0 + \frac{\gamma'}{\gamma}\int_{\tau_{scr}}^{\tau_{sep}} Idt = S_{el}Q_{tot}$. The new factor γ' can then be calculated to be:

$$\gamma' = \frac{1-\frac{1}{4}\gamma^{\frac{1}{3}}}{1-\gamma^{\frac{1}{3}}}\gamma\,. \tag{75}$$

The current is then:

$$\begin{cases} I = I_0 & \text{for } 0 \le t \le \tau_{scr} \quad \text{(screening phase)} \\ I = \gamma' I_0 \left(\dfrac{t}{\tau_{sep}}\right)^{-\frac{3}{4}} & \text{for } \tau_{scr} \le t \le \tau_{sep} \quad \text{(separation phase)} \\ I = \gamma' I_0 & \text{for } \tau_{sep} = t = \tau_{dep} \quad \text{(depletion phase)} \\ I = 0 & \text{for } \tau_{dep} \le t \quad \text{(steady state)} \end{cases} \tag{76}$$

In Eq. (66), both sides are equal to the current density J. Since J is homogeneous, they are also equal to the external current I, which allows to calculate E_{bulk}:

$$E_{bulk} = \gamma' \frac{V_A}{d}\left(\frac{t}{\tau_{sep}}\right)^{-\frac{3}{4}}. \tag{77}$$

The first order approximation of λ_{SC} in Eq. (70) can be improved by substituting Eq. (59) in Eq. (77). Using the condition $\lambda_{SC}\left(\tau_{sep}\right) = d/2$, the solution is:

$$\lambda_{SC} = \frac{d}{2}\left(1 - \frac{\gamma'}{\gamma}\left(1 - \left(\frac{t}{\tau_{sep}}\right)^{\frac{1}{4}}\right)\right). \tag{78}$$

The electric field in the space charge region on the right hand side can

then be calculated using Eq. (67), resulting in:

$$E_{SC} = \sqrt{\frac{\frac{d}{2} - x}{\lambda_{SC}} E_{bulk}^2 + \frac{x + \lambda_{SC} - \frac{d}{2}}{\lambda_{SC}} E_{int}^2}\,, \tag{79}$$

in which $E_{int}(t)$ is the electric field at the interface between the space charge region and the surface charge:

$$E_{int} = \frac{V_A}{d}\sqrt{\left(\frac{E_{bulk}}{V_A/d}\right)^2 + \frac{9}{2\gamma}\frac{E_{bulk}}{V_A/\lambda_{SC}}}\,. \tag{80}$$

Using Eqs. (58) and (80), and using the assumption of a homogeneous current density, the following expression for n_{SC} is found:

$$n_{SC} = \frac{1}{\sqrt{\frac{\frac{d}{2} - x}{\lambda_{SC}}\frac{1}{(2\bar{n})^2} + \frac{x + \lambda_{SC} - \frac{d}{2}}{\lambda_{SC}}\frac{1}{n_{int}^2}}}\,, \tag{81}$$

in which $n_{int}(t)$ is the concentration at the interface between the space charge region and the surface charge:

$$n_{int} = 2\bar{n}\frac{E_{bulk}}{E_{int}}\,. \tag{82}$$

In Fig. 24, this analytical description is compared with simulation results for $\lambda = 10^6$ and $\varphi = 10^3$, a representative situation for the space charge limited regime. As with the geometry limited regime, one can see that the dynamics are described well by the theory, although diffusion smears out the sharp variations. Fig. 24 also justifies the assumption of a homogeneous current density.

The surface charge Q_s during the depletion phase can be calculated by taking the difference between the total charge and the integral of the

concentration in Eq. (56), using Eq. (81): $Q_s = 2q\bar{n}\lambda_{SC}\left[1-2n_{int}/\left(n_{int}+2\bar{n}\right)\right]$. As in paragraph 4.2.1.1., diffusion is introduced again to find a more detailed description of the concentration and the electric field close to the electrodes. The charge near the electrode is then not described by a surface charge anymore, but forms a very narrow double layer. Using the approximation that close to the electrodes only one polarity of charges is present, one can write Eq. (41) as $J = \mu\rho E - D\,\partial\rho/\partial x$. With the assumption that the charges in the double layer are already in the steady state distribution, the current density in this double layer is zero. Using Eq. (40) and neglecting diffusion outside the double layer, this results in $E_{DL}^2 - 2V_T\,\partial E_{DL}/\partial x = E_{int}^2$, in which $E_{DL}\left(x,t\right)$ (unit: V·m^{-1}) is the electric field in the double layer near the negative electrode. A similar differential equation arises in the solution of the steady state situation of this regime, and is solved in [125]. Using the same method, the solution of this last differential equation is:

$$E_{DL} = E_{int}\coth\left(\frac{E_{int}}{2V_T}\left(\frac{d}{2}-x\right)+\operatorname{arc\,tanh}\left(\frac{E_{int}}{E_{el}}\right)\right), \tag{83}$$

in which $E_{el}\left(t\right)$ (unit: V·m^{-1}) is the electric field at the electrode:

$$E_{el} = E_{int} + \frac{Q_s}{\varepsilon\varepsilon_0}. \tag{84}$$

The concentration in the double layer can be found using Gauss's equation, resulting in:

$$n_{DL} = \frac{\varepsilon\varepsilon_0 E_{int}^2}{2qV_T}\operatorname{csch}^2\left(\frac{E_{int}}{2V_T}\left(\frac{d}{2}-x\right)+\operatorname{arc\,tanh}\left(\frac{E_{int}}{E_{el}}\right)\right). \tag{85}$$

Eqs. (83) and (85) agree very well with numerical results (Fig. 25).

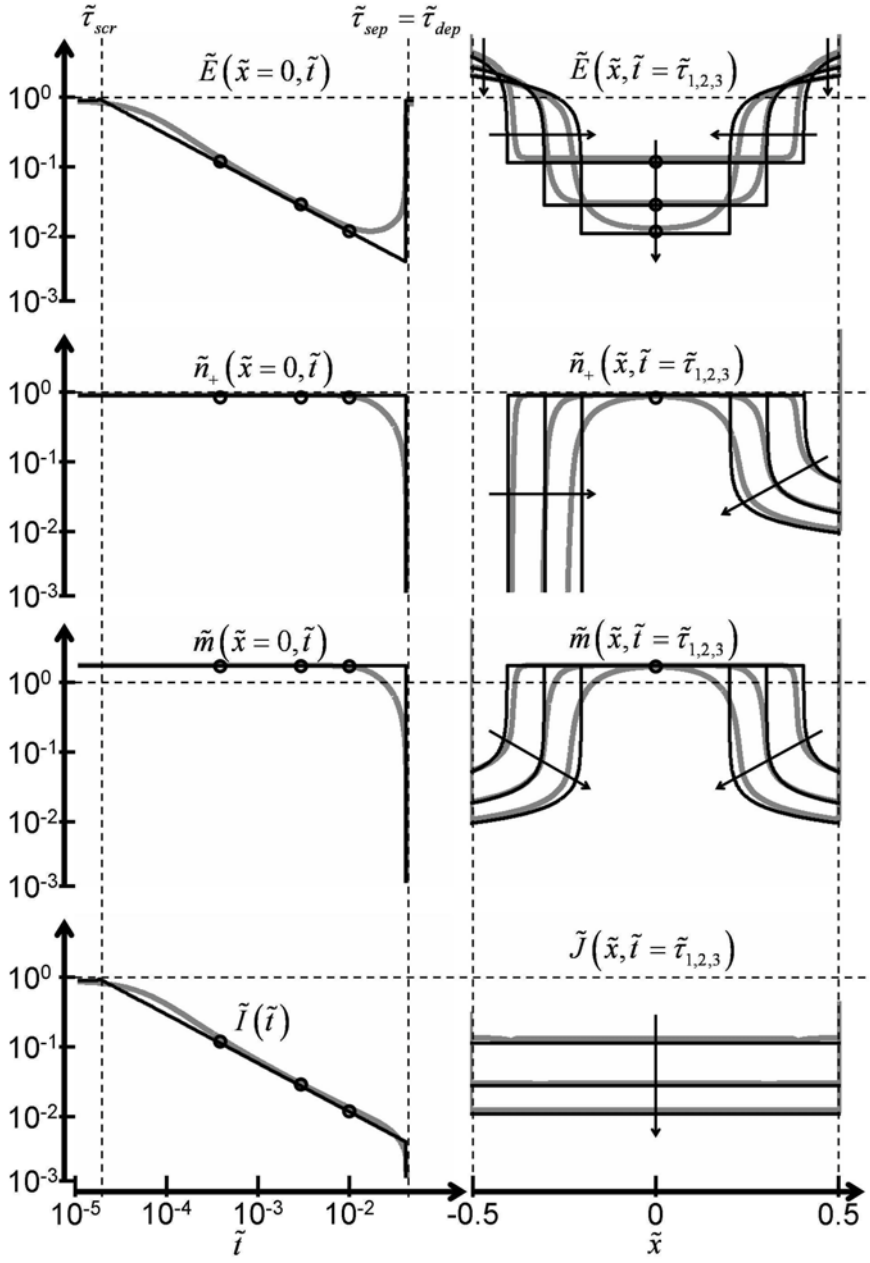
$\tilde{\tau}_{scr}$
$\tilde{\tau}_{sep} = \tilde{\tau}_{dep}$
$\tilde{E}(\tilde{x}=0,\tilde{t})$
$\tilde{E}(\tilde{x},\tilde{t}=\tilde{\tau}_{1,2,3})$
$\tilde{n}_{+}(\tilde{x}=0,\tilde{t})$
$\tilde{n}_{+}(\tilde{x},\tilde{t}=\tilde{\tau}_{1,2,3})$
$\tilde{m}(\tilde{x}=0,\tilde{t})$
$\tilde{m}(\tilde{x},\tilde{t}=\tilde{\tau}_{1,2,3})$
$\tilde{J}(\tilde{x},\tilde{t}=\tilde{\tau}_{1,2,3})$
$\tilde{I}(\tilde{t})$
10^{0}
10^{-1}
10^{-2}
10^{-3}
10^{-5}
10^{-4}
10^{-3}
10^{-2}
$\tilde{t}$
-0.5
0
0.5
$\tilde{x}$

Figure 24:

Comparison between theory (black curves) and simulation (grey curves) for $\lambda = 10^6$ and $\varphi = 1000$ (representative for the space charge limited regime). Where the grey curves are not visible, they are coinciding with the black curves. On the left, the electric field, the concentration of positive charges and the total concentration in the middle of the device, as well as the external current, are shown as a function of time. On the right, the electric field, the concentration of positive charges, the total concentration and the current density are shown as a function of position at times $\tilde{\tau}_1 = 0.00035$, $\tilde{\tau}_2 = 0.0025$ and $\tilde{\tau}_3 = 0.00935$. The dots on the left indicate these three times, the dots on the right indicate the position from the corresponding curves on the left. One can see that the assumption of a homogeneous current density at all times is justified by the simulation. The theory for the space charge limited regime agrees with the numerical results, except for the fact that in the simulation diffusion causes the sharp variations, predicted in the analytical formulas, to be more gradual. This has however no significant effect on the dynamics of the regime.

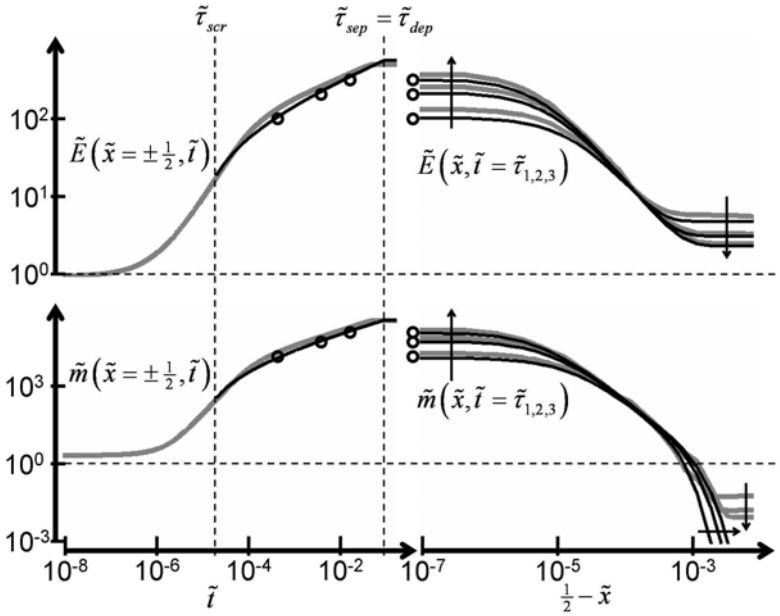

Figure 25:

Comparison between theory (black curves) and simulation (grey curves) for $\lambda = 10^6$ and $\varphi = 1000$ (representative for the space charge limited regime). Where the grey curves are not visible, they are coinciding with the black curves. On the left, the electric field and total concentration at the electrode are shown as a function of time. On the right, the electric field and total concentration in the double layer are shown as a function of position at times $\tilde{\tau}_1 = 0.00035$, $\tilde{\tau}_2 = 0.0025$ and $\tilde{\tau}_3 = 0.00935$. The dots on the left indicate these three times, the dots on the right the position from the corresponding curves on the left.

4.2.2. Regimes with diffusion

When the applied voltage is low, diffusion is the dominant transport mechanism. However, even for very low voltages, drift can not be completely neglected, otherwise the distribution of charges in the device would always remain homogeneous. Therefore, the full Nernst-Planck equation in Eq. (41) has to be used, which can be combined with the continuity Eq. (43) to give:

$$\frac{1}{D}\frac{\partial n_{\pm}}{\partial t} = \mp\frac{1}{V_T}\frac{\partial}{\partial x}\left(n_{\pm}E\right) + \frac{\partial^2 n_{\pm}}{\partial x^2}. \tag{86}$$

The boundary conditions (perfectly blocking electrodes) can be written as $V_T\,\partial n_{\pm}/\partial x\big|_{-d/2} = \pm E\left(-d/2,t\right)n_{\pm}\left(-d/2,t\right)$ for the left electrode and $V_T\,\partial n_{\pm}/\partial x\big|_{d/2} = \pm E\left(d/2,t\right)n_{\pm}\left(d/2,t\right)$ for the right electrode. In the regimes with diffusion, a discrete surface charge does not appear.

As in section 4.2.1., I discuss two limiting cases in which the electric field is either almost homogeneous (in the diffusion limited regime) or almost completely screened (in the double layer limited regime).

4.2.2.1. Diffusion limited regime

As in paragraph 4.2.1.1., Eq. (39) and (40) are replaced by $E = V_A/d$, so Eq. (86) becomes:

$$\frac{1}{D}\frac{\partial n_{\pm}}{\partial t} = \mp\frac{\varphi}{d}\frac{\partial n_{\pm}}{\partial x} + \frac{\partial^2 n_{\pm}}{\partial x^2}. \tag{87}$$

The steady state distributions $n_{\pm,ss}\left(x\right)$ (unit: m^{-3}) can then be found by setting the time derivative in Eq. (87) zero, resulting in:

$$n_{\pm,ss} = \overline{n}\frac{\varphi}{2}\operatorname{csch}\left(\frac{\varphi}{2}\right)e^{\pm\varphi\frac{x}{d}}. \tag{88}$$

The dynamic solution for this regime can be derived using standard separation of variables techniques [126] and yields:

$$n_{\pm} = n_{\pm,ss}\left(1+\frac{1}{\varphi}e^{\frac{\varphi}{2}\left(\frac{1}{2}\mp\frac{x}{d}\right)}\sum_{i=1}^{\infty}C_i X_{\pm,i}e^{-\frac{\varphi^2}{4}\left(1+\frac{4i^2\pi^2}{\varphi^2}\right)\frac{D}{d^2}t}\right), \tag{89}$$

with:

$$X_{\pm,i} = \frac{2i\pi}{\varphi}\cos\left(i\frac{\pi}{2}\pm\frac{i\pi x}{d}\right)+\sin\left(i\frac{\pi}{2}\pm\frac{i\pi x}{d}\right), \tag{90}$$

$$C_i = 8\frac{\frac{2i\pi}{\varphi}}{\left(1+\frac{4i^2\pi^2}{\varphi^2}\right)^2}\left((-1)^i e^{-\frac{\varphi}{2}}-1\right). \tag{91}$$

For low φ, $n_{\pm}$ can be approximated as:

$$n_{\pm} = \overline{n}\left(1\pm\varphi\frac{x}{d}\right)\mp\frac{4\varphi\overline{n}}{\pi^2}\sum_{i=1}^{\infty}\frac{1}{i^2}\sin\left(i\frac{\pi}{2}\right)\sin\left(\frac{x}{d}i\pi\right)e^{-i^2\pi^2\frac{D}{d^2}t}, \tag{92}$$

from which it is clear that the steady state solution is reached for $t\to\infty$. Using the expansion of the steady state solution:

$$\overline{n}\left(1\pm\varphi\frac{x}{d}\right) = \overline{n}\left(1\pm\frac{4\varphi}{\pi^2}\sum_{i=1}^{\infty}\frac{1}{i^2}\sin\left(i\frac{\pi}{2}\right)\sin\left(\frac{x}{d}i\pi\right)\right), \tag{93}$$

Eq. (92) can also be written as:

$$n_{\pm} = \overline{n}\pm\frac{4\varphi\overline{n}}{\pi^2}\sum_{i=1}^{\infty}\frac{1}{i^2}\sin\left(i\frac{\pi}{2}\right)\sin\left(\frac{x}{d}i\pi\right)\left(1-e^{-i^2\pi^2\frac{D}{d^2}t}\right), \tag{94}$$

in which it is clear that $n_{\pm}=\overline{n}$ at $t=0$, as expected. Using Eq. (47), the external current can be calculated as:

$$I = I_0 \frac{8}{\pi^2} \sum_{i=1,3,5,\ldots} \frac{1}{i^2} e^{-i^2 \pi^2 \frac{D}{d^2} t} . \quad (95)$$

With the identity $\pi^2/8 = \sum_{i=1,3,5,\ldots} i^{-2}$ it becomes clear that, for $t = 0$, $I = I_0$, as expected.

As time progresses, the term for $i = 1$ becomes very quickly dominant in Eqs. (92) and (95), and in this case one can write:

$$n_{\pm} = \overline{n}\left(1 \pm \varphi \frac{x}{d}\right) \mp \frac{4\varphi\overline{n}}{\pi^2} \sin\left(\frac{x}{d}\pi\right) e^{-\pi^2 \frac{D}{d^2} t}, \quad (96)$$

$$I = I_0 \frac{8}{\pi^2} e^{-\pi^2 \frac{D}{d^2} t} . \quad (97)$$

From Eq. (96), it can be concluded that $m = 2\overline{n}$. The fact that the total concentration is homogeneous is typical for the regimes in which diffusion is a limiting factor, as will be demonstrated in the next paragraph.

Fig. 26 shows a comparison between the theoretical description of the diffusion limited regime and simulation results for $\lambda = \varphi$=0.1, which are representative values for this regime. Except at very small times, when neglecting the higher order harmonics leads to visible deviations, the theoretical description agrees very well with the numerical results. It is clear that the electric field and the total concentration are indeed homogeneous and constant.

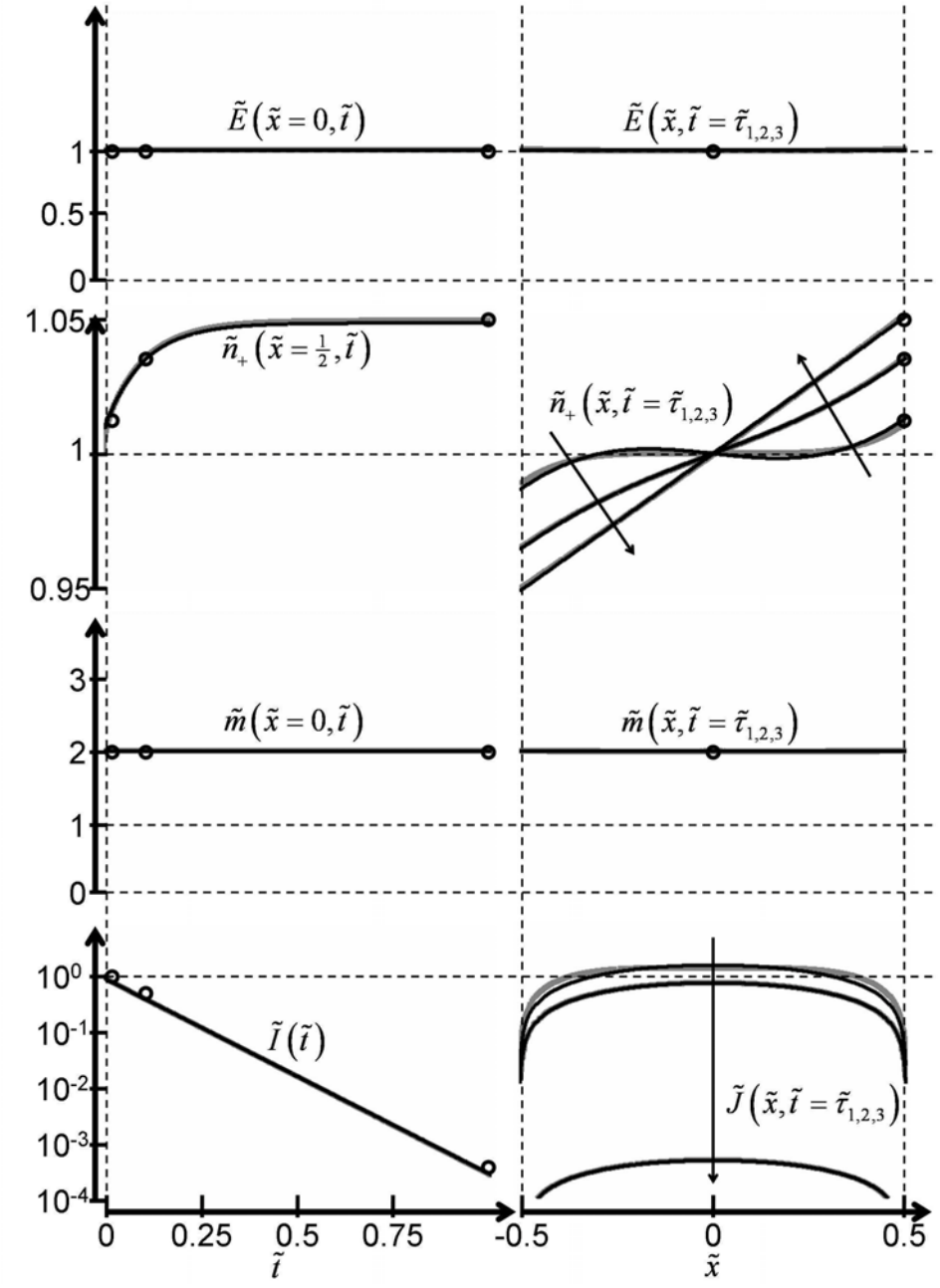
$\tilde{E}\left(\tilde{x}=0,\tilde{t}\right)$
$\tilde{E}\left(\tilde{x},\tilde{t}=\tilde{\tau}_{1,2,3}\right)$
1
0.5
0
1.05
1
0.95
$\tilde{n}_{+}\left(\tilde{x}=\frac{1}{2},\tilde{t}\right)$
$\tilde{n}_{+}\left(\tilde{x},\tilde{t}=\tilde{\tau}_{1,2,3}\right)$
3
2
1
0
$\tilde{m}\left(\tilde{x}=0,\tilde{t}\right)$
$\tilde{m}\left(\tilde{x},\tilde{t}=\tilde{\tau}_{1,2,3}\right)$
10^{0}
10^{-1}
10^{-2}
10^{-3}
10^{-4}
$\tilde{I}\left(\tilde{t}\right)$
$\tilde{J}\left(\tilde{x},\tilde{t}=\tilde{\tau}_{1,2,3}\right)$
0
0.25
0.5
0.75
$\tilde{t}$
-0.5
0
0.5
$\tilde{x}$

Figure 26:

Comparison between theory (black curves) and simulation (grey curves) for λ=0.1 and φ=0.1 (representative for the diffusion limited regime). Where the grey curves are not visible, they are coinciding with the black curves. On the left, the electric field in the middle of the device, the concentration of positive charges at the electrode and the total concentration in the middle of the device, as well as the external current, are shown as a function of time. On the right, the electric field, the concentration of positive charges, the total concentration and the current density are shown as a function of place at times $\tilde{\tau}_1$ = 0.01, $\tilde{\tau}_2$ = 0.1 and $\tilde{\tau}_3$ = 1. The dots on the left indicate these three times, the dots on the right indicate the position from the corresponding curves on the left. One can see that the assumption of a homogeneous and constant electric field and the conclusion of a homogeneous and constant total concentration are justified by the simulation. The theory for the diffusion limited regime agrees with the numerical results. Only at very short times there is a small deviation because of the neglection of higher order terms.

4.2.2.2. Double layer limited regime

When the applied voltage is low and the charge content is high, both diffusion and screening are important. The limiting regime under these circumstances has been solved in [120] and [121]. My aim in this section is to show that using a similar approach as for the other regimes discussed

in this paper leads to the same conclusions. In the space charge limited regime, the fact that screening is a limiting mechanism leads to the assumption of a homogeneous current density J. In the diffusion limited regime, it was found that the total concentration m is homogeneous. In the regime of low voltage and high concentration, both screening and diffusion are limiting mechanisms, and the two assumptions $\partial J/\partial x = 0$ and $m = 2\overline{n}$ can be combined. Using Eqs. (40) and (41), one finds then:

$$J = 2q\overline{n}\mu\left(E - \lambda_{DL}^2 \frac{\partial^2 E}{\partial x^2} \right), \tag{98}$$

in which the double layer length (or the Debye length) λ_{DL} (unit: m) is defined as:

$$\lambda_{DL} = \sqrt{\frac{\varepsilon\varepsilon_0 V_T}{2q\overline{n}}}. \tag{99}$$

Using equations (54) and (99), one can see that the dimensionless parameter λ can be interpreted in terms of the double layer length and the thickness of the device: $\lambda = d^2/\lambda_{DL}^2$.

The steady state solution $E_{ss}(x)$ (unit: V·m^{-1}) of the electric field can be found by setting the current density in Eq. (98) zero, and using Eq. (39) and the fact that the electric field is symmetric around $x = 0$:

$$E_{ss} = \frac{V_A}{d}\frac{d}{2\lambda_{DL}}\operatorname{csch}\left(\frac{d}{2\lambda_{DL}}\right)\cosh\left(\frac{x}{\lambda_{DL}}\right). \tag{100}$$

Using Eq. (40), $\rho_{ss}(x)$ (unit: C·m^{-3}), the steady state solution of the charge density, is found:

$$\rho_{ss} = q\overline{n}\varphi\operatorname{csch}\left(\frac{d}{2\lambda_{DL}}\right)\sinh\left(\frac{x}{\lambda_{DL}}\right). \tag{101}$$

Taking the derivative of (98) with respect to x, and using Eq. (40) and the

assumption of a homogeneous current density, yields $\rho = \lambda_{DL}^2 \, \partial^2 \rho / \partial x^2$. Using Eq. (101), it can be seen that the transient part $\rho_{tr}(x,t)$ (unit: C·m^{-3}) of the charge density, defined as $\rho_{tr} = \rho - \rho_{ss}$, is also a solution of this differential equation: $\rho_{tr} = \lambda_{DL}^2 \, \partial^2 \rho_{tr} / \partial x^2$. Using the fact that ρ has to be antisymmetric around $x = 0$, the solution is:

$$\rho_{tr} = C \sinh\left(\frac{x}{\lambda_{DL}}\right), \tag{102}$$

in which $C(t)$ is an integration constant that can be found by calculating the external current using two different methods.

For the first method, Eqs. (39) and (40) are used to find the electric field:

$$E = E_{ss} + \frac{\lambda_{DL}}{\varepsilon\varepsilon_0} C\left(\cosh\left(\frac{x}{\lambda_{DL}}\right) - \frac{2\lambda_{DL}}{d}\sinh\left(\frac{d}{2\lambda_{DL}}\right)\right), \tag{103}$$

which can be used in Eq. (46) to find the external current:

$$I = S_{el}\lambda_{DL}\frac{dC}{dt}\left(\cosh\left(\frac{d}{2\lambda_{DL}}\right) - \frac{2\lambda_{DL}}{d}\sinh\left(\frac{d}{2\lambda_{DL}}\right)\right). \tag{104}$$

For the second method, J is calculated using Eqs. (98) and (103):

$$J = -C\frac{2D}{d}\sinh\left(\frac{d}{2\lambda_{DL}}\right). \tag{105}$$

Since J is homogeneous, Eq. (47) shows that, multiplied with the electrode surface, it has to be equal to the external current, so the right hand sides in Eqs. (104) and (105) have to be equal, except for a factor S_{el}:

$$\left(\coth\left(\frac{d}{2\lambda_{DL}}\right) - \frac{2\lambda_{DL}}{d}\right)\frac{dC}{dt} = -\frac{2D}{\lambda_{DL}d}C. \tag{106}$$

Since at $t = 0$ the transient part of the charge density has to compensate the steady state part $C(0) = -q\bar{n}\varphi\,\mathrm{csch}\left(\frac{1}{2}d/\lambda_{DL}\right)$. The solution of Eq. (106), using this initial condition, is:

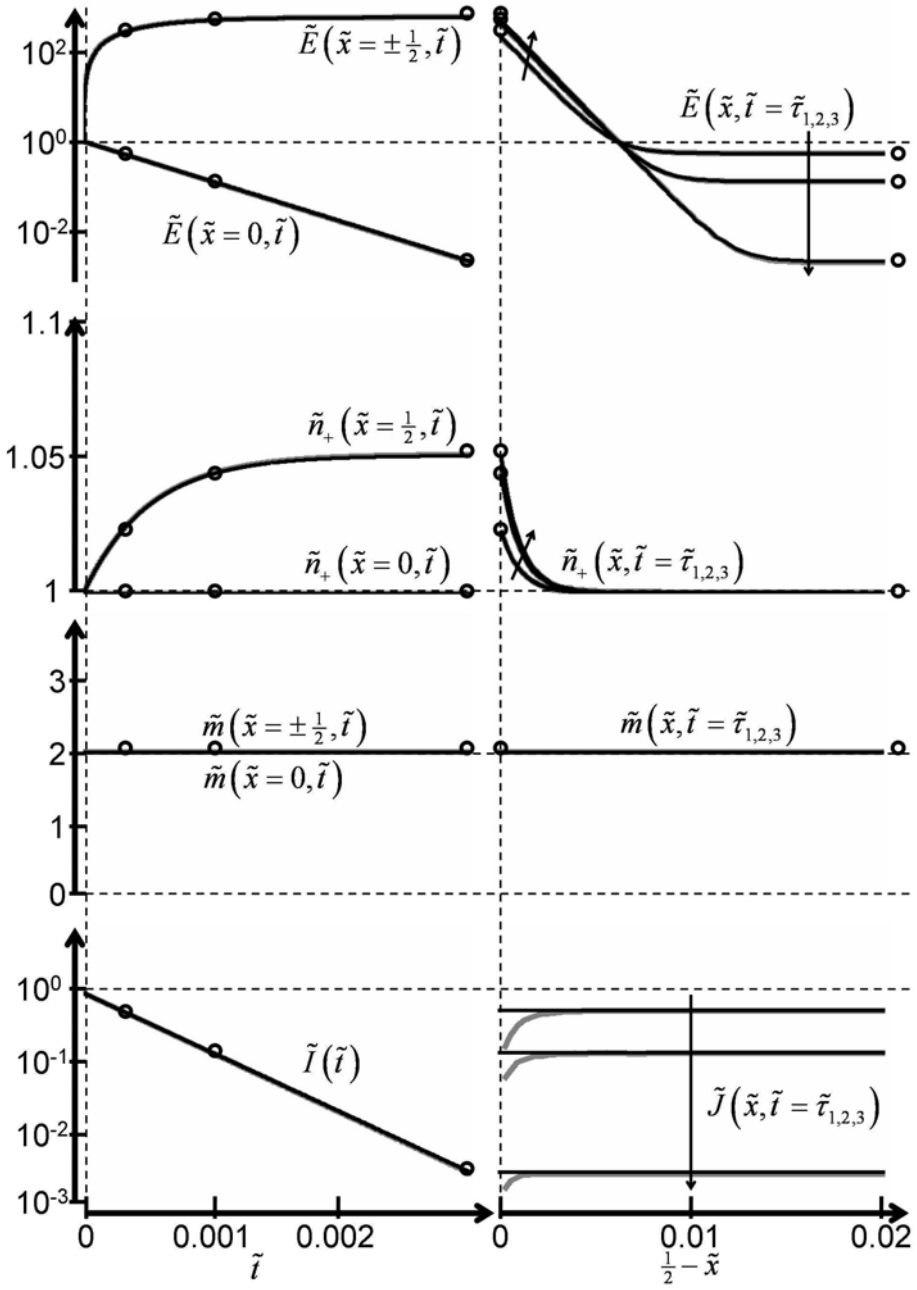
10^2
10^0
10^{-2}
$\tilde{E}\left(\tilde{x}=\pm\frac{1}{2},\tilde{t}\right)$
$\tilde{E}\left(\tilde{x}=0,\tilde{t}\right)$
$\tilde{E}\left(\tilde{x},\tilde{t}=\tilde{\tau}_{1,2,3}\right)$
1.1
1.05
1
$\tilde{n}_+\left(\tilde{x}=\frac{1}{2},\tilde{t}\right)$
$\tilde{n}_+\left(\tilde{x}=0,\tilde{t}\right)$
$\tilde{n}_+\left(\tilde{x},\tilde{t}=\tilde{\tau}_{1,2,3}\right)$
3
2
1
0
$\tilde{m}\left(\tilde{x}=\pm\frac{1}{2},\tilde{t}\right)$
$\tilde{m}\left(\tilde{x}=0,\tilde{t}\right)$
$\tilde{m}\left(\tilde{x},\tilde{t}=\tilde{\tau}_{1,2,3}\right)$
10^0
10^{-1}
10^{-2}
10^{-3}
$\tilde{I}\left(\tilde{t}\right)$
$\tilde{J}\left(\tilde{x},\tilde{t}=\tilde{\tau}_{1,2,3}\right)$
0
0.001
0.002
$\tilde{t}$
0
0.01
0.02
$\frac{1}{2}-\tilde{x}$

Figure 27:

Comparison between theory (black curves) and simulation (grey curves) for $\lambda = 10^6$ and $\varphi = 0.1$ (representative for the double layer limited regime). Where the grey curves are not visible, they are coinciding with the black curves. On the left, the electric field, the concentration of positive charges and the total concentration in the middle of the device and at the electrode, as well as the external current, are shown as a function of time. On the right, the electric field, the concentration of positive charges, the total concentration and the current density are shown as a function of place near the electrode at times $\tilde{\tau}_1 = 0.0003$, $\tilde{\tau}_2 = 0.001$ and $\tilde{\tau}_3 = 0.003$. The dots on the left indicate these three times, the dots on the right indicate the position from the corresponding curves on the left. One can see that the assumption of a homogeneous and constant total concentration and a homogeneous current density at all times are justified by the simulation. The theory for the double layer limited regime agrees with the numerical results, both close to the electrode and in the bulk of the device.

$$C = -q\bar{n}\varphi \operatorname{csch}\left(\frac{d}{2\lambda_{DL}}\right) e^{-\frac{t}{\tau_{DL}}}. \tag{107}$$

in which τ_{DL} (unit: s) is the time constant of the double layer regime:

$$\tau_{DL} = \left(\coth\left(\frac{d}{2\lambda_{DL}}\right) - \frac{2\lambda_{DL}}{d}\right)\frac{\lambda_{DL} d}{2D}, \tag{108}$$

which reduces to $\tau_{DL} = \frac{1}{2}\lambda_{DL} d/D$ for $\lambda_{DL} \ll d$. The charge concentration and electric field are then:

$$\rho = \rho_{ss}\left(1 - e^{-\frac{t}{\tau_{DL}}}\right), \tag{109}$$

$$E = \frac{V_A}{d} e^{-\frac{t}{\tau_{DL}}} + E_{ss}\left(1 - e^{-\frac{t}{\tau_{DL}}}\right). \tag{110}$$

The external current can be calculated using Eqs. (105) and (107):

$$I = I_0 e^{-\frac{t}{\tau_{DL}}}. \tag{111}$$

The comparison, in Fig. 27, between the theoretical description of the double layer limited regime and numerical results for the representative situation $\lambda = 10^6$ and $\varphi = 0.1$, justifies the assumption that the total concentration is constant and homogeneous. The other quantities are only non-homogeneous in the double layer close to the electrodes. The assumption of a homogeneous current density does not hold near the electrodes, but the variation occurs over such a small layer that the external current is still described well by Eq. (111).

4.3. Applicability of the regimes

4.3.1. Comparison between theory and simulation

To investigate in which regions of the (φ,λ) parameter-plane the respective regimes are applicable, I have performed over 20000 simulations. For each simulation, and for each of the four theoretical regimes, a value is calculated, which is a measure for the difference between the simulation result and the analytical result. Representing the difference in time- and position-dependent dynamics by a single value is somewhat arbitrary, and for different aspects of the dynamics, different regions in the (φ,λ) parameter-plane may be described well by the theory. The aim of this paragraph is to obtain a general idea of the applicability of the theoretical descriptions of the four regimes.

As a place-independent quantity which represents the dynamics of the device for a particular point in the (φ,λ) parameter-plane, I choose the external current I. For each regime, the normalized root mean square error $\Delta(\varphi,\lambda)$ (without unit) between the simulated and the theoretical current, is calculated with the following formula:

$$\Delta = \frac{1}{I_{sim}(0)} \sqrt{\frac{\int_{t_{90\%}}^{t_{10\%}} (I_{sim} - I_{th})^2 \, dt}{t_{10\%} - t_{90\%}}} . \qquad (112)$$

In this formula, $t_{90\%}$ and $t_{10\%}$ (unit: s) are the times for which the simulated current I_{sim} (unit: A) reaches 90% and 10% of its initial value $I_{sim}(0)$. I_{th} (unit: A) is the theoretical current which can be calculated for the four

regimes, using Eqs. (64), (76), (97) and (111). Depending on which equation is chosen, one obtains the values Δ_{GL} for the geometry limited regime, Δ_{SCL} for the space charge limited regime, Δ_{DL} for the diffusion limited regime or Δ_{DLL} for the double layer limited regime.

Fig. 28 shows the smallest of these four values for all of the performed simulations on the (φ,λ) parameter-plane. The four regions which correspond to the four regimes can be clearly seen. As expected, the geometry limited regime is applicable for small λ and large φ, the space charge limited regime for large λ and φ, the diffusion limited regime for small λ and φ, and the double layer limited regime for large λ and small φ.

4.3.2. Borders between the regimes

It is useful to have a 'rule of thumb' to determine quickly which regime describes best the situation for a particular combination of values for λ and φ. In order to find such rules I will compare the different time constants which are typical for the different regimes.

The time constants $\tau_{dep}=d^2/(\mu V_A)$ in the geometry limited regime, $\tau_{DL}=d\lambda_{DL}/(2D)$ in the double layer limited regime and $d^2/(\pi^2 D)$ in the diffusion limited regime all represent the initial slope of the external current. τ_{dep} becomes equal to $d^2/(\pi^2 D)$ for $\varphi=\pi^2\approx 10$, which is plotted in Fig. 28 and can be seen to be a useful rule to distinguish between the geometry limited and the diffusion limited regime. Similarly, τ_{DL} is equal to $d^2/(\pi^2 D)$ for $\lambda=\pi^4/4\approx 25$, which turns out to be a

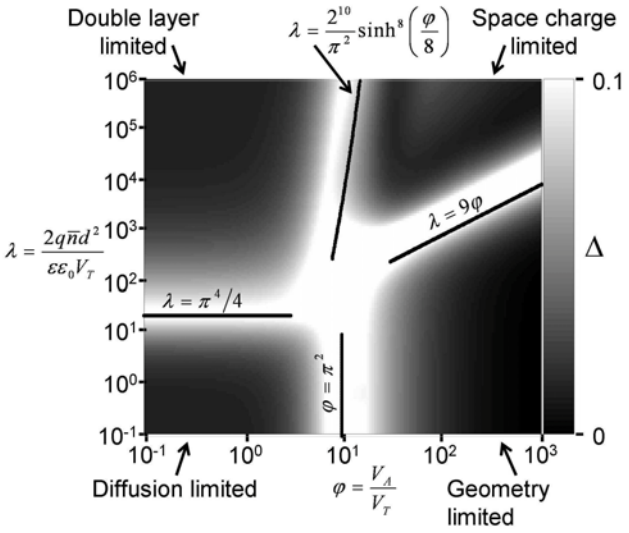

Figure 28:

The relative error between theory and simulation in the (φ, λ) parameter plane. A darker shade corresponds to a better agreement. The four different regimes and the borders between them are indicated. As expected, the geometry limited regime is applicable for small λ and large φ, the space charge limited regime for large λ and φ, the diffusion limited regime for small λ and φ, and the double layer limited regime for large λ and small φ. The borders are useful to quickly determine the applicable regime for a specific situation.

useful border between the diffusion limited and the double layer limited regime. To obtain a border between the geometry limited regime and the space charge limited regime, the separation times τ_{sep} are compared, which are given by $d^2/(2\mu V_A)$ and Eq. (71), respectively. They are equal for $\lambda = 9\varphi$, which is also plotted on Fig. 28.

A rule for the border between the space charge limited and the double layer limited regimes is not so easy to obtain because there are no time constants that have a similar meaning in both regimes. In [121], two intermediate regimes between the double layer limited regime (which is referred to as the 'linear' regime) and the space charge limited regime are discussed. The 'weakly nonlinear' regime describes the situation in which the total concentration can still be considered constant in the bulk (as in the double layer limited regime), but not near the electrodes. The 'strongly nonlinear' regime describes the situation in which space charge layers are formed (as in the space charge limited regime), but the electric field is still mostly screened by the double layers. The criterium used in [121] to distinguish between these two intermediary regimes is $\lambda = \left(2^{10}/\pi^2\right)\sinh^8\left(\varphi/8\right)$. In Fig. 28, one can see that this criterion is also useful as a border between the double layer limited and the space charge limited regimes.

4.4. Transient current measurements

The devices used for the transient current measurements consist of two glass plates, both coated with a transparent ITO-electrode of 1 cm^2. Spacer balls hold these two electrodes separated at a distance d. The space between the electrodes is filled with a mixture of high purity (99.9%) n-dodecane (ε=2) (Aldrich) and OLOA 1200, a 50% mineral oil containing surfactant polyisobutylene succinimide (Chevron). The surfactant molecules form inverse micelles, which can disproportionate resulting in a symmetric 1:1 electrolyte [17][18]. The concentration of charged inverse micelles $\overline{n}$ is proportional with the weight percentage of surfactant in the mixture, with a proportionality constant of roughly $5x10^{19}$ m^{-3} per wt% [18].

Five devices with different thicknesses and concentrations of surfactant have been made. The thickness of each device was obtained by measuring the capacitance of the device before filling. Table I gives an overview of the properties of the different devices. They are chosen in such a way that the resulting values for λ cover a large interval in Fig. 28 and Fig. 29.

Before every measurement, the devices are short-circuited for a sufficient amount of time to ensure a homogeneous distribution of charges. Then the voltage is abruptly changed to V_A and the resulting external transient current is measured. These measurements were performed for voltages of 25 mV, 100 mV, 250 mV, 1 V and 2.5 V. Fig. 29 shows the location in the (φ, λ) parameter-plane of all the measurements shown in this section.

Device number	Surfactant concentration (wt%)	Estimated $\overline{n}$ (m^{-3})	Measured d (μm)	Estimated λ (no unit)
1	0.01	5.0×10^{17}	2.2	1.75
2	0.03	1.5×10^{18}	4.5	22
3	0.10	5.0×10^{18}	9.4	320
4	0.30	1.5×10^{19}	14.8	2380
5	1.00	5.0×10^{19}	26.8	26000

Table I:

Properties of the five devices used for the transient current measurements shown in this section. The average concentrations are estimated as $5x10^{19}$ m^{-3} per wt% of surfactant. The thicknesses are derived from capacitance measurements on the empty devices. The surfactant concentrations and the thicknesses are chosen in such a way that a wide range of values for λ is covered.

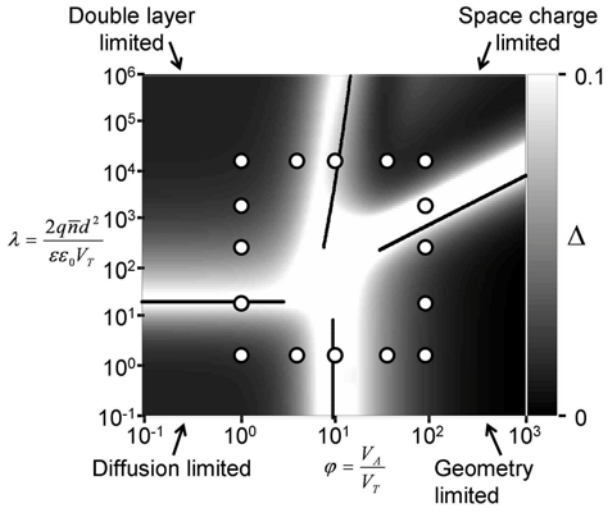

Figure 29:

Location of the (φ, λ) parameters for the measurements shown in this section, in the (φ, λ) parameter plane. The device parameters and the voltages are chosen in such a way that many effects described in this chapter can be demonstrated. The four measurements with the highest or lowest values for φ and λ are representative for the four described regimes.

4.4.1. Low voltages

The currents, measured when a voltage of 25 mV is applied on each of the five devices, are shown in Fig. 30. The concentration $\overline{n}$ and the mobility μ of the charges have been estimated by fitting simulations to these measurements. The best fits are included in Fig. 30, and are found for the values listed in the first columns of tables II and III. The values for the concentration are consistent with the expected values. Also the values for the mobility agree well with the results in other works [18][120][122].

The good agreement between the measurements and the simulations in Fig. 30 and in the following paragraphs, indicates that the dynamics of the devices during the transient phase can be modeled well by drift, diffusion and screening, as described by the Nernst-Planck-Poisson equations. The deviations at very short times are a result of the charging time of the measurement setup. At large times, other effects, such as the generation of newly charged inverse micelles [18] and reactions at the electrodes, become important, resulting in a current after the transient phase is finished.

4.4.2. High voltages

The currents, measured when a voltage of 2.5 V is applied on each of the five devices, are shown in Fig. 31, together with the corresponding simulations for the parameters found in the previous paragraph. At high voltages, one can estimate the concentration and the mobility more easily by using the fact that positive and negative charges become completely

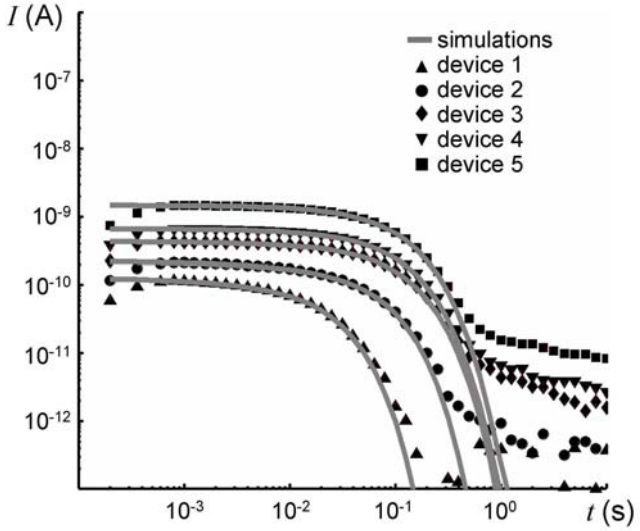

Figure 30:

Current measurements on double logarithmical scale for the five devices in table I, when a voltage step from 0 V to 25 mV is applied (points on the left in Figure 29). The grey curves are the best fitting simulations. The measurements and the simulations agree, except at very short times (when the charging time of the setup causes an error in the measurement) and at large times (because bulk and electrode reactions are not included in the simulations).

Device	$\overline{n}$ (m^{-3})			
	numerical fit	Using Eq. (113)	Theoretical fit (high V)	Theoretical fit (low V)
1	4.3×10^{17}	3.5×10^{17}	4.2×10^{17}	4.1×10^{17}
2	1.3×10^{18}	1.3×10^{18}		
3	6.6×10^{18}	6.6×10^{18}		
4	1.4×10^{19}	1.5×10^{19}		
5	7.2×10^{19}	6.2×10^{19}	8.5×10^{19}	7.8×10^{19}

Table II:

Average concentration of charges in the five devices, estimated in different ways. The values in the first column are found by fitting numerical simulations to the measured transient currents. The values in the second column are obtained from the integral of the transient current at 2.5 V, and the values in the third and the fourth column are obtained from a fit between the theoretical expressions and the transient current measurements for devices 1 and 5. All estimations agree very well.

Device	μ ($m^2V^{-1}s^{-1}$)			
	numerical fit	Using Eq. (114)	Theoretical fit (high V)	Theoretical fit (low V)
1	8.8×10^{-10}	7.1×10^{-10}	8.5×10^{-10}	8.6×10^{-10}
2	9.8×10^{-10}	8.7×10^{-10}		
3	8.0×10^{-10}	7.0×10^{-10}		
4	9.0×10^{-10}	8.1×10^{-10}		
5	7.0×10^{-10}	8.1×10^{-10}	5.9×10^{-10}	6.4×10^{-10}

Table III:

Mobility of the charges in the five devices, estimated in different ways. The values in the first column are found by fitting numerical simulations to the measured transient currents. The values in the second column are obtained from the initial current at 2.5 V, and the values in the third and the fourth column are obtained from a fit between the theoretical expressions and the transient current measurements for devices 1 and 5. All estimations agree very well.

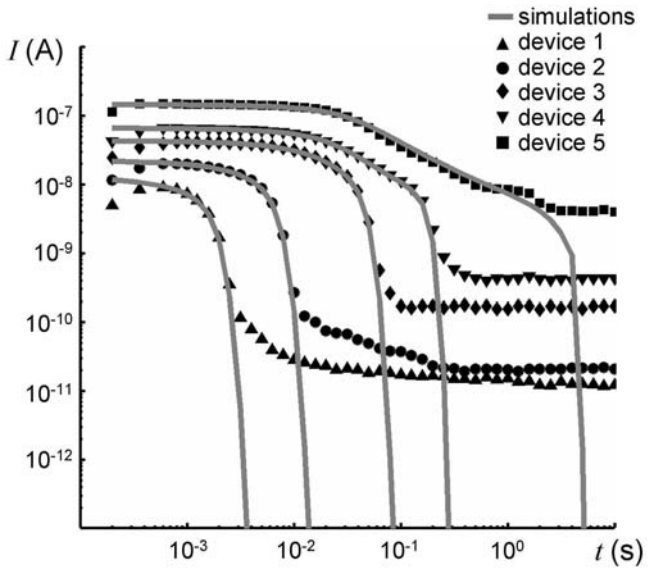

Figure 31:

Current measurements on double logarithmical scale for the five devices in table I, when a voltage step from 0 V to 2.5 V is applied (points on the right in Figure 29). The grey curves are the best fitting simulations. The measurements and the simulations agree, except at very short times (when the charging time of the setup causes an error in the measurement) and at large times (because bulk and electrode reactions are not included in the simulations). On this double-logarithmical scale, one can notice the power law behavior of the current for the highest charge contents (devices 4 and 5).

separated. Using Eqs. (48) and (62) results in:

$$\overline{n} = \frac{1}{qdS_{el}} \int_0^{\tau_{dep}} Idt \,, \tag{113}$$

$$\mu = \frac{d^2}{2V_A} I_0 \left(\int_0^{\tau_{dep}} Idt \right)^{-1} . \tag{114}$$

The integrals in these equations are only calculated until the end of the transient at the depletion time, which can be easily estimated from the measurements, to avoid including the current as a result from reactions in the bulk or at the electrodes. In estimating the initial current, an extrapolation has to be made to take into account the charging time of the measurement setup.

Applying this estimation to the measurements of Fig. 31 results in the values shown in the second column of tables II and III. The good agreement with the values obtained from the fit with simulations demonstrates that the assumption of a complete separation of charges is justified.

4.4.3. Low charge content

Fig. 32 shows the measured currents, together with the fitted simulation, for the device with the lowest λ (Device 1), and for five different voltages. On Fig. 29 it can be seen that for the lowest voltage the diffusion limited regime should apply, while for the highest voltage the geometry limited regime should apply. Therefore the derived expressions for the current can be fitted with the measurements to find the concentration and the

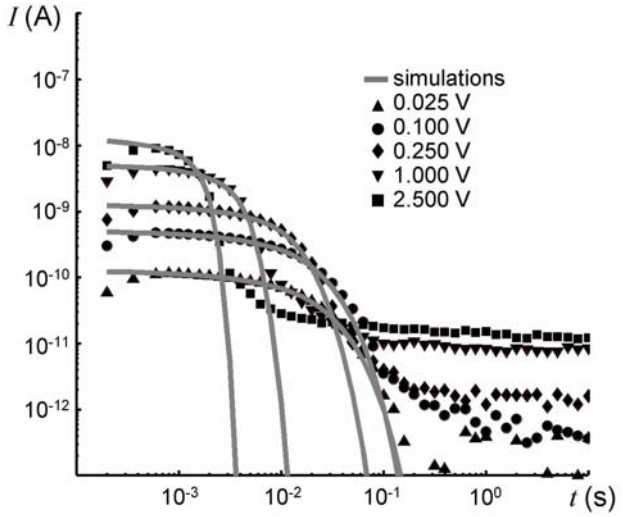

Figure 32:

Current measurements on double logarithmical scale for device 1 (with the lowest charge content), when a voltage step from 0 V to five different voltages is applied (five lowest points in Figure 29). The grey curves are the best fitting simulations. The measurements and the simulations agree, except at very short times (when the charging time of the setup causes an error in the measurement) and at large times (because bulk and electrode reactions are not included in the simulations). The measurements for the lowest and for the highest voltage are shown in the next figure on different scales.

mobility.

For the measurement at 2.5 V the best linear fit of the form $-\hat{A}t+\hat{B}$ is found, which is shown in Fig. 33(a). Using Eq. (64), the concentration and the mobility can then be calculated as:

$$\overline{n}=\frac{1}{2qdS_{el}}\frac{\hat{B}^2}{\hat{A}}, \tag{115}$$

$$\mu=\frac{d^2}{V_A}\frac{\hat{A}}{\hat{B}}. \tag{116}$$

The results for device 1 are also listed in tables II and III.

For the measurement at 25 mV the best exponential fit of the form $I=\hat{C}\exp\left(-\hat{D}t\right)$, shown in Fig. 33(b), is found. Using Eq. (97), the concentration and the mobility can then be calculated as:

$$\overline{n}=\frac{\pi^4 kT}{16q^2dV_AS}\frac{\hat{C}}{\hat{D}}, \tag{117}$$

$$\mu=\frac{qd^2}{\pi^2kT}\hat{D}. \tag{118}$$

The results for device 1 are listed in tables II and III. The good agreement between all estimations for the mobility and the concentration indicates the validity of the theoretical approximations.

It should be noted that for the above estimations one has to know the charge q of the charged inverse micelles. However, by combining the measurements at high and at low voltages, one can also estimate this charge. Combining Eqs. (116) and (118) results in:

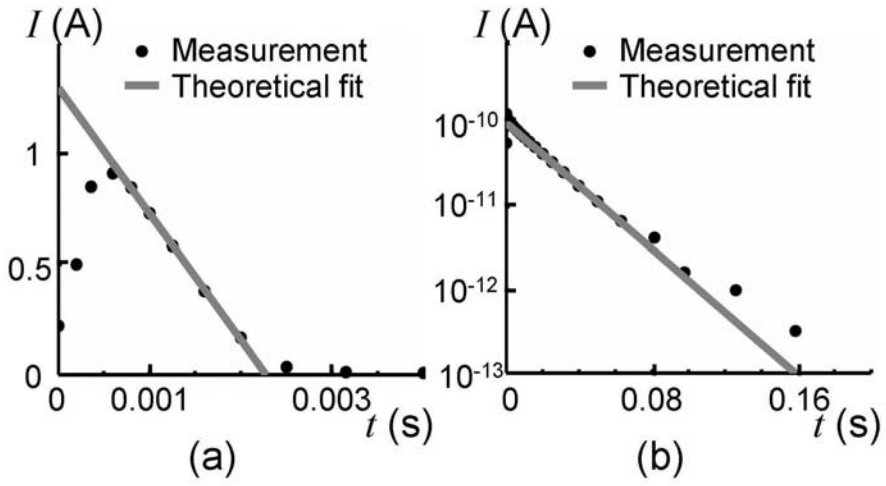

Figure 33:

Fit between theory and measurement for device 1 (with the lowest charge content), when (a) a voltage step from 0 V to 2.5 V is applied (the geometry limited regime), and (b) a voltage step from 0 V to 25 mV is applied (the diffusion limited regime). In (a), the linearly scaled axes make clear the linear decrease of the current in the geometry limited regime. In (b), the semi-logarithmical scale makes clear the exponential decrease of the current in the diffusion limited regime.

$$q = \frac{\pi^2 kT}{V_A} \frac{\hat{A}}{\hat{B}\hat{D}}. \tag{119}$$

For my measurements, this results in a charge of 1.58 x 10^{-19} C, which confirms the results in other works [18][125] that the valency of the charges in the mixture used in this work is 1.

4.4.4. High charge content

The measured currents for five different voltages for the device with the highest λ (Device 5), are shown, together with the simulations, in Fig. 34. Fig. 29 shows that in this case for the lowest voltage the double layer limited regime should apply and for the highest voltage the space charge limited regime.

Similarly as in the previous paragraph, the measurements can be compared with the theoretical expressions for the current to estimate the mobility and the concentration. For the space charge limited regime however, this results in impractical expressions. In this case, it is much easier to find the best fit between the measurement at 2.5 V and Eq. (76) graphically or numerically. This fit is found for the values listed in tables II and III, and is shown in Fig. 35(a).

For the measurement at the lowest voltage, the best exponential fit of the form $I = \hat{C}\exp\left(-\hat{D}t\right)$ is found, which is shown in Fig. 35(b). Using Eq. (111), the concentration and the mobility can be estimated as:

$$\overline{n} = \frac{2kT}{\varepsilon\varepsilon_0 q^2 V_A^2 S^2} \frac{\hat{C}^2}{\hat{D}^2}, \tag{120}$$

$$\mu = \frac{qV_A S\varepsilon\varepsilon_0 d}{4kT}\frac{\hat{D}^2}{\hat{C}}. \qquad (121)$$

The resulting values for device 5 are listed in tables II and III.

Also for this device with high λ the charge q can be estimated. Now Eq. (114) (for the measurement at the highest voltage) and Eq. (121) (for the measurement at the lowest voltage), are combined to find:

$$q = \frac{2kTd}{\varepsilon\varepsilon_0 S V_{A,low} V_{A,high}}\frac{\hat{C}}{\hat{D}^2} I_0 \left(\int_0^{\tau_{dep}} Idt \right)^{-1}. \qquad (122)$$

For my measurements, this results in a charge of 2.03 x 10^{-19} C. Again this confirms the assumption of univalent charges.

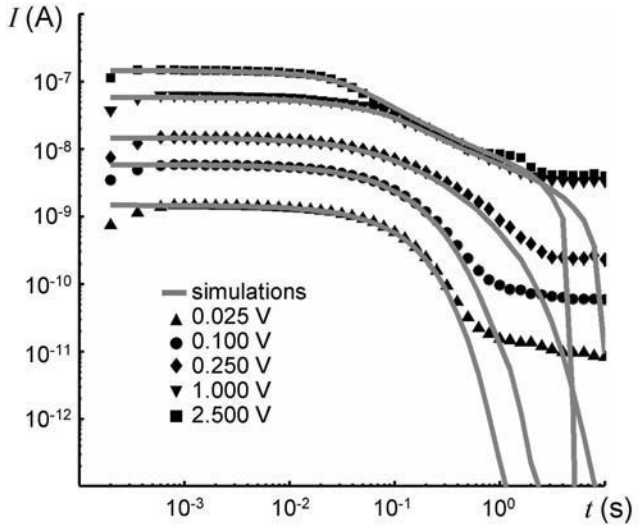

Figure 34:

Current measurements on double logarithmical scale for device 5 (with the highest charge content), when a voltage step from 0 V to five different voltages is applied (five highest points in Figure 29). The grey curves are the best fitting simulations. The measurements and the simulations agree, except at very short times (when the charging time of the setup causes an error in the measurement) and at large times (because bulk and electrode reactions are not included in the simulations). The measurements for the lowest and for the highest voltage are shown in the next figure on different scales.

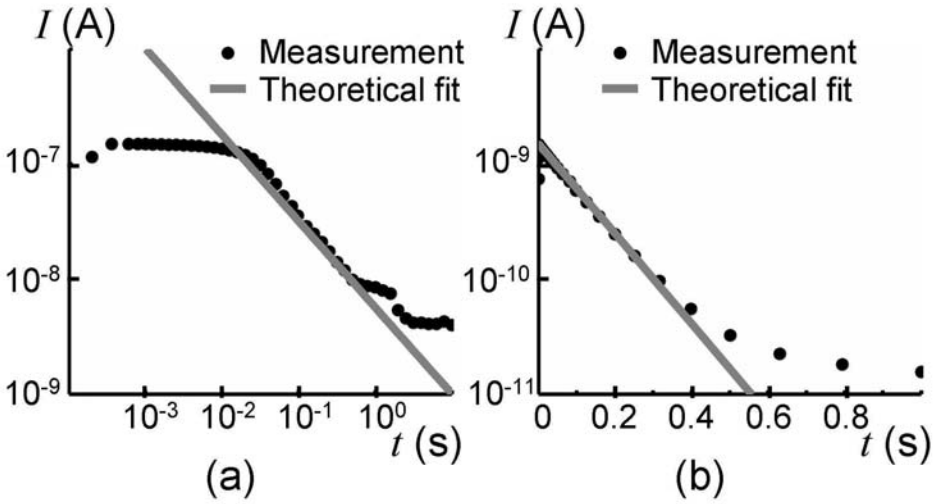

Figure 35:

Fit between theory and measurement for device 5 (with the highest charge content), when (a) a voltage step from 0 V to 2.5 V is applied (the space charge limited regime), and (b) a voltage step from 0 V to 25 mV is applied (the double layer limited regime). In (a), the double-logarithmical scale makes clear the power-law decrease of the current in the space charge limited regime. In (b), the semi-logarithmical scale makes clear the exponential decrease of the current in the double layer limited regime.

4.5. Conclusions

I have derived approximate analytical expressions which are solutions of the Nernst-Planck-Poisson equation, and describe charge transport under the influence of an electric field, in four limiting cases.

In the geometry limited regime, applicable at low charge contents and high voltages, diffusion and the effect of the charges on the electric field are neglected. The only restriction on the external current is then the condition that charges can not move out of the device. This results in a uniform movement of the charges towards the electrodes until the bulk is completely depleted. During this transient, the external current decreases linearly.

In the space charge limited regime, which occurs at high charge contents and high voltages, only diffusion is neglected. Because of the high charge content, I assume the current density in the device to be homogeneous. This results in transient space charge layers, which screen the field in the bulk almost completely, resulting in a -3/4 power law decrease of the current. When the bulk is completely depleted of charges, the space charge layers disappear, the electric field becomes homogeneous again and the current drops quickly to zero.

In the diffusion limited regime, which is valid for low charge contents and low voltages, I neglect the influence of charges on the electric field. Diffusion prevents the charges from separating, which allows me to assume that the total concentration is homogeneous at all times. The

resulting external current decreases exponentially.

In the double layer limited regime, applicable at high charge contents and low voltages, the combination of diffusion and screening of the electric field results in thin double layers in which all variations occur. In the bulk all quantities are homogeneous. I solve this regime by assuming that both the current density and the total concentration are homogeneous over the whole device. Charging the double layers results in an exponentially decreasing current.

The analytical results are tested with detailed numerical simulations. The distribution of charges, the electric field and the external current all correspond very well, both in function of time as in function of position. These results provide a better understanding of various nonlinear effects, which are becoming increasingly important in many practical applications in which the Nernst-Planck-Poisson equations are relevant.

The expressions for the external current are also tested against experiments on a mixture of dodecane and a surfactant, providing a way to determine various important properties of the devices. The good agreement between the results from the different regimes with each other, with numerical fitting and with results from other works, are a strong indication of the experimental validity of each of the four regimes.

Chapter 5
Inverse micelle reactions

After an equilibrium between drift and diffusion is reached for a certain applied voltage, the electric current should be zero. The measurements however show that a small current keeps flowing for a long time. This is a result of the movement of newly generated charged inverse micelles. I measured this 'quasi' steady state current in devices with different properties and for different voltages. An analysis of how the current depends on various parameters allows me to propose a model for the generation and recombination of charged inverse micelles in the bulk and at the electrodes. Together with drift and diffusion, these mechanisms can be combined in a model which describes both the transient and the (quasi) steady state of all the measurements I performed.

5.1. Introduction

The Nernst-Planck-Poisson equations, which model drift, diffusion and screening, describe well the measured currents on short timescales in planar devices containing a mixture of nonpolar liquid and surfactant. According to these equations, charged inverse micelles move when a voltage step is applied, until they reach a new equilibrium distribution. After this transient phase, the charges do not move anymore and the electric current should be zero. The measurements however show that a small current keeps flowing for a very long time [127].

In this chapter, I report measurements of this 'quasi' steady state current in devices with different properties and for different voltages. The measurements indicate that different mechanisms are involved. An analysis of how the current depends on various parameters allows me to propose a model for the generation and recombination of charged inverse micelles, both in the bulk and at the electrodes.

A description of the devices used for the experiments in this chapter and an overview of the measurement results are provided in section 2 of this chapter. The measurements show different behavior at high and low voltages and I treat these two situations separately. Based on the results at high voltages, a model for bulk generation and recombination of charged inverse micelles is proposed in section 3. At low voltages, the measurements can be explained by a model for surface generation and recombination, which I describe in section 4. A combination of these two models, which I treat in section 5 of this chapter, allows to explain the

quasi steady state currents in all situations.

Combined with drift, diffusion and screening, the models for bulk and surface reactions derived in this chapter describe the electric current at all timescales. The number of fitted parameters in this description is limited compared to the amount of different measurements, situations and phenomena that are explained. This gives confidence in the validity of the proposed models to predict the behavior of inverse micelles.

5.2. Measurements

5.2.1. Devices

The devices used for the measurements in this chapter have the same structure as in the previous chapters. They consist of two glass plates, coated with a transparent ITO-electrode with surface area S_{el} = 1 cm^2 (figure 11). The glass plates are attached to each other using UV-curing glue. Spacer beads keep the two plates separated at a distance d. For the measurements in this chapter I made sure that there was no overlap between the electrodes through the glue or through the spacers, to avoid any leakage current. The space between the plates is filled with a mixture of high purity (99.9%) n-dodecane (Aldrich) and different weight percentages of OLOA 1200, which contains 50 wt% mineral oil and 50 wt% of the surfactant polyisobutylene succinimide (Chevron).

I made two series of devices. In the first series, the plates are spincoated with a thin (around 50 nm) layer of polyimide covering the ITO electrode. In the other series, the plates are left uncoated. For each series, I made devices with combinations using the (spacer) diameters 7 µm, 12 µm and 23 µm and the OLOA concentrations 0.1 wt%, 0.2 wt%, 0.5 wt%, 1 wt%, 2 wt% and 5 wt%. Tables IV and V show the measured thickness (obtained from the capacitance of empty cells), the measured initial average concentration of charges (using a fit with simulations, see next paragraph), and the calculated λ-parameter (see chapter 4) for each device. It should be noted that λ is always bigger than 100. The reason why I didn't use concentrations and thicknesses which would result in

Device number	Surfactant concentration (wt%)	Measured $\overline{n}$ (m^{-3})	Measured d (μm)	Estimated λ (no unit)
1A	0.2	1.0×10^{19}	6.9	350
2A	1	5.9×10^{19}	5.7	1380
3A	5	2.2×10^{20}	5.4	4600
4A	0.1	4.9×10^{18}	12.6	560
5A	0.2	9.0×10^{18}	13.9	1260
6A	0.5	2.1×10^{19}	8.9	1190
7A	1	5.6×10^{19}	14.1	8070
8A	2	9.5×10^{19}	13.9	13340
9A	5	2.2×10^{20}	12.2	23700
10A	0.2	1.2×10^{19}	29.3	7700
11A	1	5.1×10^{19}	30.4	34250
12A	5	2.3×10^{20}	23.1	90640

Table IV:

Properties of the devices with a polyimide coating on the electrodes used for the transient current measurements shown in this chapter. The average concentrations are estimated by fitting simulations using drift, diffusion and screening to the measurements. The thicknesses are derived from capacitance measurements on the empty devices. The values for λ are in all devices high enough to be in the double layer limited or space charge limited regime.

smaller values for λ, is that the quasi steady state currents in these devices are in many cases too small to be measured accurately. This also means that the diffusion limited regime and the geometry limited regime (for the voltages up to 5 V used in this chapter) are not covered by measurements in this chapter.

5.2.2. Current measurements

Before every measurement the devices are short-circuited for at least 10000 seconds. Then, at $t = 0$, a step to a voltage between 0.01 V and 5 V is applied and the resulting electric current is measured. The long short-circuiting time ensures that the charges in the device are in equilibrium when the step is applied, not only for drift and diffusion but also for the longer term mechanisms investigated in this chapter. For the same reason, measurements at higher voltages were always performed after measurements at lower voltages.

Figure 36 shows the measured current as a function of time for the

Device number	Surfactant concentration (wt%)	Measured $\overline{n}$ (m^{-3})	Measured d (μm)	Estimated λ (no unit)
1B	0.2	5.0×10^{18}	7.4	200
2B	1	3.8×10^{19}	6.9	1320
3B	5	2.1×10^{20}	5.9	5270
4B	0.1	1.7×10^{18}	10.7	140
5B	0.2	6.3×10^{18}	9.2	390
6B	0.5	2.1×10^{19}	12.3	2300
7B	1	4.6×10^{19}	13	5570
8B	2	9.3×10^{19}	12.3	10130
9B	5	2.7×10^{20}	9.8	18550
10B	0.2	9.2×10^{18}	28.4	5370
11B	1	4.4×10^{19}	25.5	20570
12B	5	2.7×10^{20}	23.2	103580

Table V:

Properties of the devices without polyimide coating on the electrodes used for the transient current measurements shown in this chapter. The average concentrations are estimated by fitting simulations using drift, diffusion and screening to the measurements. The thicknesses are derived from capacitance measurements on the empty devices. The values for λ are in all devices high enough to be in the double layer limited or space charge limited regime.

devices with thickness around 12 μm and with 1 wt% of OLOA 1200, both with and without a polyimide coating, and for different voltages. The figure also shows the simulation, based on drift, diffusion and screening, which fits the experimental results best. One can see that at short times the current is very well described by drift and diffusion, as was already shown in the previous chapter. At longer times however, the simulated current goes to zero while the measurements still show a current, which decreases very slowly. This current can not be ascribed to drift and diffusion of the charges which were initially present in the device. It is these quasi steady state currents that I investigate in this chapter.

5.2.3. Quasi steady state current

In many cases, especially for high voltages, the distinction between the transient part and the quasi steady state part of the current is quite clear and a value for the quasi steady state current can be estimated from the measurement in a reproducible way. In other cases, mostly for low

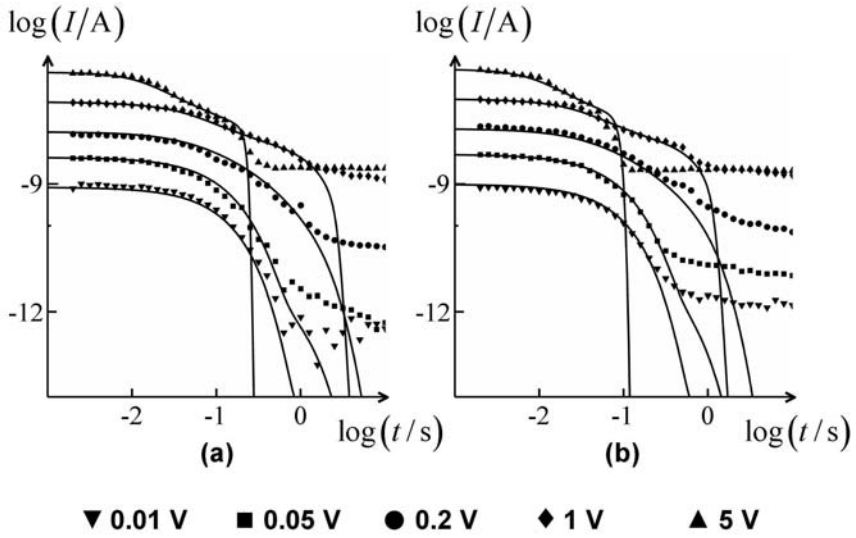

Figure 36:

Measurements of the electric current on devices with spacer thickness 12 µm and surfactant concentration 1 wt% with (a) and without (b) a polyimide coating on the electrodes, when a voltage step is applied after short-circuiting for a long time.The figure also shows the best fitting simulation, using drift, diffusion and screening. These simulations show that the electric current should go to zero as the charges assume a new equilibrium distribution. In the measurements however, a small current remains after the transient period. This 'quasi' steady state current decreases only very slowly.

voltages, the distinction is not so clear. Therefore, I use a formal procedure to obtain the values that I consider to be the quasi steady state values immediately after the transient period. First, for every measurement, the best fitting simulation using drift, diffusion and screening (at short times) is found. This simulated current goes to zero, while there is still a measured current. At the moment when the simulated current is a factor 100 smaller than the measured current I consider the transient phenomenon to be completed. The current measured at this time is used as the estimation for the quasi steady state current.

Figure 37 shows the quasi steady state currents obtained in this way as a function of the applied voltage, for devices with thickness around 12 µm and different concentrations of OLOA, both with and without a polyimide coating. Some important conclusions can be drawn from these measurements. The first one is that for the higher voltages the quasi steady state current is almost independent of the applied voltage. For high concentrations at high voltages it is approximately the same for devices with and without polyimide. At low voltages, there is, for all concentrations, a difference in the quasi steady state current for devices with and without polyimide and the current increases approximately linearly with the voltage. Similar observations can be made in figure 38, which shows the quasi steady state currents as a function of the applied voltage for devices with 1 wt% OLOA and different thicknesses, both with and without a polyimide coating. Because of the difference in behavior for low and high voltages, I will treat these two cases separately in the next two sections. In section 5, the conclusions of sections 3 and 4 will be combined to explain the measurements for all voltages.

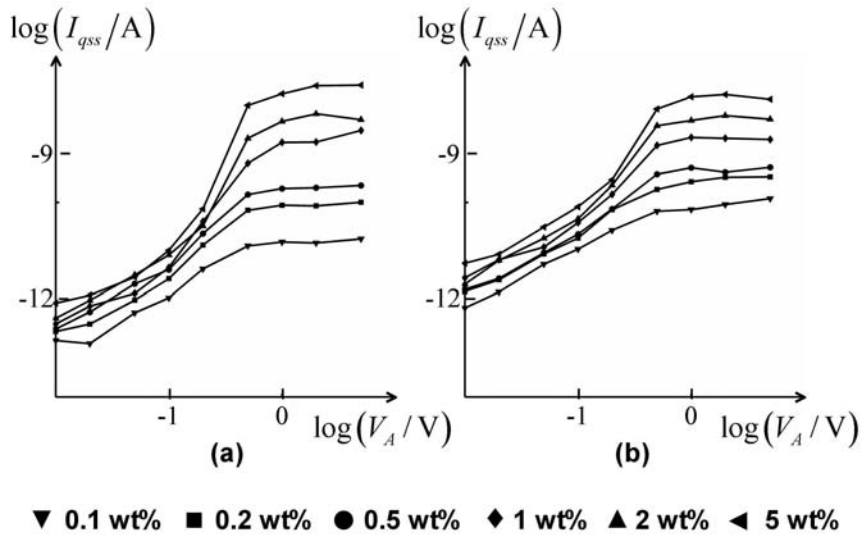

Figure 37:

Measurements of the quasi steady state current as a function of the applied voltage step, in devices with (a) and without (b) polyimide layers on the electrodes, and with a spacer thickness of 12 µm and different concentrations of surfactant. The measured quasi steady state current is, in all devices, approximately independent of the voltage for high voltages, and proportional with the voltage for low voltages. For high surfactant concentrations and high voltages, the quasi steady state current is approximately the same for devices with and without polyimide layers.

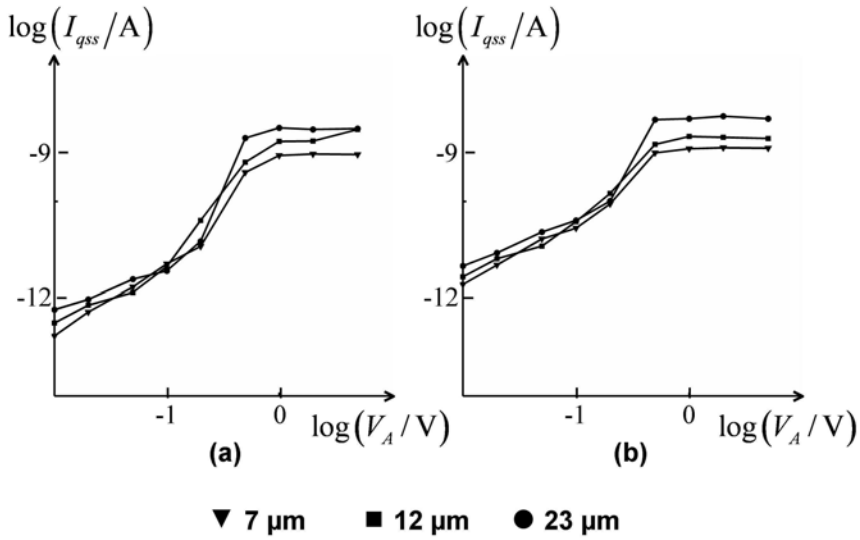

Figure 38:

Measurements of the quasi steady state current as a function of the applied voltage step, in devices with (a) and without (b) polyimide layers on the electrodes, and with a surfactant concentration of 1 wt% and different spacer thicknesses. The measured quasi steady state current is, in all three devices, approximately independent of the voltage for high voltages, and proportional with the voltage for low voltages. For high voltages, the quasi steady state current is approximately the same for devices with and without polyimide layers. For low voltages, there is a difference between the two situations.

5.3. Bulk reactions

5.3.1. Quasi steady state current at high voltages

In the measurements at high voltages, the quasi steady state current is independent of the voltage. There is however, as can be seen on figures 37 and 38, a dependency on the concentration of surfactant and on the thickness of the device. To investigate these dependencies, I measured the quasi steady state current at high voltages (2 V and 5 V) in devices with different combinations of thickness and surfactant concentration, with and without polyimide coating (Tables IV and V).

It is found that the quasi steady state current is best described by a linear dependency on the thickness of the device and a quadratic dependency on the average concentration of charged inverse micelles $\overline{n}$ (figure 39(a)). In devices without a polyimide layer these dependencies are not valid for the lower values of $\overline{n}^2 d$ (figure 39(b)). I will explain this in the following section. In this section, I concentrate on the situations in which the dependency applies.

5.3.2. Bulk generation and recombination

In chapter 3 I showed that, when the effect of surface adsorption and the critical micelle concentration can be neglected (as is the case in the experiments of this chapter), the concentrations of charged and neutral inverse micelles (and also the total concentration) are proportional to the surfactant weight fraction. For the dependency of the quasi steady state

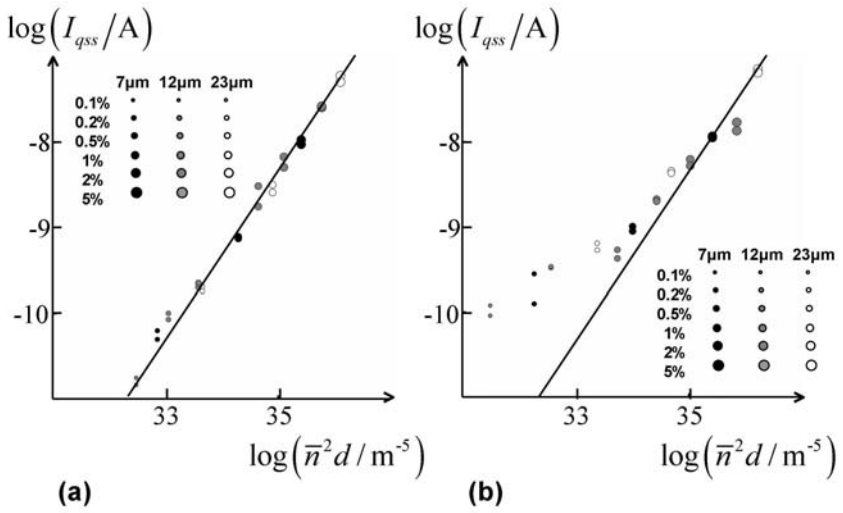

Figure 39:

The measured quasi steady state current at 2 V and 5 V as a function of the combination $\overline{n}^2 d$ of the (fitted) concentration of charged inverse micelles and the measured thickness of the device, for devices with different surfactant concentrations and thicknesses, with (a) and without (b) a polyimide layer on the electrodes. For devices with polyimide layers (a), there is a clear proportionality between the quasi steady state current and $\overline{n}^2 d$. The same proportionality is also visible for the higher values of $\overline{n}^2 d$ in devices without a polyimide coating on the electrodes (b), but not for he lower values of $\overline{n}^2 d$.

current I_{qss} (unit: A) described in the previous paragraph, one can therefore write:

$$I_{qss} \propto c^2 d \propto \overline{n}^2 d \propto \overline{n}_0^2 d \propto \overline{n}_{tot}^2 d \,. \tag{123}$$

The proportionality between the charged inverse micelle concentration and the total inverse micelle concentration was explained in chapter 3 by the disproportionation and comproportionation of inverse micelles. In this section I use these reactions to explain the quasi steady state current.

5.3.2.1. Mechanism

The inverse micelles in a mixture of nonpolar liquid and surfactant are constantly moving around due to thermal diffusion. Because of this movement collisions between two micelles occur all the time in the device. The frequency with which these collisions occur is proportional to the concentrations of both types of inverse micelle involved in the collision. For collisions between oppositely charged micelles the frequency is proportional with $n_+ n_-$, for collisions between two neutral inverse micelles the frequency is proportional with n_0^2 (in which $n_0(x,t)$ (unit: m^{-3}) is the concentration of neutral inverse micelles), and for collisions between charged and neutral inverse micelles the frequency is proportional with $n_\pm n_0$.

A disproportionation or comproportionation occurs when a collision results in the transfer of a charge from one inverse micelle to another [17][18]. One can use the concept in which two colliding inverse micelles momentarily form a bigger inverse micelle (figure 40), in which the

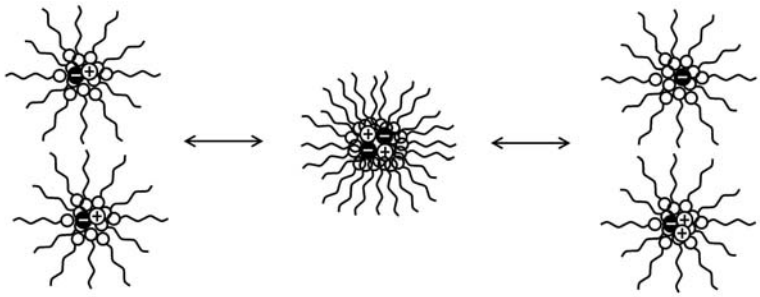

Figure 40:

Schematic representation of the generation and recombination process for inverse micelles. When two inverse micelles collide, they can form momentarily a bigger inverse micelle. This big inverse micelle is not stable and quickly splits up again in two normally sized inverse micelles. In this process, a charge can be exchanged between the two inverse micelles.

interior of the two inverse micelles is mixed. The bigger inverse micelle is not stable, and quickly splits up again in two normally sized inverse micelles. There is a chance that the charges in the interior are not distributed in the same way as they were originally, resulting in a transfer of charge. In chapter 1 I showed that it is difficult for more than univalently charged inverse micelles to remain separated by thermal motion, so only a limited number of types of exchanges are relevant. When two oppositely charged inverse micelles collide, they can exchange a charge resulting in two neutral inverse micelles and vice versa. When an exchange occurs between a charged and a neutral inverse micelle, there is no net effect on the micelle populations.

The reactions between inverse micelles imply that the average concentration of charged inverse micelles $\bar{n}$ does not remain constant over time. The continuity equation (43) does not apply anymore, and has to be replaced by:

$$\frac{\partial n_{\pm}}{\partial t} = -\frac{\partial \Psi_{\pm}}{\partial x} - \alpha n_{+} n_{-} + \beta n_0^2 , \tag{124}$$

in which the recombination constant α (unit: $m^3 \cdot s^{-1}$) and the generation constant β (unit: $m^3 \cdot s^{-1}$) are reaction rate constants describing the charge exchange between two oppositely charged or two neutral inverse micelles. The ratio of these two constants corresponds to the equilibrium constant of the disproportionation / comproportionation reaction:

$$K = \frac{\beta}{\alpha} , \tag{125}$$

for which a numerical value was derived in chapter 3.

The concentration of neutral inverse micelles is strictly speaking not constant and homogeneous, and has to be described by the position and time dependent quantity $n_0(x,t)$. The motion of neutral inverse micelles is due to diffusion and described by the equivalent of equation (41) without the drift term:

$$\Psi_0 = -D \frac{\partial n_0}{\partial x} , \tag{126}$$

in which $\Psi_0(x,t)$ (unit: $m^{-2} \cdot s^{-1}$) is the flux of neutral inverse micelles. The disproportionation and comproportionation reactions have to be included in the continuity equation for neutral inverse micelles:

$$\frac{\partial n_0}{\partial t} = -\frac{\partial \Psi_0}{\partial x} + 2\alpha n_{+} n_{-} - 2\beta n_0^2 . \tag{127}$$

The neutral inverse micelles have no effect on the electric field, but the generation of new charged inverse micelles and their motion will result in an electric current and a continuing change of the field.

5.3.2.2. Bulk generation current

The external electric current is, according to equation (46), proportional to the change of the electric field near the electrode:

$$I = \varepsilon\varepsilon_0 \frac{dE_{el}}{dt} S_{el} . \tag{128}$$

In chapter 4, E_{el} was defined as the field near the electrode, not including any surface charge on the 'liquid side' of the electrode. In this chapter I use the same definition in the case when there is no polyimide layer. However, when there is an insulating polyimide layer on the electrode, I define E_{el} as the field at the interface between the liquid and the polyimide layer, again without including a surface charge on the 'liquid side' of the interface. With this definition, equation (128) is always valid, whether there is a polyimide layer or not.

In the quasi steady state situation for high voltages, all charges are near the electrodes (or near the insulating layers), and the charge on the electrodes can be calculated using equations (13) and (14). The electric field E_{el} near the electrode is directly related to this charge and its quasi steady state value $E_{el,qss}$ (unit: V·m^{-1}) can be expressed as:

$$E_{el,qss} = \left(1 + 2 \frac{d_{IL}/\varepsilon_{IL}}{d/\varepsilon} \right)^{-1} \left(\frac{V_A}{d} + \frac{q_e}{\varepsilon\varepsilon_0} \overline{n} d \right). \tag{129}$$

In this equation, d_{IL} (unit: m) is the thickness of the insulating layers (which is 0 when there are no insulating layers), and ε_{IL} (without unit) is the relative dielectric constant of the insulating layers (which is irrelevant when there are no insulating layers). I assume that the capacitance of the insulating layer is much larger than the capacitance of the device, so in this case one can always write:

$$E_{el,qss} = \frac{V_A}{d} + \frac{q_e}{\varepsilon\varepsilon_0}\bar{n}d\,. \tag{130}$$

In addition, I assume that equation (130) still holds when generation and recombination are important. The average concentration $\bar{n}$ in this case is not constant in time anymore, which is why I call this situation 'quasi' steady state. Combining equations (128) and (130) results in:

$$I_{qss} = q_e \frac{d\bar{n}}{dt} S_{el} d\,. \tag{131}$$

The change over time of the average concentration $\bar{n}$ can be found by integrating equation (124) over the whole device and dividing the result by the device thickness:

$$\frac{\partial\bar{n}}{\partial t} = -\frac{1}{d}\left(\Psi_{\pm}\left(\frac{d}{2}\right) - \Psi_{\pm}\left(-\frac{d}{2}\right)\right) - \frac{\alpha}{d}\int_{-d/2}^{d/2} n_+ n_- dx + \frac{\beta}{d}\int_{-d/2}^{d/2} n_0^2 dx\,. \tag{132}$$

The first term in the right hand side of this equation is zero because of the blocking electrode boundary conditions. The second term is approximately zero because, for high voltages, the steady state distributions (and thus, by assumption, also the quasi steady state distributions) of positive and negative charges are completely separated. For the third term I assume that the distribution of neutral inverse micelles is approximately homogeneous. Equations (131) and (132) can

then be combined to find:

$$I_{qss} = q_e S_{el} \beta \overline{n}_0^2 d \,, \tag{133}$$

which explains the dependencies in equation (123).

Equation (130) is valid for the geometry limited regime and in the space charge limited regime. For the regimes at low voltages, it does not apply. The diffusion limited regime is not relevant in this chapter, but one can easily see that the generation current would be negligible according to the proposed mechanism, since the electric field near the electrodes is practically undisturbed by the charges in the device. The measurements at low voltages in this chapter are all examples of the double layer limited regime. The quasi steady state current predicted by the model of bulk generation and recombination in the double layer limited regime has been derived in [18] and can be expressed as:

$$I_{qss} = \frac{\varepsilon\varepsilon_0 \alpha S_{el} \overline{n}}{16 d} \left(\frac{q_e}{kT} \right)^2 f^4 V_A^2 \,, \tag{134}$$

with

$$f = \left(1 + \frac{d_{IL}/\varepsilon_{IL}}{\lambda_{DL}/\varepsilon} \right)^{-1} . \tag{135}$$

The correction factor f (without unit) takes into account the influence of the insulating layer. Unlike the correction factor in equation (129), one can not simply assume that $f = 1$, because the Debye length can be of the same order of magnitude as the thickness of the insulating layers. However, I found that all measurements (with and without polyimide layers) can be explained best by simulations which do not include insulating layers. A possible explanation is that the polyimide is in fact not

a good insulator, but allows charges from the electrodes to move through it. Therefore, I do not set $f = 1$ in the theoretical description (because for other materials it may be relevant), but I do assume $f = 1$ when I fit theoretical expressions to the measurements.

5.3.3. Agreement with measurements

Using equations (26) and (29), equation (133) can be fitted with the measurements in figure 39(a) to find a value for the generation constant β:

$$\beta = 6.4 \times 10^{-25} \text{ m}^3 \cdot \text{s}^{-1}. \tag{136}$$

Using equation (125), the following value for the recombination constant is found:

$$\alpha = 1.8 \times 10^{-21} \text{ m}^3 \cdot \text{s}^{-1}. \tag{137}$$

The best fit in figure 39(a) is also plotted on figure 39(b), and shows that for high concentrations and thicknesses, the quasi steady state current at high voltages is explained well by the model of bulk generation and recombination, both for devices with and without polyimide layers on the electrodes. For low concentrations and thicknesses the quasi steady state current is not well explained by the model of bulk generation and recombination.

In figure 41, the external electric current as a function of time, resulting from a simulation including generation and recombination is compared to the measurements of figure 36. One can see that for high voltages the

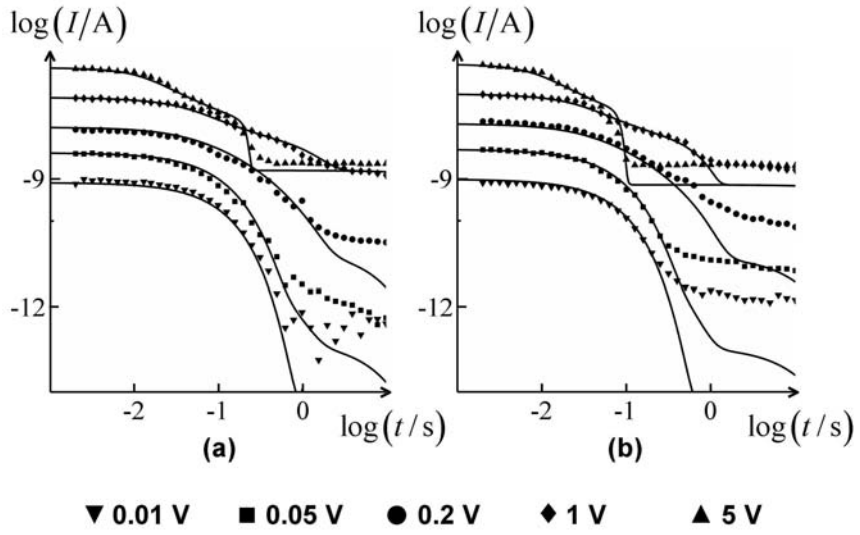

Figure 41:

Measurements of the electric current on devices with spacer thickness 12 µm and surfactant concentration 1 wt% with (a) and without (b) a polyimide coating on the electrodes, when a voltage step is applied after short-circuiting for a long time.The figure also shows the best fitting simulation, using drift, diffusion, screening and bulk generation and recombination. For high voltages the simulations are in agreement with the measurements, especially for the device with polyimide layers. For low voltages however, the measured current is higher than predicted by bulk generation and recombination.

quasi steady state current is described well. However, for low voltages there is a clear difference between measurement and simulation.

The same conclusion can be drawn from figures 42 and 43, which show the measured and simulated quasi steady state current as a function of voltage, for a fixed thickness and different concentrations of surfactant (figure 42) and for a fixed concentration and different thicknesses (figure 43). For low voltages, it is clear that another mechanism is involved. The important difference between the measurement results for devices with and without polyimide layers indicates that this effect is related to the surfaces of the device rather than to the bulk of the liquid.

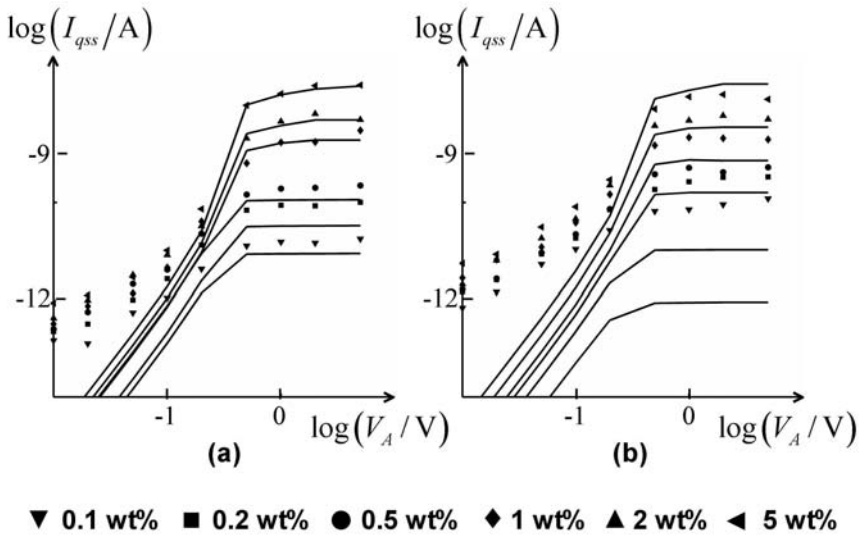

Figure 42:

Measurements of the quasi steady state current as a function of the applied voltage step (dots), in devices with (a) and without (b) polyimide layers on the electrodes, and with a spacer thickness of 12 µm and different concentrations of surfactant. The figure also shows the results of simulations using bulk generation and recombination (lines). The simulations are in agreement with the measurements at high voltages, except at the devices without polyimide and with lower surfactant concentrations. For low voltages, the current is not well described by bulk generation and recombination.

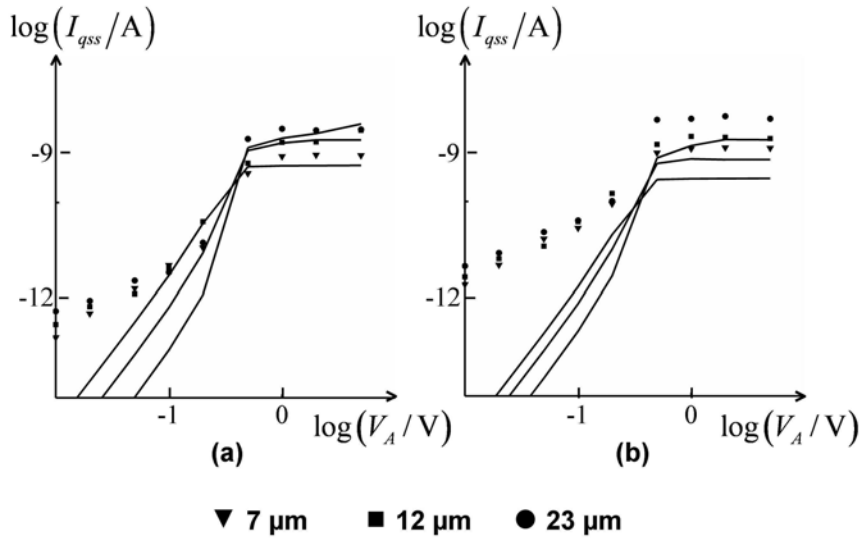

Figure 43:

Measurements of the quasi steady state current as a function of the applied voltage step (dots), in devices with (a) and without (b) polyimide layers on the electrodes, and with a surfactant concentration of 1 wt% and different spacer thicknesses. The figure also shows the results of simulations using bulk generation and recombination (lines). The simulations are in agreement with the measurements at high voltages in the devices without polyimide. For low voltages, the current is not well described by bulk generation and recombination.

5.4. Surface generation and recombination

5.4.1. Quasi steady state current at low voltages

The fact that, for low voltages, the measured quasi steady state current is significantly different for devices with and without polyimide layers, suggests that reactions near the surfaces of the device are responsible for this current. An additional argument for this hypothesis is that in the double layer limited regime, which is applicable for all low voltage measurements in this chapter, all quantities only vary in a thin double layer near the electrodes. In the bulk the concentrations are approximately equal to the initial homogeneous distribution, and the electric field is almost zero. The situation in the bulk is therefore almost the same as during the equilibrium before the voltage step was applied (and in which there was no current).

Based on the important role of the double layer, I looked for a relation between the quasi steady state current and quantities near the electrodes (or near the polyimide layers). An important quantity is the electric field near the electrodes which (for the double layer limited regime in steady state) follows from equation (100), but more accurately from [18] or [120], in which the influence of the insulating layers is taken into account:

$$E_{el,qss} = f\frac{V_A}{2\lambda_{DL}} = f\frac{\sqrt{kT}}{V_T\sqrt{2\varepsilon\varepsilon_0}}V_A\sqrt{n}\,, \tag{138}$$

Two other quantities are the quasi steady state concentrations $n_{\pm,el,qss}$ (unit: m^{-3}) of positively and negatively charged inversed micelles near the electrodes, which can also be found in [18] or [120] for the case of the

double layer limited regime with insulating layers:

$$n_{\pm,el,qss} = \overline{n}\left(1 \mp \frac{f}{2}\frac{V_A}{V_T}\right). \tag{139}$$

This equation is valid for the electrode at $x = -d/2$. At the other electrode the concentration of positive charges is equal to the concentration of negative charges at $x = -d/2$ and vice versa. The remaining quantity near the surface is the concentration of neutral inverse micelles in steady state $n_{0,el,qss}$ (unit: m^{-3}), which I assume to be equal to the initial average concentration of neutral inverse micelles:

$$n_{0,el,qss} = \overline{n}_0 = \overline{n}\sqrt{\frac{\alpha}{\beta}}\,. \tag{140}$$

I find that the quasi steady state current at low voltages is best described as being proportional to the electric field near the electrodes. Figure 44 shows the measured quasi steady state current for voltages up to 0.1 V, as a function of the steady state electric field at the electrode, obtained from a fitted simulation including only drift and diffusion. The proportionality of the quasi state current with the electric field at the electrodes is remarkable, both for devices with and without polyimide layers. However, the proportionality constant is not the same for the two cases.

5.4.2. Surface generation and recombination

The fact that the quasi steady state current only depends on the electric field near the electrodes (and not on the surfactant concentration) is surprising. If the mechanism responsible for the quasi steady state current

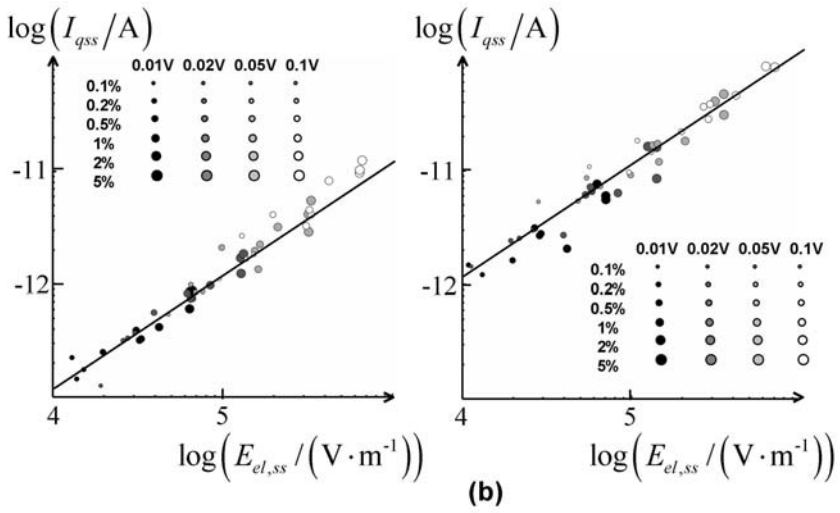

Figure 44:

The measured quasi steady state current at low voltages (0.01 V, 0.02 V, 0.05 V and 0.1 V) as a function of the steady state electric field at the electrodes, obtained from simulations using drift, diffusion and screening, for devices with different thicknesses and surfactant concentrations. Both for devices with (a) and without (b) a polyimide coating on the electrodes, there is a linear dependence between the quasi steady state current and the steady state electric field at the electrodes. The proportionality constant is not the same for the two series of devices.

at low voltages would involve a reaction with inverse micelles, one would expect the current to depend on the concentration of (one or more kinds of) inverse micelles. This is apparently not the case. In the model that I propose, I explain this by assuming that the reactions at the surface are not limited by the availability of inverse micelles. The physical mechanism that I describe in this section explains the measurements well. However, there may be alternative explanations. Additional experiments to confirm or falsify the mechanism I propose have to be carried out.

5.4.2.1. Mechanism

In order to explain the quasi steady state current, I will make a number of assumptions. First, I assume that there is a layer of adsorbed surfactant molecules on the surfaces (figure 45), which corresponds to the conclusion of chapter 3 for the case of devices without a polyimide coating. In the case of devices with a polyimide coating I could not conclude on the existence of an adsorbed surfactant layer from the measurements in chapter 2. This does not necessarily mean that there is no such layer, it could also be explained by a low surface concentration of adsorbed surfactant molecules, which is not discernible in the measurements. The layer enclosed between the adsorbed surfactant and the electrode (or polyimide) is polar, and can contain (positive and negative) charges (figure 45). If there is an electric field in this layer, these charges feel a force. In the case of an electric field pointing towards the liquid (near the left electrode), positive charges can lower their potential energy by moving into the liquid. I assume that this energy disturbs the preference of adsorption of surfactant molecules, compared to the

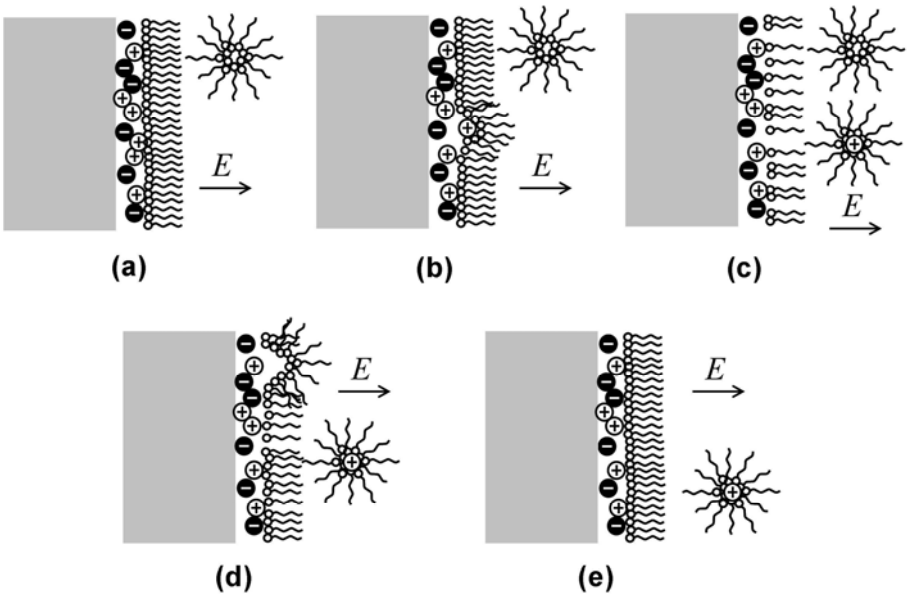

Figure 45:
Schematic representation of the model for surface generation and recombination proposed in this chapter. (a) Surfactant molecules do not only form inverse micelles, but also adsorb at surfaces, resulting in a small polar layer in which charges exist. (b) When there is an electric field, the charges feel a force, disturbing the equilibrium between micellization and surafce adsorption. (c) This results in the generation of charged inverse micelles at the surface. (d) The surfactant molecules which formed the inverse micelle are replaced by molecules from another inverse micelle. (e) The overall result of the reaction is that a (charged or neutral) inverse micelle has been replaced by a charged inverse micelle.

formation of inverse micelles. In other words, the electric field causes adsorbed surfactant molecules to desorb together with the positive charge and form a positively charged inverse micelle (figure 45). I model the generation of charged inverse micelles at the surfaces by a flux $\Psi_{\pm,inj}$ (unit: $m^{-2} \cdot s^{-1}$), proportional to the electric field:

$$\begin{aligned} \Psi_{+,inj}\left(-\frac{d}{2}\right) &= -\Psi_{-,inj}\left(\frac{d}{2}\right) = \zeta E_{el} \quad \left(E_{el} > 0\right) \\ \Psi_{-,inj}\left(-\frac{d}{2}\right) &= -\Psi_{+,inj}\left(\frac{d}{2}\right) = \zeta E_{el} \quad \left(E_{el} < 0\right) \end{aligned} \quad . \tag{141}$$

In these equations, the surface generation constant ζ (unit: $m^{-1} \cdot V^{-1} \cdot s^{-1}$) describes the proportionality with the electric field at the electrodes.

If there would only be generation of inverse micelles at the surfaces, the adsorbed surfactant layers would quickly disappear and the process would stop. Therefore, I assume that the surfactant molecules which form new inverse micelles are instantly replaced by surfactant molecules from existing inverse micelles (figure 45). I assume that each type of inverse micelle (positive, negative or neutral) has the same affinity for adsorption at the surface, so the different fluxes are weighed by the concentrations of the different types of inverse micelles at the surfaces. I assume that the availability of inverse micelles is not a limiting factor in this process: every generated inverse micelle at the surface is immediately replaced by another inverse micelle. The adsorption flux for the different kinds of inverse micelles is described by the following equations:

$$\Psi_{\bullet,ads}\left(\pm\frac{d}{2}\right)=-\frac{n_{\bullet}\left(\pm\frac{d}{2}\right)}{n_{tot}\left(\pm\frac{d}{2}\right)}\Psi_{\mp,inj}\left(\pm\frac{d}{2}\right)\qquad\left(for\ E_{el}>0\right)$$
$$\Psi_{\bullet,ads}\left(\pm\frac{d}{2}\right)=-\frac{n_{\bullet}\left(\pm\frac{d}{2}\right)}{n_{tot}\left(\pm\frac{d}{2}\right)}\Psi_{\pm,inj}\left(\pm\frac{d}{2}\right)\qquad\left(for\ E_{el}<0\right)$$, (142)

in which the '•' can be replaced by either '+', '-' or '0'. In theory, these equations are unphysical when there are no inverse micelles near the surface. In practice however, for the situations that I investigated this case does not occur.

The total fluxes for each type of inverse micelle, which replace the blocking electrode boundary conditions, are the sum of the contributions in equations (141) and (142). They can be written concisely for all situations (positive and negative electrode, positive and negative field, positive, negative and neutral inverse micelles) as:

$$\Psi_{\bullet}\left(\pm\frac{d}{2}\right)=\mp\left(\bullet\frac{\bullet E_{el}\mp\left|E_{el}\right|}{2E_{el}}-\frac{n_{\bullet}\left(\pm\frac{d}{2}\right)}{n_{tot}\left(\pm\frac{d}{2}\right)}\right)\zeta\left|E_{el}\right|, \qquad (143)$$

in which the '•', when it is not used as an index, has to be interpreted as either '1×', '-1×' or '0×', for positive, negative and neutral inverse micelles, respectively.

5.4.2.2. Surface generation current

In quasi steady state, the current density $J_{el,qss}$ (unit: C·m^{-2}·s^{-1}) at the surfaces which corresponds to the fluxes in equation (143) can be written as:

$$J_{el,qss} = J_{qss}\left(\frac{d}{2}\right) = J_{qss}\left(-\frac{d}{2}\right) = \left(1 - \frac{n_{+,el,qss} - n_{-,el,qss}}{n_{+,el,qss} + n_{0,el,qss} + n_{-,el,qss}}\right)\zeta q_e E_{el,qss} \quad . \tag{144}$$

For low voltages, the concentrations of charged inverse micelles near the electrodes are much smaller than the concentration of neutral inverse micelles, because of the very low value of the equilibrium constant K. In this case, equation (144) reduces to:

$$J_{el,qss} = \zeta q_e E_{el,qss} \, , \tag{145}$$

For high voltages, the concentration of positively charged inverse micelles near the positive electrode is zero, and the concentration of neutral inverse micelles can be neglected compared to the concentration of negative inverse micelles. In this case, equation (144) can be written as:

$$J_{el,qss} = 2\zeta q_e E_{el,qss} \, . \tag{146}$$

When the electrodes are not perfectly blocking, equation (128) is not valid anymore, because a conduction current must be added:

$$I_{qss} = \left(J_{el,qss} + \varepsilon\varepsilon_0 \frac{dE_{el,qss}}{dt} \right) S_{el} . \tag{147}$$

In this section, I assume that the second term in this equation can be neglected compared to the first term. This assumption is not obviously valid, so it requires some justification. Consider the limit of a very low voltage. The surfactant molecules used to generate charged inverse micelles at the surface are then almost all replaced by the molecules from neutral inverse micelles in the bulk. This means that the average amount of charged inverse micelles increases over time. One can calculate that this increase is described (in the case of a positive voltage and thus a positive current density at the electrodes) by:

$$\frac{d\bar{n}}{dt} = \frac{J_{el,qss}}{q_e d} . \tag{148}$$

Combining this equation with the derivative with respect to time of equation (138) results in:

$$\frac{dE_{el,qss}}{dt} = f \frac{\sqrt{kT}}{2q_e\sqrt{2\varepsilon\varepsilon_0}} \frac{V_A}{V_T} \frac{1}{d\sqrt{\bar{n}}} J_{el,qss} . \tag{149}$$

With λ and φ defined as in the previous chapter, equation (147) can then be written as:

$$I = \left(1 + \frac{f}{2} \frac{\varphi}{\sqrt{\lambda}} \right) J_{el,qss} S_{el} . \tag{150}$$

Even for f =1, its maximal value, and λ =100, the lowest value for the measurements in this chapter, the value of the second term between the brackets is 0.2 for 100 mV, the largest voltage used in figure 44. This justifies that, for low voltages, the second term in equation (147) can be neglected. For high voltages, the reason is different. In this case every

generated charged inverse micelle is replaced by an oppositely charged inverse micelle. This happens symmetrically at both electrodes, so the effect is that $\overline{n}$, and thus $E_{el,qss}$, does not change over time.
With the assumption that the second term in equation (147) can be neglected, the quasi steady state current at low voltages can be found by combining equations (145) and (147):

$$I_{qss} = \zeta q_e S_{el} E_{el,qss}, \tag{151}$$

which is consistent with the results in figure 44. Using equation (138) the quasi steady state current at low voltages is then:

$$I_{qss} = \zeta q_e S_{el} f \frac{\sqrt{kT}}{V_T \sqrt{2\varepsilon\varepsilon_0}} V_A \sqrt{\overline{n}}\,. \tag{152}$$

At high voltages, the current can be calculated in a similar way to be:

$$I_{qss} = 2\zeta q_e S_{el} \left(\frac{V_A}{d} + \frac{q_e}{\varepsilon\varepsilon_0} \overline{n} d \right). \tag{153}$$

5.4.3. Agreement with measurements

Equation (152) can be fitted to the measurements in figure 44 to find the surface generation constant ζ. The best fits are shown on the figure. In the case of devices with a polyimide layer, the resulting value is:

$$\zeta = 6.8\times10^{5}\ \mathrm{m^{-1}\cdot V^{-1}\cdot s^{-1}}. \tag{154}$$

For devices without a polyimide layer on the electrodes, the best fit is found for:

$$\zeta = 7.3\times10^{6}\ \mathrm{m^{-1}\cdot V^{-1}\cdot s^{-1}}. \tag{155}$$

In figure 46, the external electric current as a function of time, resulting from a simulation including surface generation and recombination is compared with the measurements of figure 36. One can see that for low voltages the quasi steady state current is described well. For high voltages and devices without polyimide the agreement is also good, but for devices with polyimide there is a clear difference between measurement and simulation.

Similar conclusions can be drawn from figures 47 and 48, which show the measured and simulated quasi steady state current in function of voltage, for a fixed thickness and different concentrations of surfactant (figure 47) and for a fixed concentration and different thicknesses (figure 48).

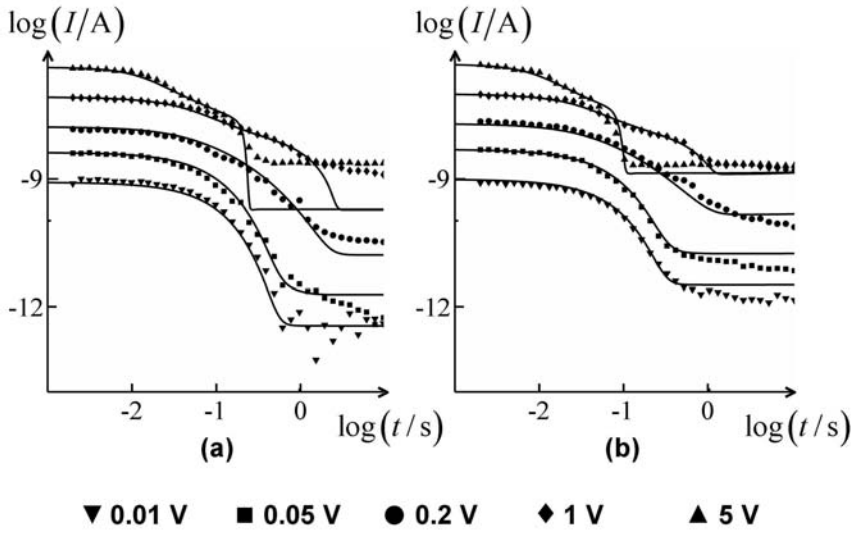

Figure 46:

Measurements of the electric current on devices with spacer thickness 12 µm and surfactant concentration 1 wt% with (a) and without (b) a polyimide coating on the electrodes, when a voltage step is applied after short-circuiting for a long time.The figure also shows the best fitting simulation, using drift, diffusion, screening and surface generation and recombination. For low voltages the simulations are in agreement with the measurements. For low voltages however, the measured current in the device with a polyimide layer on the electrodes is higher than predicted by the model for surface generation and recombination.

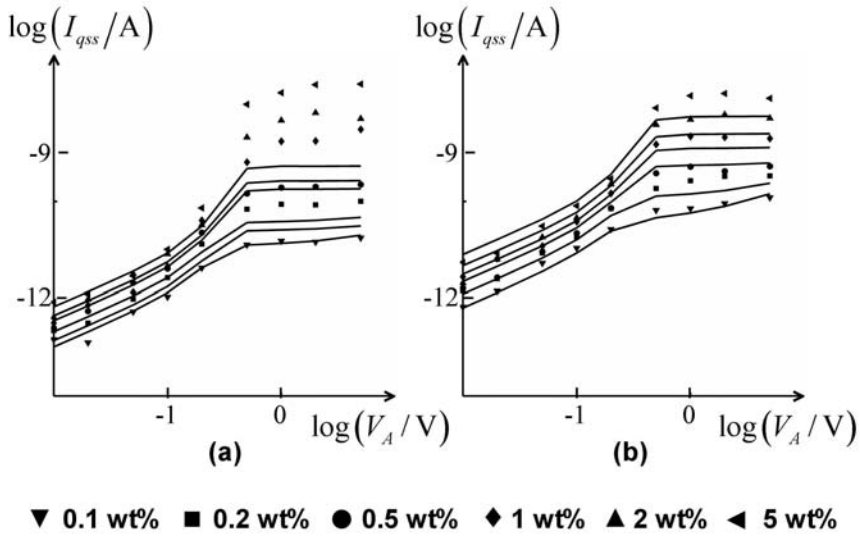

Figure 47:

Measurements of the quasi steady state current as a function of the applied voltage step (dots), in devices with (a) and without (b) polyimide layers on the electrodes, and with a spacer thickness of 12 µm and different concentrations of surfactant. The figure also shows the results of simulations using surface generation and recombination (lines). At low voltages, measurements and simulations agree very well, both in devices with and without polyimide layers. At high voltages the simulated currents agree fairly well with the measurements on devices without polyimide, but are too low in devices with polyimide.

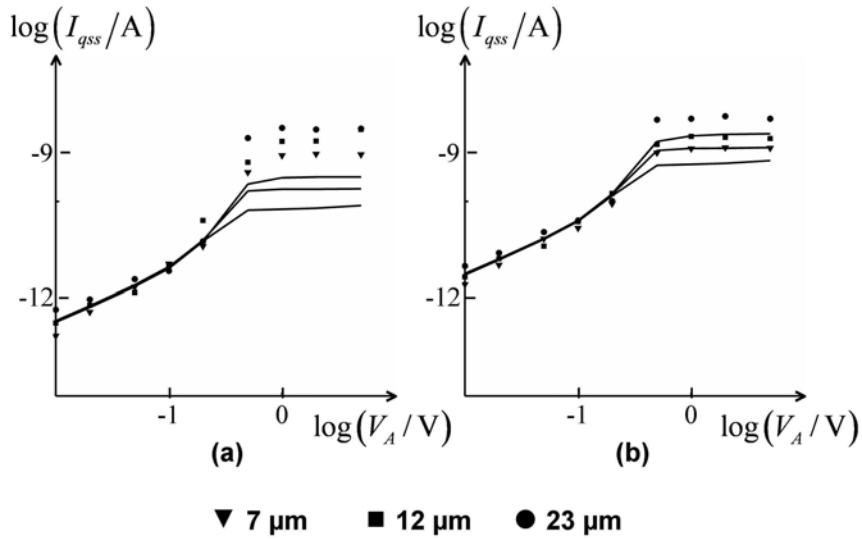

Figure 48:

Measurements of the quasi steady state current as a function of the applied voltage step (dots), in devices with (a) and without (b) polyimide layers on the electrodes, and with a surfactant concentration of 1 wt% and different spacer thicknesses. The figure also shows the results of simulations using surface generation and recombination (lines). At low voltages, measurements and simulations agree very well, both in devices with and without polyimide layers. At high voltages the simulated currents agree fairly well with the measurements on devices without polyimide, but are too low in devices with polyimide.

5.5. Combined bulk and surface reactions

In the previous two sections I showed that the model for bulk generation and recombination describes the measurements well at high voltages, but results in a too low quasi steady state current at low voltages. The model for surface generation and recombination is in good agreement with the measurements at low voltages, but results in a too low quasi steady state current at high voltages. Neither of the two models alone can explain all measurements. The logical next step is to combine them into one model.

5.5.1. Complete model

The full set of differential equations describing the behavior of inverse micelles in planar devices (in the case of a positive applied voltage and no insulating layer) includes the Nernst Planck equations, which model drift and diffusion:

$$\Psi_{\bullet} = \bullet \mu n_{\bullet} E - D \frac{\partial n_{\bullet}}{\partial x}, \tag{156}$$

In which, as in the previous section, for positive, negative or neutral inverse micelles, • should be replaced by '+', '-' or '0' respectively, when it is used as an index, and by '+1×', '-1×' or '0×', respectively, when it is not used as an index. The influence of the charges on the electric field is modeled by the equation of Gauss:

$$\varepsilon\varepsilon_0 \frac{\partial E}{\partial x} = q_e \left(n_+ - n_- \right), \tag{157}$$

together with the condition:

$$\int_{-d/2}^{d/2} E dx = V_A \,. \tag{158}$$

Bulk generation and recombination are included in the continuity equations:

$$\begin{aligned} \frac{\partial n_{\pm}}{\partial t} &= -\frac{\partial \Psi_{\pm}}{\partial x} - \alpha n_+ n_- + \beta n_0^2 \\ \frac{\partial n_0}{\partial t} &= -\frac{\partial \Psi_0}{\partial x} + 2\alpha n_+ n_- - 2\beta n_0^2 \end{aligned}, \tag{159}$$

and surface generation and recombination are included in the boundary conditions:

$$\Psi_{\bullet}\left(\pm\frac{d}{2}\right) = \mp\left(\bullet\frac{\bullet 1 \mp 1}{2} - \frac{n_{\bullet}\left(\pm\frac{d}{2}\right)}{n_{tot}\left(\pm\frac{d}{2}\right)}\right)\zeta E_{el} \,. \tag{160}$$

The set of equations is completed with the initial distribution of inverse micelles, which is in the context of this work always homogeneous:

$$\begin{aligned} n_+(t=0) &= n_+(t=0) = \overline{n} \\ n_0(t=0) &= \overline{n}\sqrt{\frac{\alpha}{\beta}} \end{aligned} \,. \tag{161}$$

5.5.2. Agreement with measurements

In figure 49, the external electric current as a function of time, resulting from a simulation of the full model in the previous paragraph is compared with the measurements of figure 36. The current for all voltages is described well by the model, both for devices with and without a

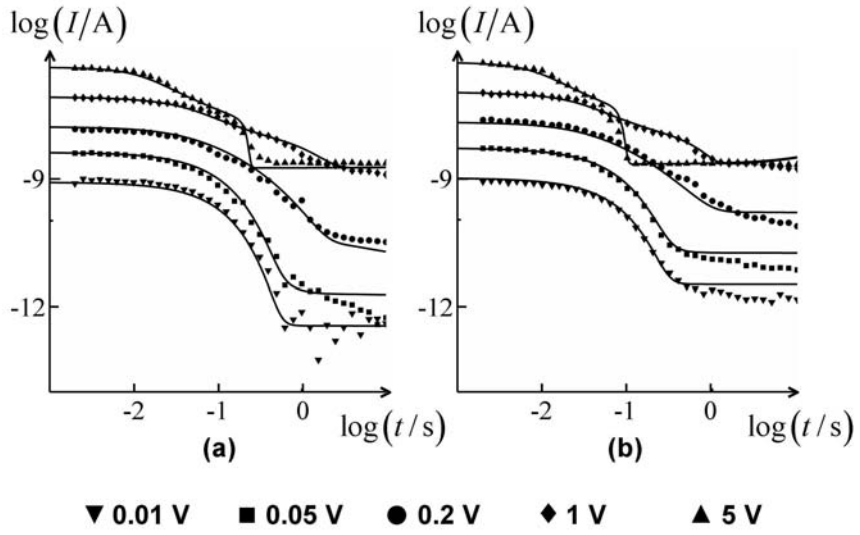

Figure 49:

Measurements of the electric current on devices with spacer thickness 12 µm and surfactant concentration 1 wt% with (a) and without (b) a polyimide coating on the electrodes, when a voltage step is applied after short-circuiting for a long time.The figure also shows the best fitting simulation, using drift, diffusion, screening and both bulk and surface generation and recombination. The measurements and the simulations are in good agreement, both for devices with and without polyimide layers, and both for low and high voltages.

polyimide layer on the electrodes.

The good agreement can also be seen on figures 50 and 51, which show the measured and simulated quasi steady state current in function of voltage, for a fixed thickness and different concentrations of surfactant (figure 50) and for a fixed concentration and different thicknesses (figure 51).

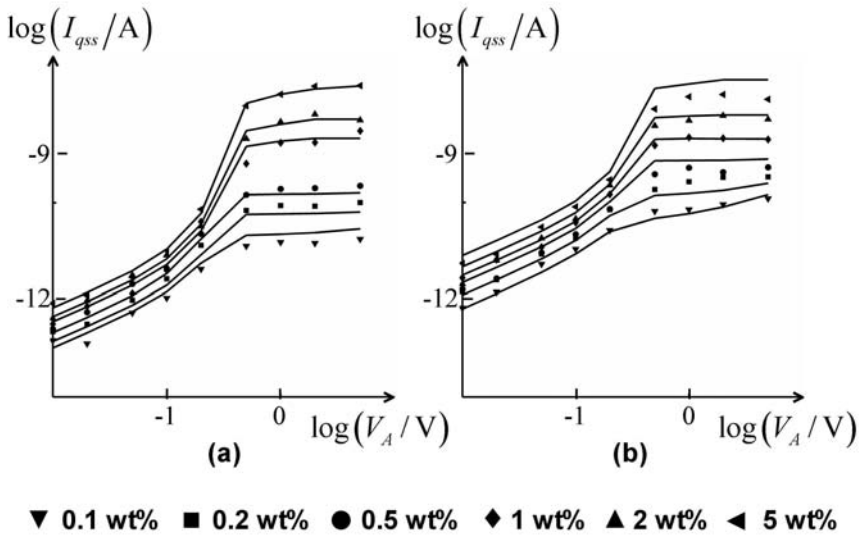

Figure 50:

Measurements of the quasi steady state current as a function of the applied voltage step (dots), in devices with (a) and without (b) polyimide layers on the electrodes, and with a spacer thickness of 12 µm and different concentrations of surfactant. The figure also shows the results of simulations combining bulk and surface generation and recombination (lines). The measurements and the simulations are in good agreement, both for devices with and without polyimide layers, and both for low and high voltages.

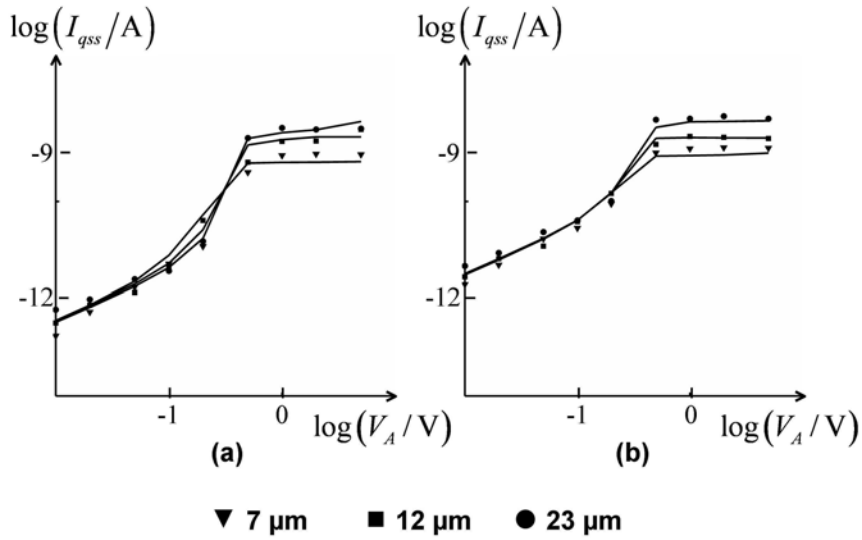

Figure 51:

Measurements of the quasi steady state current as a function of the applied voltage step (dots), in devices with (a) and without (b) polyimide layers on the electrodes, and with a surfactant concentration of 1 wt% and different spacer thicknesses. The figure also shows the results of simulations combining bulk and surface generation and recombination (lines). The measurements and the simulations are in good agreement, both for devices with and without polyimide layers, and both for low and high voltages.

5.6. Conclusions

When a voltage step is applied over the electrodes of a planar device containing a mixture of nonpolar liquid and surfactant, charged inverse micelles move to reach a new equilibrium distribution. This movement results in an external electric current, which should go to zero if there would be only drift, diffusion and screening. The measurements however show that a small current remains after the transient period. This 'quasi' steady state current decreases only very slowly.

I measured this quasi steady state current for different voltages in devices with different thicknesses and surfactant concentrations, with and without a polyimide layer on the electrodes. The observed dependencies allowed me to propose a model to explain the quasi steady state currents. This model includes two mechanisms for generation and recombination of charged inverse micelles. In the first mechanism, the reactions happen in the bulk of the liquid. In the second mechanism, the reactions happen at the surfaces. Both mechanisms are necessary to describe the measurements.

Together with drift, diffusion and screening, the proposed mechanisms provide a full description of the electric current on different timescales when a voltage step from 0 V is applied on a planar device with nonpolar liquid and surfactant. The number of fitted parameters in this description is far less than the amount of different measurements, situations and phenomena that are explained. This gives confidence about the ability of the proposed models to predict the behavior of inverse micelles.

Chapter 6
Conclusions

Surfactant molecules in nonpolar liquids adsorb at interfaces and self-aggregate into inverse micelles. The layers of surfactant which are formed in this way provide a barrier which keeps opposite charges separated, stabilizing them on the surface of colloidal particles or in the interior of inverse micelles. Surfactants are used as charging agents in many applications, one of which is electrophoretic display technology. In electrophoretic displays, the movement of charged pigment particles in a nonpolar liquid under the influence of an electric field causes the pixels to change color. Charged inverse micelles can influence the behavior of these displays.

During my PhD research, I investigated inverse micelles in a nonpolar liquid by performing current measurements on one-dimensional devices

with planar ITO electrodes, containing a mixture of n-dodecane and OLOA 1200. Nonpolar liquids, even with surfactant, contain few charges and the electric currents are small. I developed a setup which can measure electric currents fast and accurately over a wide range and during a long time. This measurement setup is especially suited to measure currents when a voltage step is applied over the electrodes.

Analysis of transient current measurements allowed me to estimate the mobility and concentration of charged inverse micelles. From these values, I derived characteristics about the structure and concentration of the inverse micelles, the charging mechanism leading to charged inverse micelles and the surface density of surfactant molecules in an adsorbed surface layer. Micellization and surface adsorption of surfactant molecules are processes that are widely accepted. Although it was already recognized in the past that these are competing processes, this work shows for the first time experiments in which the effects of both are visible.

The movement of charged inverse micelles as a result of drift and diffusion and their influence on the electric field, are described by the Nernst-Planck-Poisson equations. I derived analytical expressions in four limiting cases. The analytical results are tested with detailed numerical simulations. The distribution of charges, the electric field and the external current all correspond very well, both as a function of time or as a function of position. The expressions for the external current are also tested against experiments on a mixture of dodecane and a surfactant, providing a way to determine various important properties of the devices.

The good agreement between results obtained from the different regimes, from numerical fitting and from results in other works, are a strong indication for the validity of each of the four regimes. In particular the theoretical description of the space charge limited regime, at high voltages and high charge content, is a new result. Also new is the fact that all the different regimes could be measured and compared for the same type of liquid.

The measured current does not go to zero after the transient period. This indicates that additional mechanisms are present, resulting in a small current remaining for a long time. I measured this quasi steady state current for different voltages in devices with different thicknesses and surfactant concentrations, with and without a polyimide layer on the electrodes. The observed dependencies allowed me to propose a model to explain the quasi steady state currents. This model includes two mechanisms for generation and recombination of charged inverse micelles. In the first mechanism, the reactions happen in the bulk of the liquid. In the second mechanism, the reactions happen at the surfaces. Both mechanisms are necessary to describe the measurements. The fact that bulk generation and recombination are a result of a disproportionation and comproportionation reaction is not new. My colleague Filip Strubbe was the first to measure and explain the effects of these reactions on the quasi steady state current, during his master thesis in collaboration with Philips Research Eindhoven. The mechanism of surface generation and recombination, which explains the quasi steady state current at low voltages, is an original contribution in this PhD thesis.

The results reported in this work are all based on one specific type of experiment: electric current measurements on planar devices when a voltage step is applied after short-circuiting the device. This work presents a systematic analysis of these measurements, starting with the structure of the inverse micelles responsible for the current, and ending with a 'complete' model to explain the current measurements. Many aspects of the behavior of mixtures of nonpolar liquids and surfactant are not treated in this work, and a lot of research remains to be done. During my PhD research I also investigated a number of related topics. Some results have lead to publications, but are outside of the scope of this thesis.

The modeling of charge transport is the most important part of my research, and the results are reported in this work. Some investigations did not lead to conclusions, and indicate that not all aspects of the behavior of mixtures of nonpolar liquid and surfactant are understood yet. In particular, I did also measure currents for the case in which the electrodes are short-circuited after applying a voltage, or when the voltage is changed from one nonzero voltage to another. These measurements can partly be explained by the model reported in this work, but in certain situations the measured current indicates the existence of other mechanisms, for which I could not find a good explanation.

In addition to measurements for voltage steps starting from a nonzero voltage, there are many more possibilities for research that may lead to interesting results. The quasi steady state currents are not constant in

time, but change slowly. In this work, I made no attempt to explain this 'transient of the quasi steady state'. However, a study of this behavior may lead to interesting findings about the long term processes in the device. Also worth investigating is the effect of hydrodynamic flow. I always considered the liquid to be static, but in some cases the movement of inverse micelles causes a flow of liquid in the device. To describe this, the Navier-Stokes equations have to be included in the model. The effects of flow are best noticeable in devices which do not have a simple one-dimensional geometry. The addition of colloidal particles also opens a whole new range of phenomena to be studied. Finally, current measurements are not the only way to study mixtures of nonpolar liquids and surfactants. Different techniques, such as light scattering methods (DLS, PALS, …), nuclear magnetic resonance measurements, spectroscopic methods, … could be used to provide independent confirmation (or not) of my results, and to provide additional information which can not be obtained through electric current measurements.

Although many questions remain, I think that the results of my work contribute to the understanding of mixtures of nonpolar liquid and surfactant. Many results are also applicable in other situations where charges move in a viscous medium. The model for the movement of and the reactions between inverse micelles provide the necessary basis to be able to simulate the behavior of electrophoretic ink.

Appendix
Numerical simulation method

For the numerical simulations presented in this work, I used a forward Euler algorithm. This is not the fastest numerical method, nor is the stability guaranteed for a given timestep. However, one can always find (by trial and error) a timestep and a slab-thickness so that, for given simulation parameters, the algorithm remains stable. The main advantage of the forward Euler method is that it is simple to implement, because it is an explicit method, and therefore does not involve matrix inversions.

The simulation results for every timestep are calculated using the results of the previous timestep (except for the initial condition which is provided separately). The device (with thickness d), is divided in N slabs, all with the same thickness $\Delta x = d/N$ (see figure 52). The concentrations $n_+^{i,j}$,

$n_{-}^{i,j}$ and $n_{0}^{i,j}$ of positive, negative and neutral inverse micelles, respectively, are defined in the middle of each slab $i = 0 \ldots N-1$ and for every timestep $j \geq 0$ (with length Δt). The electric field $E^{i,j}$ and the fluxes $\Psi_{+}^{i,j}$, $\Psi_{-}^{i,j}$ and $\Psi_{0}^{i,j}$ are defined at the borders between the slabs, including the interfaces ($i = 0 \ldots N$, see figure 52), and for every timestep $j \geq 0$. The applied voltage is, in this appendix, considered to be positive. The following calculations are performed in every timestep.

First, the values $F^{i,j} = E^{i,j} - E^{0,j}$ are calculated, using the law of Gauss, as:

$$\begin{aligned} F^{0,j} &= 0 \\ F^{i,j} &= F^{i-1,j} + \frac{e}{\varepsilon\varepsilon_0}\left(n_{+}^{i-1,j} - n_{-}^{i-1,j}\right)\Delta x \,. \\ F^{N,j} &= 0 \end{aligned} \qquad \text{(A1)}$$

Then, the electric field at the interfaces is calculated in such a way that the correct voltage is applied over the device:

$$E^{0,j} = E^{N,j} = \frac{V_A}{d} - \frac{1}{d}\sum_{i=1}^{N-1} F^{i,j}\Delta x \,, \qquad \text{(A2)}$$

and the electric field in the device is calculated as:

$$E^{i,j} = E^{0,j} + F^{i,j} \,. \qquad \text{(A3)}$$

Boundary conditions are imposed for the fluxes at the interfaces. The concentrations are not known in these points, but are estimated using a linear interpolation of the two slabs closest to the interfaces. When there are no surface reactions, the fluxes at the interfaces are zero, otherwise they are calculated using:

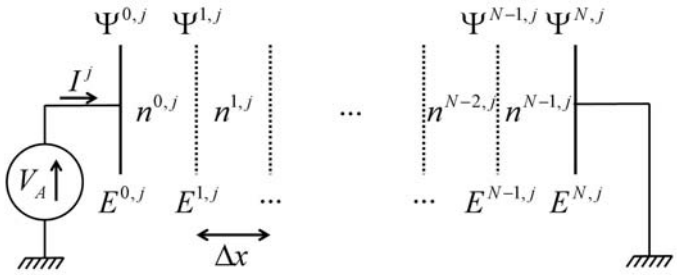

Figure 52:

Overview of the division in slabs of the device and of the definition of the different variables.

$$\Psi_+^{0,j} = \left(1 - \frac{\frac{3}{2}n_+^{0,j} - \frac{1}{2}n_+^{1,j}}{\frac{3}{2}\left(n_+^{0,j} + n_-^{0,j} + n_0^{0,j}\right) - \frac{1}{2}\left(n_+^{1,j} + n_-^{1,j} + n_0^{1,j}\right)}\right)\zeta E^{0,j}$$

$$\Psi_-^{0,j} = -\frac{\frac{3}{2}n_-^{0,j} - \frac{1}{2}n_-^{1,j}}{\frac{3}{2}\left(n_+^{0,j} + n_-^{0,j} + n_0^{0,j}\right) - \frac{1}{2}\left(n_+^{1,j} + n_-^{1,j} + n_0^{1,j}\right)}\zeta E^{0,j} \quad , \qquad \text{(A4)}$$

$$\Psi_0^{0,j} = -\frac{\frac{3}{2}n_0^{0,j} - \frac{1}{2}n_0^{1,j}}{\frac{3}{2}\left(n_+^{0,j} + n_-^{0,j} + n_0^{0,j}\right) - \frac{1}{2}\left(n_+^{1,j} + n_-^{1,j} + n_0^{1,j}\right)}\zeta E^{0,j}$$

and

$$\Psi_+^{N,j} = \frac{\frac{3}{2}n_+^{N-1,j} - \frac{1}{2}n_+^{N-2,j}}{\frac{3}{2}\left(n_+^{N-1,j} + n_-^{N-1,j} + n_0^{N-1,j}\right) - \frac{1}{2}\left(n_+^{N-2,j} + n_-^{N-2,j} + n_0^{N-2,j}\right)}\zeta E^{N,j}$$

$$\Psi_-^{N,j} = \left(-1 + \frac{\frac{3}{2}n_-^{N-1,j} - \frac{1}{2}n_-^{N-2,j}}{\frac{3}{2}\left(n_+^{N-1,j} + n_-^{N-1,j} + n_0^{N-1,j}\right) - \frac{1}{2}\left(n_+^{N-2,j} + n_-^{N-2,j} + n_0^{N-2,j}\right)}\right)\zeta E^{N,j} \qquad \text{(A5)}$$

$$\Psi_0^{N,j} = \frac{\frac{3}{2}n_0^{N-1,j} - \frac{1}{2}n_0^{N-2,j}}{\frac{3}{2}\left(n_+^{N-1,j} + n_-^{N-1,j} + n_0^{N-1,j}\right) - \frac{1}{2}\left(n_+^{N-2,j} + n_-^{N-2,j} + n_0^{N-2,j}\right)}\zeta E^{N,j}$$

The fluxes in the interior of the device are calculated using the discretized drift and diffusion equations:

$$\begin{aligned}
\Psi_{+}^{i,j} &= \mu \frac{n_{+}^{i-1,j} + n_{+}^{i,j}}{2} E_{i,j} - D \frac{n_{+}^{i,j} - n_{+}^{i-1,j}}{\Delta x} \\
\Psi_{-}^{i,j} &= -\mu \frac{n_{-}^{i-1,j} + n_{-}^{i,j}}{2} E_{i,j} - D \frac{n_{-}^{i,j} - n_{-}^{i-1,j}}{\Delta x} \\
\Psi_{0}^{i,j} &= -D \frac{n_{0}^{i,j} - n_{0}^{i-1,j}}{\Delta x}
\end{aligned} . \qquad \text{(A6)}$$

The external current can then be calculated from the average of the current density (from Ramo's theorem):

$$I^{j} = \frac{eS\Delta x}{d}\left(\frac{\Psi_{+}^{0,j} - \Psi_{-}^{0,j}}{2} + \sum_{i=1}^{N-1}\left(\Psi_{+}^{i,j} - \Psi_{-}^{i,j}\right) + \frac{\Psi_{+}^{N,j} - \Psi_{-}^{N,j}}{2} \right). \qquad \text{(A7)}$$

Finally, the concentrations in the next timestep are calculated using the continuity equations:

$$\begin{aligned}
n_{+}^{i,j+1} &= n_{+}^{i,j} - \frac{\Psi_{+}^{i+1,j} - \Psi_{+}^{i,j}}{\Delta x}\Delta t - \alpha n_{+}^{i,j} n_{-}^{i,j} + \beta n_{0}^{i,j} n_{0}^{i,j} \\
n_{-}^{i,j+1} &= n_{-}^{i,j} - \frac{\Psi_{-}^{i+1,j} - \Psi_{-}^{i,j}}{\Delta x}\Delta t - \alpha n_{+}^{i,j} n_{-}^{i,j} + \beta n_{0}^{i,j} n_{0}^{i,j} \\
n_{0}^{i,j+1} &= n_{0}^{i,j} - \frac{\Psi_{0}^{i+1,j} - \Psi_{0}^{i,j}}{\Delta x}\Delta t + 2\alpha n_{+}^{i,j} n_{-}^{i,j} + 2\beta n_{0}^{i,j} n_{0}^{i,j}
\end{aligned} . \qquad \text{(A8)}$$

References

[1] H. Eicke, '**Surfactants in nonpolar solvents**', Topics in Current Chemistry, Vol. 87 (1980), pp. 85-145.

[2] E. Ruckenstein and R. Nagarajan, '**Aggregation of amphiphiles in nonaqueous media**', Journal of Physical Chemistry, Vol. 84 (1980), pp. 1349-1358.

[3] S. Salaniwal, S. T. Cui, P. T. Cummings and H. D. Cochran, '**Self-assembly of reverse micelles in water/surfactant/carbon dioxide systems by molecular simulation**', Langmuir, Vol. 15 (1999), pp. 5188-5192.

[4] S. P. Moulik, '**Micelles: Self-organized surfactant assemblies**', Current Science, Vol. 71 (1996), pp. 368-376.

[5] M. P. Pileni, '**Reverse micelles as microreactors**', Journal of Physical Chemistry, Vol. 97 (1993), pp. 6961-6973.

[6] N. L. Klyachko and A. V. Levashov, '**Bioorganic synthesis in reverse micelles and related systems**', Current Opinion in Colloid and Interface Science, Vol. 8 (2003), pp. 179-186.

[7] Y. L. Khmelnitsky, A. K. Gladilin, V. L. Roubailo, K. Martinek and A. V. Levashov, '**Reversed micelles of polymeric surfactants in nonpolar organic solvents**', European Journal of Biochemistry, Vol. 206 (1992), pp. 737-745.

[8] Y. Chen, Q. S. Wu and Y. Dingibi, '**Stepwise assembly of nanoparticles, -tubes, -rods, and -wires in reverse micelle systems**', European Journal of Inorganic Chamistry, Vol. 31 (2007), pp. 4906-4910.

[9] Y. Won, S. P. Meeker, V. Trappe, D. A. Weitz, N. Z. Diggs and J. I. Emert, '**Effect of temperature on carbon-black agglomeration in hydrocarbon liquid with adsorbed dispersant**', Langmuir, Vol. 21 (2005), pp. 924-932.

[10] M. J. Lawrence, '**Surfactant systems: their use in drug delivery**', Chemical Society Reviews, Vol. 23 (1994), pp. 417-424.

[11] A. S. Dukhin and P. J. Goetz, '**How non-ionic "electrically neutral" surfactants enhance electrical conductivity and ion stability in non-polar liquids**', Journal of Electroanalytical Chemistry, Vol. 588 (2006), pp. 44-50.

[12] I. D. Morrison, '**Electrical charges in nonaqueous media**', Colloids and Surfaces A: Physicochemical and Engineering Aspects, Vol. 71 (1993), pp. 1-37.

[13] J. D. Piper, A. G. Fleiger, C. C. Smith and N. A. Kernstein, '**Chemical, physical, electrical properties of systems containing lead or copper soaps in liquid paraffin**', Industrial and Engineering Chemistry, Vol. 31 (1939), pp. 307-317.

[14] A. Klinkenberg and J. L. van der Minne, '**Electrostatics in the petroleum industry**', Elsevier, New York, 1958.

[15] R. M. Fuoss, '**Ionic Association. III. The equilibrium between ion pairs and free ions**', Journal of the American Chemical Society, Vol. 80 (1958), pp. 5059-5061.

[16] A. Kitahara, S. Karasawa and H. Yamada, '**The effect of water on electrokinetic potential and stability of suspensions in nonpolar media**', Journal of Colloid and Interface Science, Vol. 25 (1967), pp. 490-495.

[17] M. F. Hsu, E. R. Dufresne and D. A. Weitz, '**Charge stabilization in nonpolar solvents**', Langmuir, Vol. 21 (2005), pp. 4881-4887.

[18] F. Strubbe, A. R. M. Verschueren, L. J. M. Schlangen, F. Beunis and K. Neyts, '**Generation current of charged micelles in nonaqueous liquids: Measurements and simulations**', Journal of Colloid and Interface Science, Vol. 300 (2006), pp. 396-403.

[19] J. A. Dahlquist and I. Brodie, '**Electrophoretic development of electrostatic charge images from colloidal suspensions of carbon**', Journal of Applied Physics, Vol. 40 (1969), pp. 3020-3027.

[20] D. A. Hays, I. D. Morrison and L. S. Smith, '**Role of particles and dispersions in electrophotography**', Particulate Science and Technology, Vol. 5 (1987), pp. 39-51.

[21] G. Percin, T. S. Lundgren and B. T. Khuri-Yakub, '**Controlled ink-jet printing and deposition of organic polymers and solid particles**', Applied Physics Letters, Vol. 73 (1998), pp. 2375-2377.

[22] P. Sarkar and P. S. Nicholson, '**Electrophoretic deposition (EPD): Mechanisms, kinetics, and application to ceramics**', Journal of the American Ceramic Society, Vol. 79 (1996), pp. 1978-2002.

[23] A. Yethiraj and A. van Blaaderen, '**A colloidal model system with an interaction tunable from hard sphere to soft and dipolar**', Nature, Vol. 421 (2003), pp. 513-517.

[24] H. Block and J. P. Kelly, '**Electro-rheology**', Journal of Physics D, Vol. 21 (1988), pp. 1661-1677.

[25] A. P. Gast and C. F. Zukoski, '**Electrorheological fluids as colloidal suspensions**', Advances in Colloid and Interface Science, Vol. 30 (1989), pp. 153-202.

[26] J. Jacobson, B. Comiskey, C. Turner, J. Albert and P. Tsao, '**The last book**', IBM Systems Journal, Vol. 36 (1997), pp. 457-463.

[27] J. A. Rogers, '**Towards paperlike displays**', Science, Vol. 291 (2001), pp. 1502-1503.

[28] A. Henzen and J. van de Kamer, '**The present and future of electronic paper**', Journal of the Society for Information Display, Vol. 14 (2006), pp. 437-442.

[29] R. C. Lean, '**Physics and performance optimization of electronic paper**', Journal of Imaging Science and Technology, Vol. 46 (2002), pp. 562-574.

[30] K. K. Shieh and D. S. Lee, '**Preferred viewing distance and screen angle of electronic paper displays**', Applied Ergonomics, Vol. 38 (2007), pp. 601-608.

[31] H. E. A. Huitema, G. H. Gelinck, P. J. G. van Lieshout, E. van Veenendaal and F. J. Touwslager, '**Flexible electronic-paper active-matrix displays**', Journal of the Society for Information Display, Vol. 14 (2006), pp. 729-733.

[32] J. A. Rogers and Z. Bao, '**Printed plastic electronics and paperlike displays**', Journal of Polymer Science A - Polymer Chemistry, Vol. 40 (2002), pp. 3327-3334.

[33] N. K. Sheridon and M. A. Berkovitz, '**Gyricon - Twisting ball display**', Proceedings of the SID, Vol. 18 (1977), pp. 289-293.

[34] J. M. Crowley, N. K. Sheridon and L. Romano, '**Dipole moments of gyricon balls**', Journal of Electrostatics, Vol. 55 (2002), pp. 247-259.

[35] D. K. Yang, J. L. West, L. C. Chien and J. W. Doane, '**Control of reflectivity and bistability in displays using cholesteric liquid-crystals**', Journal of Applied Physics, Vol. 76 (1994), pp. 1331-1333.

[36] C. H. Wang and P. J. Bos, '**Bistable C1 ferroelectric liquid crystal device for e-paper application**', Displays, Vol. 25 (2004), pp. 187-194.

[37] T. Z. Kosc, K. L. Marshall, A. Trajkovska-Petkoska, E. Kimball and S. D. Jacobs, '**Progress in the development of polymer cholesteric liquid crystal flakes for display applications**', Displays, Vol. 25 (2004), pp. 171-176.

[38] T. Z. Kosc, K. L. Marshall, S. D. Jacobs and J. C. Lambropoulos, '**Polymer cholesteric liquid-crystal flake reorientation in an alternating-current electric field**', Journal of Applied Physics, Vol. 98 (2005), pp. 013509/1-6.

[39] D. Corr, U. Bach, D. Fay, M. Kinsella, C. McAtamney, F. O'Reilly, S.N. Rao and N. Stobie, '**Coloured electrochromic "paper-quality" displays based on modified mesoporous electrodes**', Solid State Ionics, Vol. 165 (2003), pp. 315-321.

[40] M. Grätzel, '**Ultrafast colour displays**', Nature, Vol. 409 (2001), pp. 575-576.

[41] P. M. S. Monk, F. Delage and S. M. Costa Vieira, '**Electrochromic paper: utility of electrochromes incorporated in paper**', Electrochimica Acta, Vol. 46 (2001), pp. 2195-2202.

[42] M. Marescaux, F. Beunis, F. Strubbe and K. Neyts, '**Electrochromic materials for electronic paper**', 8th FirW PhD Symposium (Ghent, Belgium, 2007).

[43] R. A. Hayes, B. J. Feenstra, '**Video-speed electronic paper based on electrowetting**', Nature, Vol. 425 (2003), pp. 383-385.

[44] T. Roques-Carmes, R. A. Hayes and L. J. M. Schlangen, '**A physical model describing the electro-optic behavior of switchable optical elements based on electrowetting**', Journal of Applied Physics, Vol. 96 (2004), pp. 6267-6271.

[45] A. L. Dalisa, '**Electrophoretic displays**', Topics in Applied Physics, Vol. 40 (1980), pp. 213-232.

[46] B. Comiskey, J. D. Albert, H. Yoshizawa, J. Jacobson, '**An electrophoretic ink for all-printed reflective electronic displays**', Nature, Vol. 394 (1998), pp. 253-255.

[47] J. H. Park, M. A. Lee, B. J. Park and H. J. Choi, '**Preparation and electrophoretic response of poly(methyl methacrylate-co-methacrylic acid) coated TiO2 nanoparticles for electronic paper application**', Current Applied Physics, Vol. 7 (2007), pp. 349-351.

[48] M. K. Kim, C. A. Kim, S. D. Ahn, S. R. Kang and K. S. Suh, '**Density compatibility of encapsulation of white inorganic TiO2 particles using dispersion polymerization technique for electrophoretic display**', Synthetic Metals, Vol. 146 (2004), pp. 197-199.

[49] M. A. Hopper and V. Novotny, '**Characteristics of a TiO2-based electrophoretic display**', Journal of the Electrochemical Society, Vol. 126 (1979), pp. 339-339.

[50] J. Y. Kim, S. Garoff, J. L. Anderson, L. J. M. Schlangen, '**Movement of colloidal particles in two-dimensional electric fields**', Langmuir, Vol. 21 (2005), pp. 10941-10947.

[51] P. T. Kazlas and M. D. McCreary, '**Paperlike microencapsulated electrophoretic materials and displays**', Mrs Bulletin, Vol. 27 (2002), pp. 894-897.

[52] G. Li, Y. Q. Feng, X. G. Li, P. Gao, J. Wang and J. Y. Xie, '**Preparation and characterization of polyurea microcapsules containing colored electrophoretic responsive fluid**', Journal of Materials Science, Vol. 42 (2007), pp. 4838-4844.

[53] J. K. Song, H. J. Choi and I. Chin, '**Preparation and properties of electrophoretic microcapsules for electronic paper**', Journal of Microencapsulation, Vol. 24 (2007), pp. 11-19.

[54] D. G. Yu, S. H. Kim and J. H. An, '**Preparation and characterization of electronic inks encapsulation for microcapsule-type electrophoretic displays (EPDs)**', Journal of Industrial and Engineering Chemistry, Vol. 13 (2007), pp. 438-443.

[55] R. J. Pugh and F. M. Fowkes, '**The dispersibility and stability of coal particles in hydrocarbon media with a polyisobutene succinamide dispersing agent**', Colloids and Surfaces, Vol. 11 (1984), pp. 423-427.

[56] C. J. Chung and J. H. Jean, '**Dispersion of titania powder in an electronic ink for electrophoretic display**', Journal of the American Ceramic Society, Vol. 90 (2007), pp. 3490-3495.

[57] P. Murau and B. Singer, '**Understanding and elimination of some suspension instabilities in an electrophoretic display**', Journal of Applied Physics, Vol. 48 (1978), pp. 4820-4829.

[58] L. S. Park, J. W. Park, H. Y. Choi, Y. S. Han, Y. Kwon and H. S. Choi, '**Fabrication of charged particles for electrophoretic display**', Current Applied Physics, Vol. 6 (2006), pp. 644-648.

[59] H. S. Choi, J. W. Park, L. S. Park, J. K. Lee, Y. S. Han and Y. Kwon, '**Preparation of panel and charged particles for electrophoretic display**', Journal of Nonlinear Optical Physics & Materials, Vol. 14 (2005), pp. 521-528.

[60] A. Kitahara, M. Amano, S. Kawasaki and K. Konno, '**Concentration effect of surfactants on zeta-potential in non-aqueous dispersions**', Colloid and Polymer Science, Vol. 255 (1977), pp. 1118-1121.

[61] F. M. Fowkes, H. Jinnai, M. A. Mostafa, F. W. Anderson and R. J. Moore, '**Mechanism of electric charging of particles in non-aqueous liquids**', ACS Symposium Series, Vol. 200 (1982), pp. 307-324.

[62] M. E. Labib and R. Williams, '**The effect of moisture on the charge at the interface between solids and organic liquids**', Journal of Colloid and Interface Science, Vol. 115 (1987), pp. 330-338.

[63] N. Garbow, M. Evers and T. Palberg, '**Optical tweezing electrophoresis of isolated, highly charged colloidal spheres**', Colloids and Surfaces A - Physicochemical and Engineering Aspects, Vol. 195 (2001) pp. 227-241.

[64] F. Strubbe, F. Beunis, M. Marescaux and K. Neyts, '**Charging mechanism in colloidal particles leading to a linear relation between charge and size**', Physical Review E, Vol. 75 (2007), pp. 031405/1-8.

[65] V. Novotny and M. A. Hopper, '**Electrical conduction in surfactant-water-nonaqueous liquid systems**', Journal of the Electrochemical Society, Vol. 133 (1986), pp. 1629-1636.

[66] V. Novotny and M. A. Hopper, '**Transient conduction of weakly dissociating species in dielectric fluids**', Journal of the Electrochemical Society, Vol. 126 (1979), pp. 925-929.

[67] T. K. De and A. Maitra, '**Solution behaviour of aerosol OT in non-polar solvents**', Advances in Colloid and Interface Science, Vol. 59 (1995), pp. 95-193.

[68] D. Liu, J. Ma, H. Cheng and Z. Zhao, '**Solubilization in mixed reverse micellar systems of AOT/nonionic surfactants/n-heptane**', Journal of Dispersion Science and Technology, Vol. 19 (1998), pp. 599-611.

[69] M. Ueda and Z. A. Schelly, 'Mean aggregation number and water vapor pressure of AOT Reverse micellar systems determined by controlled partial pressure-vapor pressure osmometry (CPP-VPO)', Langmuir, Vol. 4 (1988), pp. 653-655.

[70] A. Kitahara, T. Kobayashi and T. Tachibana, '**Light scattering study of solvent effect on micelle formation of Aerosol OT**', Journal of Physical Chemistry, Vol 66 (1962), pp. 363-365.

[71] M. B. Mathews and E. Hirschhorn, '**Solubilization and micelle formation in a hydrocarbon medium**', Journal of Colloid Science, Vol. 8 (1953), pp. 86-96.

[72] K. S. Kim, J. Y. Lee, B. J. Park, J. H. Sung, I. Chin, H. J. Choi and J. H. Lee, '**Synthesis and characteristics of microcapsules containing electrophoretic particle suspensions**', Colloid and Polymer Science, Vol. 284 (2006), pp. 813-816.

[73] R. C. Liang, M. C. Park, Z. G. Wu, X. Chen and H. Zang, '**Manufacturing process for electrophoretic display**', US Patent No. 6,672,921 B1 (2004).

[74] K. R. Amundson, R. W. Zehner, R. M. Webber, K. Geramita, L. Zhang, A. Loxley, G. M. Duthaler, J. E. Ritter, M. L. Steiner, M. M. Holman, J. J. Abramson and G. Crossley, '**Electro-optic display and materials for use therein**', US Patent No. 0,035,808 A1 (2007).

[75] M. L. Huber, A. Laesecke and R. Perkins, '**Transport properties of n-dodecane**', Energy and Fuels, Vol. 18 (2004), pp. 968-975.

[76] J. G. Gordon, M. W. Hart, A. M. Homola, D. R. McKean, L. B. Schein, B. A. Smith and S. A. Swanson, '**Electrophoretic display**', US Patent No. 5,745,094 (1998).

[77] J. D. Albert and B. Comiskey, '**Process for creating an encapsulated electrophoretic display**', US Patent No. 6,067,185 (2000).

[78] K. K. Papok, V. A. Gladkikh, B. S. Zuseva and A. N. Zaitseva, '**Rapid method of determination of oil and additive grades in wide-range varnish former (Dil instrument)**', Chemistry and Technology of Fuels and Oils, Vol. 13 (1977), pp. 357-360.

[79] I. F. Blagovidov, V. P. Lapin, G. L. Trofimpva and G. I. Shor, '**Mechanism of the stabilizing effect of motor-oil additives**', Chemistry and Technology of Fuels and Oils, Vol. 7 (1971), pp. 439-443.

[80] R. J. Pugh, T. Matsunaga and F. M. Fowkes, 'The dispersability and stability of carbon black in media of low dielectric constant. 1. Electrostatic and steric contribution to colloidal stability', Colloids and Surfaces, Vol. 7 (1983), pp. 183-207.

[81] R. J. Pugh and F. M. Fowkes, 'The dispersability and stability of carbon black in media of low dielectric constant. 2. Sedimentation volume of concentrated dispersions, adsorption and surface calorimetry studies', Colloids and Surfaces, Vol. 9 (1984), pp. 33-46.

[82] R. E. Kornbrekke, I. D. Morrison and T. Oja, '**Electrophoretic mobility measurements in low conductivity media**', Langmuir, Vol. 8 (1992), pp. 1211-1217.

[83] P. D. Calvert, R. R. Lalanandham and M. V. Parish, '**Dispersion of ceramic particles in organic liquids**', Material Resource Society Symposium, Vol. 73 (1986), pp. 579-584.

[84] P. D. Calvert, R. R. Lalanandham, M. V. Parish and E. Tormey, '**Dispersants in ceramic processing**', British Ceramic Proceedings, Vol. 37 (1986), pp. 249-253.

[85] I. R. Collins and S. E. Taylor, '**The preparation and stability of colloidal metal dispersions prepared by a two-phase non-aqueous route**', Journal of Dispersion Science and Technology, Vol. 12 (1991), pp. 403-415.

[86] Y. Chevalier, M.-C. Dubois-Clochard, J.-P. Durand, B. Delfort, P. Gateau, L. Barré, D. Frot, Y. Briolant, I. Blanchard and R. Gallo, '**Adsorption of poly(isobutenylsuccinimide) dispersants at a solid-hydrocarbon interface**', Progress in Colloid and Polymer Science, Vol. 118 (2001), pp. 110–114.

[87] Y. Shigesato, I. Yasui and D. C. Paine, '**ITO thin-film transparent conductors: Microstructure and processing**', JOM, Vol. 47 (1995), pp. 47-50.

[88] J. R. Bellingham, W. A. Phillips and C. J. Adkins, '**Electrical and optical properties of amorphous indium oxide**', Journal of Physics: Condensed Matter, Vol. 2 (1990), pp. 6207-6221.

[89] J. Hanna and I. Shimizu, '**Materials in active-matrix liquid-crystal displays**', Materials Research Society Bulletin, Vol. 21 (1996), pp. 35-38.

[90] P. D. Rack, A. Naman, P. H. Holloway, S. S. Sun and R. T. Tuenge, '**Materials used in electroluminescent displays**', Materials Research Society Bulletin, Vol. 21 (1996), pp. 49-58.

[91] J. F. Keithley, J. R. Yeager and R. J. Erdman, '**Low level measurements**', Keithley, Cleveland, 1984.

[92] S. Ramo, '**Currents induced by electron motion**', Proceedings of the IRE, Vol. 27 (1939), pp. 584-585.

[93] P. De Visschere, '**The validity of Ramo's theorem**', Solid-State Electronics, Vol. 33 (1989), pp. 455-459.

[94] Z. He, '**Review of the Shockley-Ramo theorem and its application in semiconductor gamma-ray detectors**', Nuclear Instruments and Methods in Physics Research, Vol. 463 (2001), pp. 250-267.

[95] K. Neyts, J. Beeckman and F. Beunis, '**Quasistationary current contributions in electronic devices**', Opto-Electronics Review, Vol. 15 (2007), pp. 41-46.

[96] E. A. Richley and J. C. Mikkelsen, '**Electrical processes in nonpolar liquids based on initial transient response and recovery**', Journal of Applied Physics, Vol. 86 (1999), pp. 7029-7038.

[97] P. Kohn, K. Schröter and T. Thurn-Albrecht, '**Determining the mobility of ions by transient current measurements at high voltages**', Physical Review Letters, Vol. 99 (2007), Art. No. 086104.

[98] D. C. Prieve, J. D. Hoggard, R. Fu, P. J. Sides and R. Bethea, '**Two independent measurements of Debye lengths in doped nonpolar liquids**', Langmuir, Vol. 24 (2008), pp. 1120-1132.

[99] P. Somasundaran, S. Krishnakumar and S. C. Mehta, '**A new model to describe the sorption of surfactants on solids in non-aqueous media**', Journal of Colloid and Interface Science, Vol. 292 (2005), pp. 373-380.

[100] B. Y. Zhu and T. R. Gu, '**Surfactant adsorption at solid liquid interfaces**', Advances in Colloid and Interface Science, Vol. 37 (1991), pp. 1-32.

[101] Y. L. Chen, Z. H. Xu and J. Israelachvili, 'Structure and interactions of surfactant-covered surfaces in nonaqueous (oil surfactant water) media', Langmuir, Vol. 8 (1992), pp. 2966-2975.

[102] K. A. Egorova and A. I. Kupreev, 'Infrared spectroscopic investigation of dynamics of adsorption processes in systems comprising nonpolar solvent, metal and surfactant', Colloid Journal of the USSR, Vol. 40 (1978), pp. 280-282.

[103] B. L. Papke and L. M. Robinson, 'Factors affecting poly(isobutenyl)succinimide dispersant adsorption onto surfactant-coated colloidal particles in nonaqueous media', Langmuir, Vol. 10 (1994), pp. 1741-1748.

[104] M. Arellano, I. Michelhaciski, D. L. Feke and I. Manaszloczower, 'Compatibilization of titanium dioxide powders with non-polar media: Adsorption of anionic surfactants and its influence on dispersion stability', Journal of Coatings Technology, Vol. 68 (1996), pp. 103-112.

[105] J. S. H. Lee, I. Barbulovic-Nad, Z. Wu, X. Xuan and D. Li, '**Electrokinetic flow in a free surface-guided microchannel**', Journal of Applied Physics, Vol. 99 (2006), Art. No. 054905.

[106] R. Rodríguez, S. Vargas and D. A. Fernández-Velasco, '**Reverse micelle systems composed of water, triton X-100, and phospholipids in organic solvents**', Journal of Colloid and Interface Science, Vol. 197 (1998), pp. 21-28.

[107] C. Petit, P. Lixon and M. P. Pileni, '**Structural study of bimetallic bis(2-ethylhexyl) sulfosuccinate aggregates**', Langmuir, Vol. 7 (1991), pp. 2620-2625.

[108] P. Becher, '**Micelle formation in aqueous and nonaqueous solutions**', Nonionic Surfactants, Vol. 1 (1967), pp. 478-515.

[109] N. Muller, 'Attempt at a unified interpretation of the self-association of 1-1 ionic surfactants in solvents of low dielectric constant', Journal of Colloid and Interface Science, Vol. 63 (1978), pp. 383-393.

[110] C. Yan, M. Zharnikov, A. Goelzhaeuser and M. Grunze, '**Preparation and characterization of self-assembled monolayers on indium tin oxide**', Langmuir, Vol. 16 (2000), pp. 6208-6215.

[111] I. Borukhov, D. Andelman and H. Orland, '**Adsorption of large ions from an electrolyte solution: A modified Poisson-Boltzmann equation**', Electrochimica Acta, Vol. 46 (2000), pp. 221-229.

[112] T. Li, P. P. Ruden, I. H. Campbell and D. L. Smith, '**Investigation of bottom-contact organic field effect transistors by two-dimensional device modeling**', Journal of Applied Physics, Vol. 93 (2003), pp. 4017-4023.

[113] D. B. Graves and K. F. Jensen, '**A continuum model of DC and RF discharges**', IEEE Transactions on Plasma Science, Vol. 14 (1986), pp. 78-91.

[114] A. M. Kol'chuzhkin, A. M. Timokhin, V. D. Ababii and V. A. Lebedev, '**Iteration method of solving the integrodifferential Nernst-Planck-Poisson equations**', Russian Journal of Electrochemistry, Vol. 35 (1999), pp. 1007-1010.

[115] R. C. Kumar, 'The Nernst-Planck equation or the current-density equation in the context of semiconductor heterojunction theory', Physica Status Solidi A, Vol. 126 (1991), pp. 383-396.

[116] S. Mafe, J. Pellicer and V. M. Aguilella, 'Ionic transport and space-charge density in electrolytic solutions as described by Nernst-Planck and Poisson equations', Journal of Physical Chemistry, Vol. 90 (1986), pp. 6045-6050.

[117] S. Jayaram and J. D. Cross, 'Influence of electrode processes on transient conduction phenomena in non-polar liquids', Journal of Electrostatics, Vol. 29 (1992), pp. 55-72.

[118] M. S. Kilic, M. Z. Bazant and A. Ajdari, 'Steric effects in the dynamics of electrolytes at large applied voltages: I. Double-layer charging', Physical Review E, Vol. 75 (2007), Art. No. 021502.

[119] M. S. Kilic, M. Z. Bazant and A. Ajdari, 'Steric effects in the dynamics of electrolytes at large applied voltages: II. Modified Poisson-Nernst-Planck equations', Physical Review E, Vol. 75 (2007), Art. No. 021503.

[120] F. Beunis, F. Strubbe, M. Marescaux, K. Neyts and A. R. M. Verschueren, '**Diffuse double layer charging in nonpolar liquids**', Applied Physics Letters, Vol. 91 (2007), Art. No. 182911.

[121] M. Z. Bazant, K. Thornton and A. Ajdari, '**Diffuse-charge dynamics in electrochemical systems**', Physical Review E, Vol. 70 (2004), Art. No. 021506.

[122] F. Beunis, F. Strubbe, K. Neyts and A. R. M. Verschueren, '**Power-law transient charge transport in a nonpolar liquid**', Applied Physics Letters, Vol. 90 (2007), Art. No. 182103.

[123] H. De Vleeschouwer, F. Bougrioua and H. Pauwels, '**Importance of ion transport in industrial LCD applications**', Molecular Crystals and Liquid Crystals, Vol. 360 (2001), pp. 29-39.

[124] P. L. Castillo, N. Bennis, M. Geday, J. M. Otón, F. Beunis, K. Neyts and V. Urruchi, '**Erasing strategies for asymmetric antiferroelectric liquid crystal driving schemes**', Molecular Crystals and Liquid Crystals, Vol. 450 (2006), pp. 239-253.

[125] A. R. M. Verschueren, P. H. L. Notten, L. J. M. Schlangen, F. Strubbe, F. Beunis and K. Neyts, '**Screening and separation of charges in microscale devices: Complete planar solution of the Poisson-Boltzmann equation**', Journal of Physical Chemistry A, submitted.

[126] M. N. Ozisik, '**Heat conduction**', Wiley, New York, 1980.

[127] T. Bert, F. Beunis, H. De Smet and K. Neyts, '**Steady state currents in EPIDs**', Displays, Vol. 27 (2006), pp. 35-38.

Publications

[i] F. Beunis, F. Strubbe, M. Marescaux, K. Neyts and A. R. M. Verschueren, '**Micellization and surface adsorption of surfactant in micrometer scale geometries**', in preparation.

[ii] F. Beunis, F. Strubbe, M. Marescaux, J. Beeckman, K. Neyts and A. R. M. Verschueren, '**The dynamics of charge transport in planar devices**', submitted.

[iii] A. R. M. Verschueren , P. H. L. Notten, L. J. M. Schlangen, F. Strubbe, F. Beunis and K. Neyts, '**Screening and separation of charges in microscale devices: Complete planar solution of the Poisson-Boltzmann equation**', submitted.

[iv] F. Strubbe, F. Beunis and K. Neyts, '**Detection of elementary charges on colloidal particles**', submitted.

[v] M. Marescaux, F. Beunis, F. Strubbe and K. Neyts, '**Electrochromic materials for electronic paper**', 8th FirW PhD Symposium (Ghent, Belgium, 2007).

[vi] F. Beunis, F. Strubbe, M. Marescaux, K. Neyts and A. R. M. Verschueren, '**Diffuse double layer charging in nonpolar liquids**', Applied Physics Letters, Vol. 91 (2007), Art. No. 182911.

[vii] F. Beunis, F. Strubbe, K. Neyts and A.R.M. Verschueren, '**Power-law transient charge transport in a nonpolar liquid**', Applied Physics Letters, Vol. 90 (2007), Art. No. 182103.

[viii] F. Strubbe, F. Beunis, M. Marescaux and K. Neyts, '**Charging mechanism in colloidal particles leading to a linear relation between charge and size**', Physical Review E, Vol. 75 (2007), Art. No. 031405.

[ix] G. Stojmenovik, S. Vermael, F. Beunis, K. Neyts and A. R. M. Verschueren, '**Monte Carlo algorithm for drift and diffusion of ions in anisotropic, non-homogeneous media**', Opto-electronics Review, Vol. 15 (2007), pp. 13-19.

[x] K. Neyts, J. Beeckman and F. Beunis, '**Quasistationary current contributions in electronic device**s', Opto-electronics Review, Vol. 15 (2007), pp. 41-46.

[xi] K. Neyts and F. Beunis, '**Ion transport and switching currents in smectic liquid crystal devices**', Ferroelectrics, Vol. 344 (2006), pp. 255-266.

[xii] F. Beunis, F. Strubbe, M. Marescaux, K. Neyts and A. R. M. Verschueren, '**Charge transport in electronic paper**', 7th FirW PhD Symposium (Ghent, Belgium, 2006).

[xiii] F. Strubbe, F. Beunis and K. Neyts, '**Determination of the effective charge of individual colloidal particles**', Journal of Colloid and Interface Science, Vol. 301 (2006), pp. 302-309.

[xiv] F. Strubbe, A. R. M. Verschueren, L. J. M. Schlangen, F. Beunis and K. Neyts, '**Generation current of charged micelles in nonaqueous liquids: Measurements and simulations**', Journal of Colloid and Interface Science, Vol. 300 (2006), pp. 396-403.

[xv] P. Castillo, N. Bennis, M. Geday, X. Quintana, J. M. Otón, F. Beunis, K. Neyts and V. Urruchi, '**Erasing strategies for asymmetric antiferroelectric liquid crystal driving schemes**', Molecular Crystals and Liquid Crystals, Vol. 450 (2006), pp. 239-253.

[xvi] F. Beunis, F. Strubbe, K. Neyts and A. R. M. Verschueren, '**Electrical transient behavior of a low dielectric fluid between planar electrodes**', International Conference on Electrokinetic Phenomena (Nancy, France, 2006).

[xvii] F. Strubbe, F. Beunis and K. Neyts, '**Determination of the effective charge of individual colloidal particles**', International Conference on Electrokinetic Phenomena (Nancy, France, 2006).

[xviii] G. Stojmenovik, F. Beunis, K. Neyts, S. Vermael and A. R. M. Verschueren, '**Monte Carlo algorithm for drift and diffusion of ions in anisotropic, non-homogeneous media**', International Workshop on Liquid Crystals for Photonics (Ghent, Belgium, 2006).

[xix] T. Bert, H. De Smet, F. Beunis and K. Neyts, '**Complete electrical and optical simulation of electronic paper**', Displays, Vol. 27 (2006), pp. 50-55.

[xx] T. Bert, H. De Smet, F. Beunis and K. Neyts, '**Steady state current in EPIDs**', Displays, Vol. 27 (2006), pp. 35-38.

[xxi] F. Strubbe, F. Beunis, M. Marescaux, A. R. M. Verschueren and K. Neyts, '**Determination of the valency of pigment particles in electrophoretic ink**', 6th FirW PhD Symposium (Ghent, Belgium, 2005).

[xxii] C. Desimpel, F. Beunis, H. Desmet and K. Neyts, '**Experiments on azimuthal degenerated anchoring surfaces**', 16th Conference on Liquid Crystals (Warsaw, Poland, 2005).

[xxiii] F. Beunis, F. Strubbe, K. Neyts, T. Bert, H. De Smet, A. R. M. Verschueren and L. J. M. Schlangen, '**Electric field compensation in electrophoretic ink displays**', 25th International Display Research Conference (Edinburgh, United Kingdom, 2005).

[xxiv] T. Bert, H. De Smet, F. Beunis and F. Strubbe, '**Numerical simulation of the transport of particles in electrophoretic displays**', Opto-electronics Review, Vol. 13 (2005), pp. 281-286.

[xxv] T. Bert, F. Beunis, H. De Smet and K. Neyts, '**Transient current properties in electronic paper**', 11th International Display Workshops (Niigata, Japan, 2004).

[xxvi] F. Beunis, K. Neyts, A. Adamski, J. M. Otón, X. Quintana, P. L. Castillo and N. Bennis, '**Charge transport in AFLC cells with asymmetric boundaries**', 5th FTW PhD Symposium (Ghent, Belgium, 2004).

[xxvii] T. Bert, F. Beunis, H. De Smet and K. Neyts, '**Transient current properties in electronic paper**', SID-ME 10th Anniversary Meeting (Stuttgart, Germany, 2004).

[xxviii] F. Beunis, K. Neyts, A. Adamski, J. M. Otón, X. Quintana, P. L. Castillo and N. Bennis, '**Leakage currents in AFLC cells with asymmetric boundaries**', 20th International Liquid Crystal Conference (Ljubljana, Slovenia, 2004).

[xxix] S. Vermael, K. Neyts, G. Stojmenovik, F. Beunis and L. J. M. Schlangen, '**A 1-dimensional simulation tool for electrophoretic displays**', 4th FTW PhD Symposium (Ghent, Belgium, 2003).

[xxx] S. Vermael, K. Neyts, G. Stojmenovik, F. Beunis and L. J. M. Schlangen, '**A 1-dimensional simulation tool for electrophoretic displays**', 23rd International Display Research Conference (Phoenix, Arizona, United States, 2003).

[xxxi] F. Beunis and A. De Vos, '**Designing a reversible chip**', 5th International Conference on Thermal Problems in Electronics (Lodz, Poland, 2003).

[xxxii] A. De Vos and F. Beunis, '**Optimizing reversible chips**', 10th International Conference on Mixed Design of Integrated Circuits and Systems (Lodz, Poland, 2003).